AD-A058 265 WASHINGTON UNIV SEATTLE APPLIED PHYSICS LAB F/G 8/12
COMPREHENSIVE STUDIES OF ARCTIC PACK ICE IN APRIL 1976.(U)
MAY 78 G R GARRISON, R E FRANCOIS, E W EARLY N000123-74-C-2064

UNCLASSIFIED APL-UW 7724 NL

1 OF 1
AD A058265

END
DATE FILMED
10-78
DDC

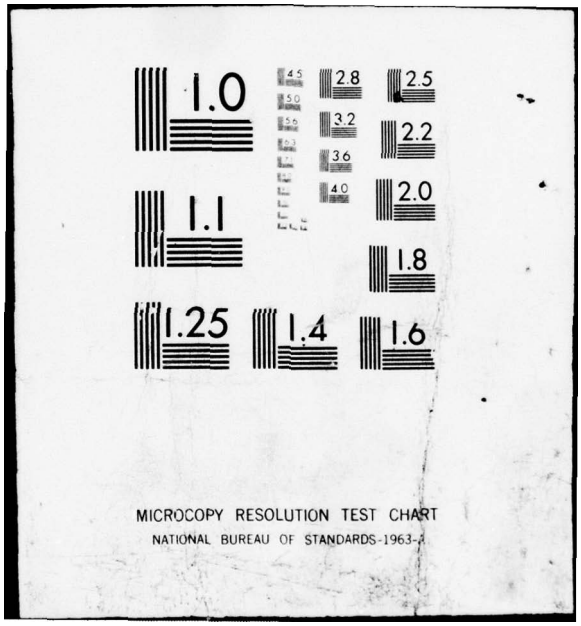
1.0
1.1
1.25
1.4
1.6
1.8
2.0
2.2
2.5
2.8
3.2
3.6
4.0
4.5
5.0
5.6
MICROCOPY RESOLUTION TEST CHART
NATIONAL BUREAU OF STANDARDS-1963-A

AD A058265

LEVEL II

12

COMPREHENSIVE STUDIES OF ARCTIC PACK ICE IN APRIL 1976

DDC
RECEIVED
AUG 29 1978
E

PREPARED FOR:

ARCTIC SUBMARINE LABORATORY, CODE 54
NAVAL UNDERSEA CENTER, SAN DIEGO, CALIFORNIA
UNDER CONTRACTS N00123-74-C-2064 AND N00123-77-C-1013

APL-UW 7724
May 1978

J No.
DDC FILE COPY

APPLIED • PHYSICS • LABORATORY
A DIVISION OF THE UNIVERSITY OF WASHINGTON

DISTRIBUTION STATEMENT A
Approved for public release;
Distribution Unlimited

78 08 21 034

(9) Data presentation and analysis kept.

(2)

COMPREHENSIVE STUDIES OF ARCTIC PACK ICE IN APRIL 1976

(10)

by G.R. Garrison
R.E. Francois
E.W. Early
T. Wen

(15) N0014-73-C-2061
N0014-73-C-1073

(16) F52555

(17) 7F525550P1

(14) APL-UW 7724

(11) May 1978

(12) 73p.

DISTRIBUTION STATEMENT A
Approved for public release;
Distribution Unlimited

031700
78 08 21 034

Ice Camp APLIS in April 1976.

ABSTRACT

During the occupancy of a camp on an ice floe in the Chukchi Sea, studies were made of both the upper and lower surfaces of the pack ice surrounding the camp. Hole drilling and surface observations provided accurate information on ice thickness and composition. A submarine was tracked acoustically as it profiled the underside of the ice. Two aircraft examined the upper surface using photography, infrared imagery, laser profiling and microwave imagery. The highly detailed under-ice profiles show the underside of the ice to be very irregular with little erosion regardless of the age of the ice. The upper surface erodes much faster, and thus gives little evidence of the roughness below. Radiation patterns reveal thickness and age characteristics of the floe but their interpretation requires further investigation.

ACCESSION for
NTIS White Section X
DDC Buff Section ☐
UNANNOUNCED ☐
JUSTIFICATION.....
BY.....
DISTRIBUTION/AVAILABILITY CODES
Dist. AVAIL. and/or SPECIAL
A

TABLE OF CONTENTS

I. INTRODUCTION

The April 1976 field studies were a continuation of oceanographic and acoustic investigations that were started in 1971.[1-5] The studies are sponsored by the Arctic Submarine Laboratory of the Naval Ocean Systems Center at San Diego in a search for knowledge and techniques applicable to submarine operations in arctic seas.

The April 1976 field project was a coordinated effort between APL scientists stationed on an ice floe, a nuclear submarine operating under the ice, and instrumented Navy aircraft. The Naval Arctic Research Laboratory (NARL) at Barrow served as a base for the operation and headquarters for a coordinator from the Arctic Submarine Laboratory. Helicopter support for the APL ice camp was shared with the Polar Research Laboratory which was conducting studies on an ice flow several miles away. The final phase of the project was conducted at AIDJEX ice camp Caribou further east in the Beaufort Sea.

APL established the ice floe camp in the shallow Chukchi Sea and conducted a study of the sea and the ice, with emphasis on properties important to acoustics. The ice camp was occupied for 20 days, beginning in late March.

The oceanographic and weather observations have been described in a previous report.[6] The temperature remained near freezing and the salinity remained near 32‰ throughout the water column except for a small layer near the bottom. Currents were small and the weather was moderate with air temperatures from -31 to -17°C.

The acoustic investigations began with the installation of an underwater tracking range for tracking a submarine, which was used to take under-ice profiles. Measurements were made of the acoustic reflections from the surrounding under-ice features and the reverberation from nearby areas of flat ice. A comparison was made between the keel properties seen in the under-ice profiles and the echoes from those keels in an attempt to determine a meaningful relationship.

Aerial observations were made several times during the occupation of the ice camp. Photographs, infrared images, microwave images, and laser profiles were obtained from several altitudes. This information is compared with the under-ice profiles to improve interpretation of aerial observations.

A brief schedule of events is given below:

17-19 March 1976	Searched for a floe.
20	Established camp with three men, one hut.

21	Helicopter brought three more huts.
22	Outfitted huts. Fifth hut and two men arrived.
23	Augered several holes.
24	Started weather and CTD recording.
25	Installed tracking transducers.
26	Lowered tracking transducers. Augered rotator hole.
27	FH-1100 helicopter with two men arrived. Set up a helicopter base.
28	Installed rotator (to rotate transducer for echoing).
29	Improved markers for the overflights.
30	Measured ice reflection at 60 kHz.
31	Checked out tracking system.
1 April 1976	Took photographs and CTD profiles from helicopter.
2	Measured ice reflections at 20 kHz.
3	Made acoustic propagation measurements.
4	Obtained under-ice profiles.
5	Completed profiling. Two men departed for ice camp Caribou.
6-8	Took CTD profiles from helicopter. Packed equipment.
8-9	Took acoustic propagation measurements at Caribou.
9	Obtained CTD profiles in Beaufort Sea.
11	Obtained CTD profiles near Pt. Franklin.
10-12	Personnel transported to Barrow and to Seattle.

II. SUMMARY

A. AIRBORNE SENSING

Aerial photographs of the surface, taken in good light from low altitudes, often indicate the general character of the under-ice surface. This is especially true for recent ridging. For multi-year floes, however, the surface will often have weathered smooth while the underside remains a ragged jumble of blocks. To accurately estimate ice thickness and bottom-side roughness, one must resort to sensing that penetrates the surface.

Infrared images were very helpful in determining underwater characteristics because the ice temperature, presented as a gray scale, is very indicative of the ice thickness. Microwave images were a valuable addition because they distinguish between first-year and multi-year ice. A comparison of the imagery with under-ice profiles and photographs of the area indicates that the changes in emissivity (at 33.6 GHz) can be adequately explained by correlation with ice age.

Laser profiles of the top of the ice were of little value for indicating conditions underwater because the surface erodes so much faster than the bottom. Also, the actual height of the ice above sea level is difficult to determine because of variations in the height of the aircraft during the measurement. Even when the data are corrected by removing low-frequency variations, some uncertainty remains. The corrected data indicate the ratio of ice draft to ice elevation was 7.5. Analysis of ridge sails showed 4.6 sails per kilometer; the average height was 1.5 m. The distribution of sail heights agrees well with the Hibler equation,[7]

$$P(h) = 2.19\ e^{-0.45h^2},$$

in which the average and minimum heights have been inserted. There is an equally good fit to the Wadhams equation,[8]

$$n(h) = 51.5\ e^{-1.82h},$$

in which the average and minimum sail heights and the sail spacing have been inserted.

B. UNDER-ICE PROFILING

In the past most under-ice profiles have been taken with relatively wide beam sonars. Under-ice profiles taken from a submarine with a narrowbeam sonar revealed that the jagged surface produced when pressure ridges are formed is fairly permanent. The profiles showed numerous

steep inclines 1-3 m in vertical extent with slopes of 75° to 80°. There were several inclines 10-15 m in vertical extent with slopes of 88° to 89° which may result from gaps above tilted blocks of ice. Such slopes, found in both annual and multi-year ice, indicate that erosion beneath the pack is minimal. This extreme roughness causes a high acoustic reflectivity and may mean that the drag coefficients are higher than currently expected. The upper surface, on the other hand, appears to weather smooth in one or two seasons.

Examination of 143 km of under-ice profiles showed 11.7 keels per kilometer with drafts exceeding 3.5 m. The average draft was 6.4 m. The distribution is well represented by the Hibler equation when evaluated for the minimum and average keel drafts observed:

$$P(h) = 0.338\, e^{-0.021h^2} .$$

The high keel density found here is thought to be a result of using a narrower beam for the under-ice profiling than was used by other investigators.

III. THE ICE FLOE CAMP

An ice floe of considerable size was required to support the tracking range. The tracking hydrophones required a stable area nearly 1 km in diameter. Any breaks in this area would have disrupted the system beyond recovery in the short time allotted for work with the submarine. Therefore, a thick floe was desired, but not too thick for the drilling of several holes. A suitable landing strip for fixed-wing aircraft--namely, a long lead that had refrozen with no subsequent breaks and ridging--was also required. The location had to be in an ice pack that would not drift too far from Barrow, would not drift over the deep Barrow canyon, and would not drift southwestward into a coastal current which, though small in the spring, is sometimes in the direction of the Bering Strait.

This section describes in detail how a suitable floe was found and occupied, the arrangement and facilities of the camp, and the equipment and work involved in maintaining it.

A. SEARCH FOR A SUITABLE FLOE

The condition and movement of the ice in the desired area were studied in early March by Dr. M. Allan Beal, the Technical Coordinator for the project, using satellite photographs provided by the Geophysical Institute at the University of Alaska and some reconnaisance flights provided by NARL. At first the desired area was very open, but later a solid pack of ice began moving into the area from the north (see the satellite photograph, Figure 1). Laboratory representatives joined the search party on 18 March. Several floes were sighted that would have been suitable except that there was no adjacent refrozen lead to provide a landing strip for the Twin Otter airplane.

By 20 March more ice had moved into the area. A floe with a good landing strip was found at 71°21'N, 160°12'W (see Figure 2); the plane was landed, and a radio beacon was installed. The floe was 3 km in diameter and contained several large ridges that would provide a variety of acoustic reflections for the measurements. When the decision was made to occupy this floe, a radio call to NARL started the carpenters on the assembly of one of the pre-fabricated huts. The plane returned to NARL and by nightfall a plane load of personnel and gear and one hut, slung beneath a helicopter, were deposited on the ice. On the following day the Twin Otter brought more equipment and supplies (Figure 3).

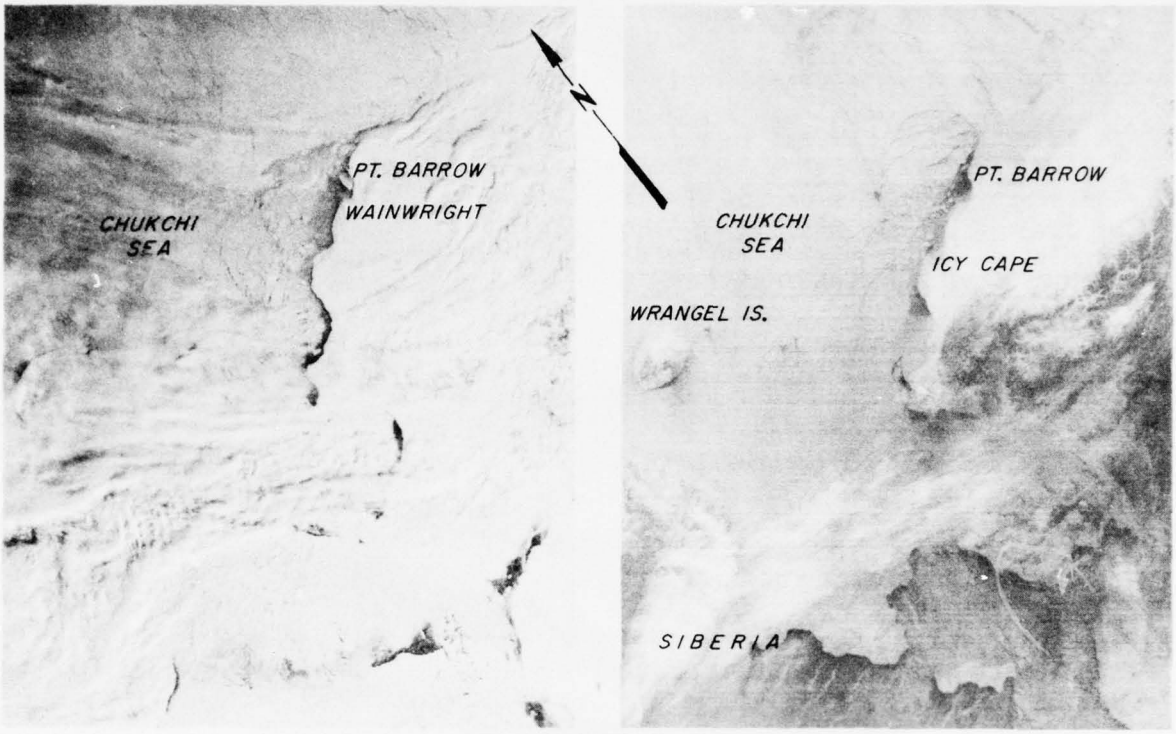

9 MARCH 1976

21 MARCH 1976

Figure 1. Satellite photographs of eastern Chukchi Sea prior to installation of APLIS at location shown in Figure 2.

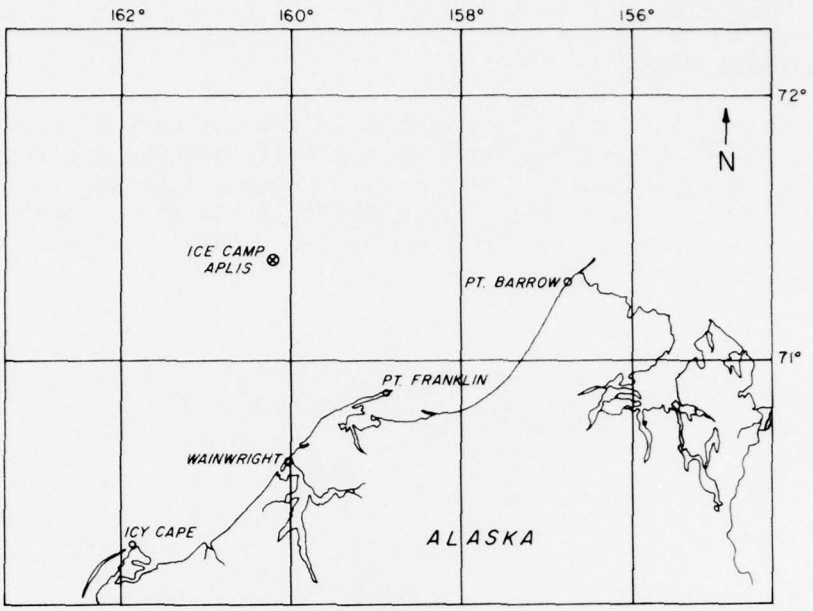

Figure 2. Location of Ice Camp APLIS. The satellite tracking provided only a rough plot of the floe's drift, since the jitter in the data (σ = 2 km) was nearly equal to the drift. However, during the 15 days that the floe was tracked, it appeared to oscillate 5 km each way in a northeast-southwest direction, finally moving another 5 km southwest.[6]

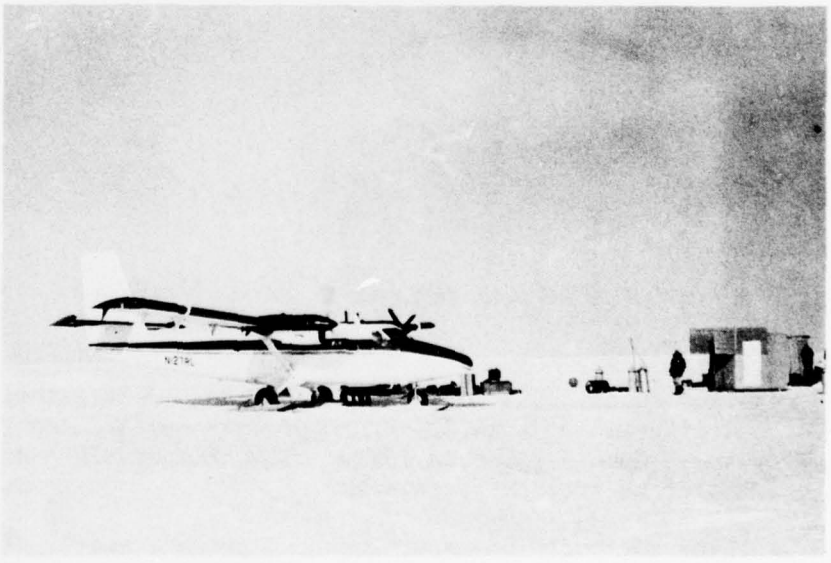

Figure 3. A delivery of equipment by NARL's Twin Otter aircraft.

B. CAMP FACILITIES

The next three days were occupied in the delivery of more huts, the building of shelves and bunks in the huts, and the drilling of some holes through the ice. The final layout of the camp is shown in Figure 4. The huts were 8x12 ft and built of 1/4-in. plywood on 2x3 in. studs with Styrofoam insulation between the studs. A window and a door were provided in each hut.

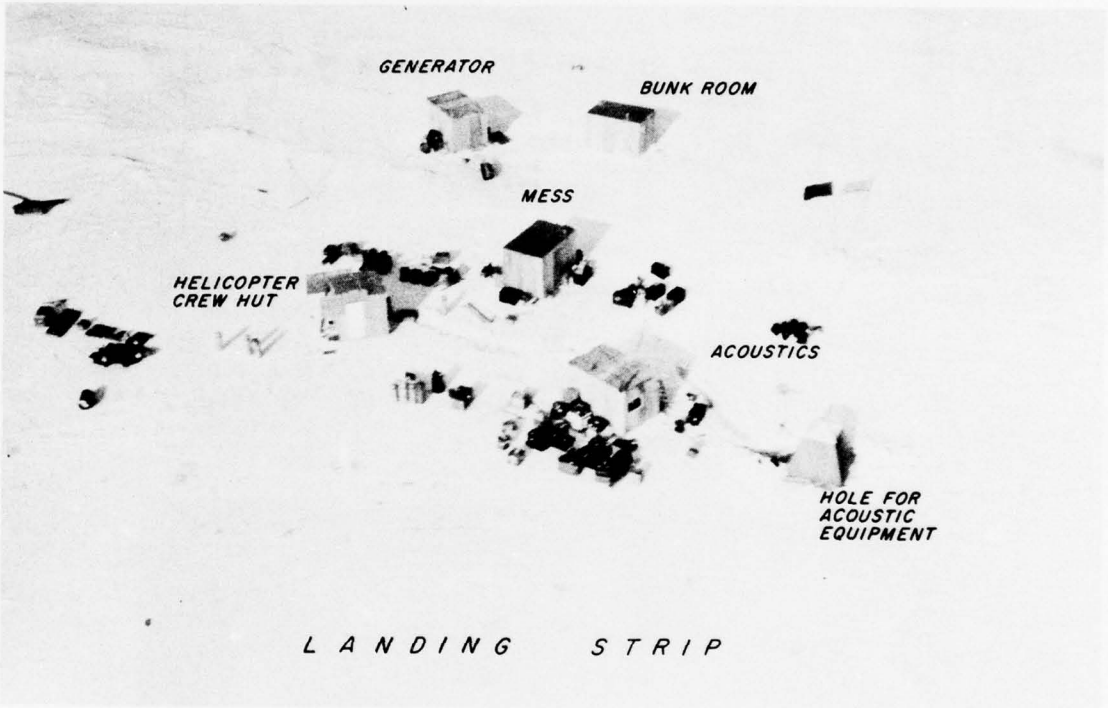

Figure 4. Hut assignments at Ice Camp APLIS.

The mess hut contained a work table, a three-burner gasoline cooking stove, a dining table, a 15,000 Btu/h propane heater, and the weather recording system. Open 5-gal cans filled with chipped ice and snow were kept on the heater to provide fresh water.

The sleeping hut contained four bunks, a propane heater, clothing, and personal items.

The acoustics hut contained one folding bunk, a propane heater, and the electronic equipment for the acoustic measurements. Four men working at once seemed to be the maximum possible in this space. Antennae were mounted on the roof for the radio and the transmitter for satellite tracking. A large hole was augered through the ice about 15 ft (4.5 m) away from the hut for acoustic work. The hole was covered by a tent and heated with small propane heaters.

The generator hut contained a 3.5-kVA generator connected to a 50-gal fuel drum on the outside of the building. A work bench and mechanical tools and stores filled one side. A small propane heater was available, but the heat from the generator was usually sufficient. A toilet was installed in one corner over a 9-in. (23-cm) diameter hole 5 ft (1.5 m) deep. This hut served as a storage place for ice augers and other large items that were not in use. A 16-in. (40-cm) hole through the floor and ice gave access to the water below. A CTD winch was attached to the wall above the hole. The current meter was also stored and operated here. Operations in this hut had to be scheduled to avoid chaotic overcrowding.

The 8x8 ft helicopter hut housed the two-man crew of the FH-1100 helicopter shown in Figure 5. The helicopter was leased primarily to assist the Polar Research Laboratory's studies on an ice floe several miles away. The helicopter was used at APLIS for aerial photography and for oceanographic measurements between APLIS and the mainland.

Figure 5.
The FH-1100 helicopter based at APLIS.

C. CAMP EQUIPMENT

Several items of equipment are important for the operation and safety of the camp.

Radio communication with the Coast Guard station at NARL was accomplished using a Northern Radio Co., Mod 550 radio at either 4625 or 6230 kHz. Sometimes the atmospheric conditions were so poor during the day that we were unable to communicate for several hours. All stations on the network experienced the same difficulty. Nighttime communications were usually very good.

The radio beacon installed during the reconaissance flight performed well and was used routinely by aircraft approaching the camp. The navigation system on the Twin Otter was capable of finding the camp, perhaps with a few passes; however, the helicopter that was based at the camp relied heavily on the beacon.

Two satellite navigation transmitters were installed and both worked well. The data were radioed from the satellite to a station in Maryland, and the calculated track was not obtained until after the camp was abandoned. By special arrangement, the results for a particular satellite pass could be obtained about 10 hours later by telephone.

Spare generators proved very important. The first one installed had bad voltage regulation. After running for 6 days, a connecting rod in the Dayton engine failed. The generator was replaced by a Sears 3.5-kVA unit which produced considerable electrical noise interference to the acoustic experiments, but ran for the remaining 10 days.

A fire extinguisher for each hut was obtained from NARL. The huts were spaced well apart to avoid the danger of a fire spreading throughout the camp.

D. HOLE DRILLING AND MAINTENANCE

A Jiffy® auger, powered with a 3-hp gasoline motor, drilled 23-cm holes quickly and easily; a 40-cm hole was made by reaming out a 23-cm pilot hole with a special reamer powered by the Jiffy motor. The reamer merely cut up the ice which had to be removed by hand when the hole was dry and by bucket after it flooded. Evacuating the 3-m deep hole in the generator hut proved a difficult task by this method. The 100x75 cm hole for the acoustic work was made by cutting several 40-cm holes close together. Fortunately, the ice was only 1.3 m thick, and the hole was completed in 2.5 h by two men (see Figure 6).

The 40-cm hole in the generator hut had to be reamed daily. This began as a 45-min job, but shortened each day as the ice around the hole warmed.

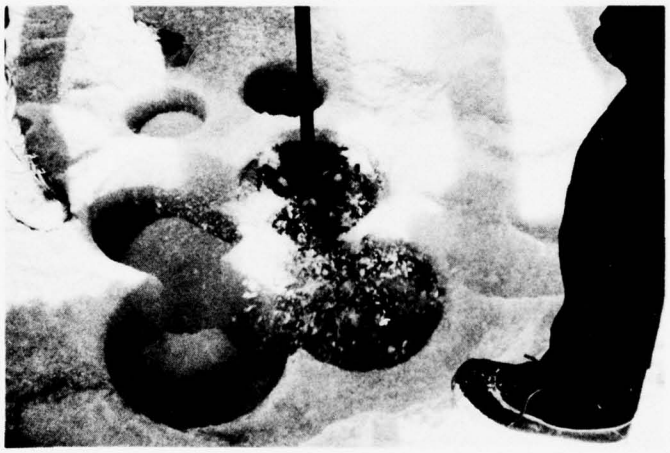

Figure 6.
Cutting six holes with the reamer to make a large acoustic instrumentation hole.

The broad, shallow hole for the acoustic work was covered by a 2-m square tent. Two propane heaters were placed over the hole in a box so that the heat radiated into the hole. This arrangement seemed to work quite well. A thin sheet of ice formed around the edge each night, but was easily removed. In 10 days there was very little decrease in the size of the hole.

The tracking transducers were installed through a 23-cm auger hole and allowed to freeze in. Unfortunately, these transducers had to be lowered the next day because of deep ice keels that blocked the acoustic transmission path. Considerable difficulty was encountered in freeing the cables from the newly formed ice. With electric melting (at 1 kW) and considerable chipping, the cables were finally freed. Recovery of these transducers at the end of the operation was accomplished by drilling another 23-cm hole alongside, lowering a special handle-hook through the hole, catching the cable, and drawing the transducer up through the hole where the cable could be cut free from the portion frozen into the ice.

IV. SUBMARINE TRACKING SYSTEM

An accurate tracking system was obtained by installing three widely spaced hydrophones which picked up special acoustic pulses from the submarine. The transmission of these pulses was synchronized with timing equipment at the ice camp; thus the transmission times could be accurately measured and the position of the submarine computed.

A. EQUIPMENT

The equipment used in the tracking operation is diagrammed in Figure 7. At the heart of the tracking system were two synchronized autonomous clocks. Each clock generated a trigger pulse at 10-sec intervals. One clock was placed aboard the submarine and connected to the transmitter while the other was built into the data processor for referencing the timers.

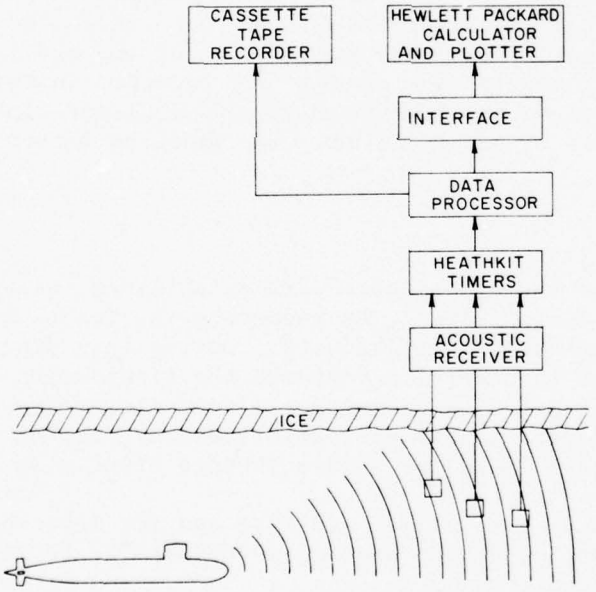

Figure 7. Block diagram of tracking system.

The transmitter on the submarine was connected to an existing transducer located 4 m from the bow on the starboard side and 8 m above the keel. The output level was 190 dB re 1 μPa at 1 m, and the pulse length was 3 msec. The transducer pattern itself was sufficiently broad, but because of the transducer's position on the submarine some variability due to hull shadowing was experienced.

The receiving transducers were lowered through holes in the ice, and connected to the acoustics hut by cables laid over the surface. These transducers were first placed at a depth of 9 m but had to be lowered to 18 m because of the deep ice keels in the area. The pattern of the receiving transducer was sufficiently broad to pick up signals from all submarine depths involved in the operation. The acoustic receivers in the hut had a bandwidth of 1.8 kHz. An automatic gain control adjusted the gain and threshold according to the noise level present in order to register the tracking pulse. A Heathkit timer connected to each receiver measured the time between the synchronizing pulse that signalled the emission of a pulse from the submarine and the receipt of a pulse.

B. OPERATION

Every 10 sec, a trigger pulse from the autonomous clock aboard the submarine triggered the transmitter which in turn sent out a pulse from the transducer. At this same instant, a pulse from the synchronized clock in the data processor reset the three Heathkit timers which then started counting time in increments of 1/10 msec. When the acoustic pulse was received by one of the receiving transducers and recognized by the receiver, the corresponding timer was stopped. Near the end of the 10-sec period, the time stored in each counter was recorded on the cassette tape and also provided to the Hewlett-Packard calculator-plotter for real-time processing. This 10-sec cycle was then repeated to obtain a continuous plot.

C. TRACKING CALCULATIONS

The relative locations of the transducers were established, using an average sound velocity of 1437.2 $msec^{-1}$, by recording the travel time of an acoustic pulse from transducer to transducer. During this process, it was found that because of deep under-ice features the transducers had to be lowered to a depth of 18 m for an unobstructed acoustic transmission. A rectangular coordinate system was established by passing the Y-axis through transducers 1 and 2 and the X-axis through transducer 3.

For tracking transducers at X_1Y_1, X_2Y_2, and X_3Y_3 and for measured distances to the tracked object of D_1, D_2 and D_3, we obtain the coordinates of the object by the equations

$$X = \frac{(M_2-M_1)(Y_1-Y_3) - (M_3-M_1)(Y_1-Y_2)}{2\ DEN}$$

and

$$Y = \frac{(M_3-M_1)(X_1-X_2) - (M_2-M_1)(X_1-X_3)}{2\ DEN} \quad ,$$

where

$$M_n = D_n^2 - X_n^2 - Y_n^2 \qquad n = 1,\ 2 \text{ or } 3$$

$$DEN = (X_1-X_2)(Y_1-Y_3) - (X_1-X_3)(Y_1-Y_2) \ .$$

With the three tracking transducers at Z=0 we can obtain the relative depth of the object from any one of the following equations:

$$Z^2 = D_n^2 - (X_n-X)^2 - (Y_n-Y)^2 \qquad n = 1,\ 2,\ \text{or } 3.$$

By selecting axes that place transducer 1 at (o,a), transducer 2 at (o,-b), and transducer 3 at (c,o) (see Figure 8) the equations can be simplified and written in a form convenient for computer programming:

$$Y = \frac{(D_2-D_1)(D_2+D_1) + a^2 - b^2}{2\ (a+b)}$$

and

$$X = \frac{1}{c}\left[aY - \frac{1}{2}(D_3-D_1)(D_3+D_1) + a^2 - c^2)\right] \ . \qquad (1)$$

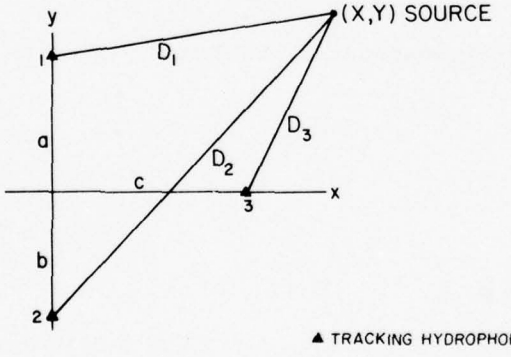

Figure 8.
Tracking from three hydrophones.

For tracking from only two transducers, the object's depth must be approximately known. Knowing this depth difference, we can convert sound travel measurements to horizontal distances. For transducers 1 and 2 at (e,f) and (g,h), with horizontal distances D_1 and D_2, respectively, to the object (see Figure 9), we have

$$\ell^2 = (f-h)^2 + (g-e)^2$$

and we define

$$s = \frac{\ell + D_1 + D_2}{2} \quad .$$

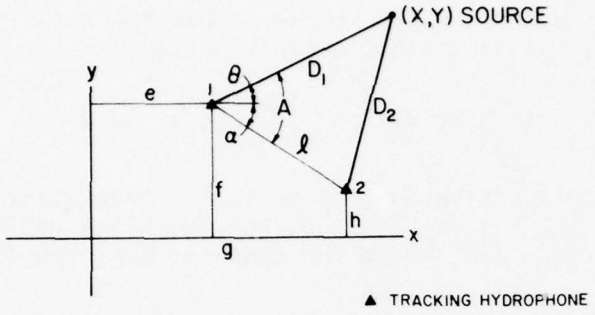

Figure 9. Tracking from two hydrophones.

The angle A at transducer 1 between transducer 2 and the object is given by

$$\sin \frac{A}{2} = \pm \sqrt{\frac{(s-\ell)(s-D_1)}{\ell D_1}} \quad . \qquad (2)$$

The angle at transducer 1 between transducer 2 and the X direction is given by α, where

$$\tan \alpha = \frac{f-h}{g-e}$$

$$\theta = A-\alpha \ ,$$

and the coordinates become

$$Y = f + D_1 \sin\theta$$

$$X = e + D_1 \cos\theta \ .$$

There are two solutions to Eq. 2 and sometimes the choice is difficult. Two-transducer tracking was therefore limited to occasions when there were only two good time measurements, which occurred often because one transmission was frequently blocked by the hull of the submarine.

Real-time tracking (with a 10-15 sec delay) was performed using a desk calculator and plotter. A Hewlett-Packard Extended Memory was necessary so that various options, such as two- or three-hydrophone tracking, could be selected quickly when a change was required.

Further analysis of the tracking data was performed at the Applied Physics Laboratory using a CDC 6400 computer. During the operation, tracking data and time of day had been recorded on a tape cassette. Later at the Laboratory these data were transcribed onto a standard 1/2-in. seven-track tape. From this tape, a listing of the tracking data, containing time and three acoustic distances, was obtained. The list was scanned manually and each data point was assigned a code to denote whether it was good, and which of the three acoustic travel distances were valid. The code and the data together were then fed into a program designed for calculating and plotting the data. A sample tracking plot is shown in Figure 10. Further analysis smoothed the plot and interpolated across the gaps. Tracking often failed completely when the submarine headed away from the hydrophones and the hull blocked the transmission.

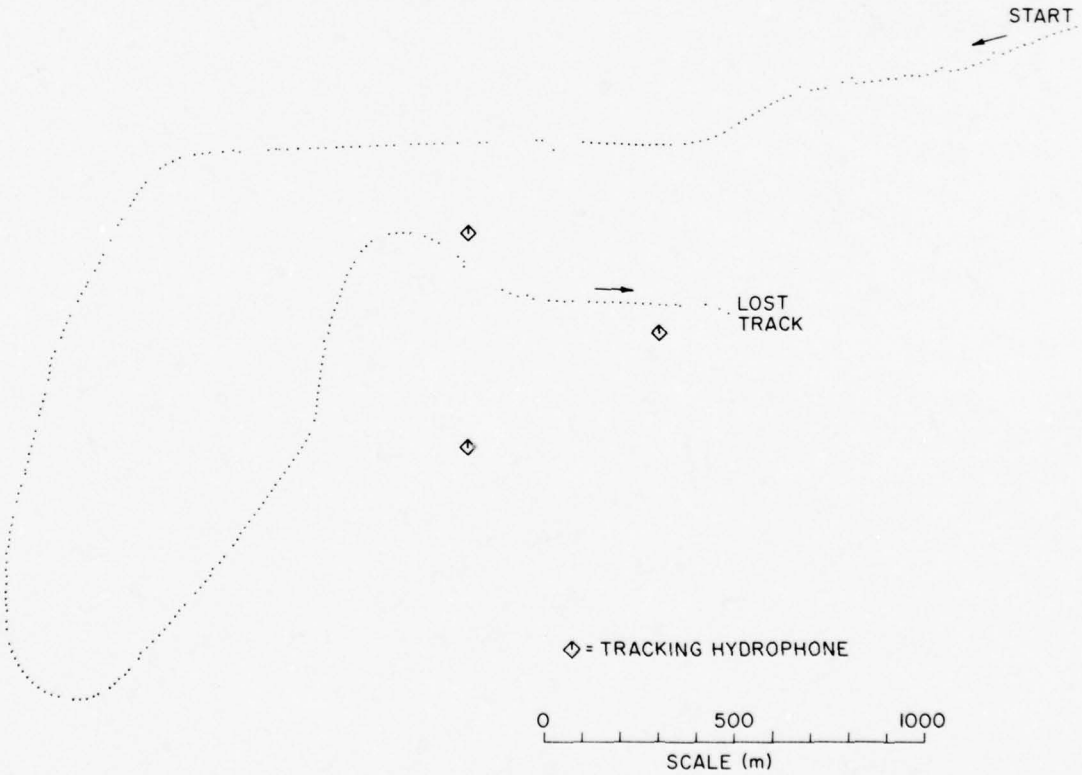

Figure 10. An example of a submarine track plotted using data from any two of the hydrophones or all three.

Examination of the computed tracks shows that, with a tracking transducer spacing of 600 m, tracking accuracy is about 5 m. The maximum range of good tracking was 3000 m, although pulses were received from 4500 m. The greatest hindrance to tracking during this operation was blockage of the submarine's transmission by the hull. For good three-hydrophone tracking, the source must be located at a point that has clearance in all directions, preferably on the highest point, because in this type of range the receiving transducers are always shallower than the submarine.

Some of the plotted tracks were compared to the inertial navigation system on the submarine. The satellite records we obtained gave latitude and longitude readings to 0.01' which is equivalent to 20 m north-south and 7 m east-west. Our computed track was accurate to about 5 m, therefore the submarine's latitude readings were a little too coarse for comparison. With some smoothing of data, the tracks differed by 5-10 m. In one case our track showed a 30 m loop and the submarine data showed a 20 m loop. However, the more central location for the submarine's navigation system, compared to the forward location of the tracking transducer, could have resulted in a smaller turning circle. Other distortions noted are probably due to ice drift which caused our reference system to move and rotate.

V. UNDER-ICE PROFILING

The submarine was tracked from the ice camp as it cruised along a network of lines around the area taking profiles of the underside of the ice.

A. PROFILING INSTRUMENTATION

The submarine has a narrowbeam sonar (2°) with a maximum repetition rate of six pulses per second. At a speed of 3 kn this gave an ice depth measurement every 0.26 m. A pressure transducer on board compensated automatically for the submarine's depth. The profile data were recorded digitally on magnetic tape which was processed at the Naval Ocean Systems Center in a manner described in the appendix. Accurate time of day was recorded by the submarine and at the ice camp so that the tracking data and the profile data could be correlated.

B. RUN PLANS

During the first profiling period on 4 April, the submarine followed the perimeter of the 2x3 km area selected for study and then spiraled inward on a line spacing of about 100 m. During a second period the next morning, two runs were made around the area to fill in some of the gaps that occurred during the first session. However, as some of the gaps resulted from the submarine avoiding ice keels, this attempt was not very successful. A third session was held in the afternoon in an attempt to obtain closely spaced lines near the camp and lines perpendicular to the previous lines. Once again the grid was distorted by the presence of ice keels too deep to pass beneath. The tracks of the four profiling runs, superimposed on an aerial photograph of the area, are shown in Figures 11 to 14.

C. UNDER-ICE TOPOGRAPHY

Many of the profiles show extremely sharp under-ice features. A change of many meters of depth often occurs in the space of one data point. This could represent a cliff or an overhang (inverted slope) and indicates that the jumble of blocks formed during ridging remains unchanged for some time. A continuous portion of an under-ice profile showing both extremes, flat refrozen leads and jumbled blocks in the ridges, is reproduced in Figure 15.

When looking at profiles, one often assumes that some slopes appear steep because of the exaggerated vertical scale. In Figure 16, we have replotted a section of the profile with the vertical scale the same as the horizontal scale. Many of the slopes are still very steep, showing that the underside of the ice was very irregular and had neither eroded nor consolidated appreciably.

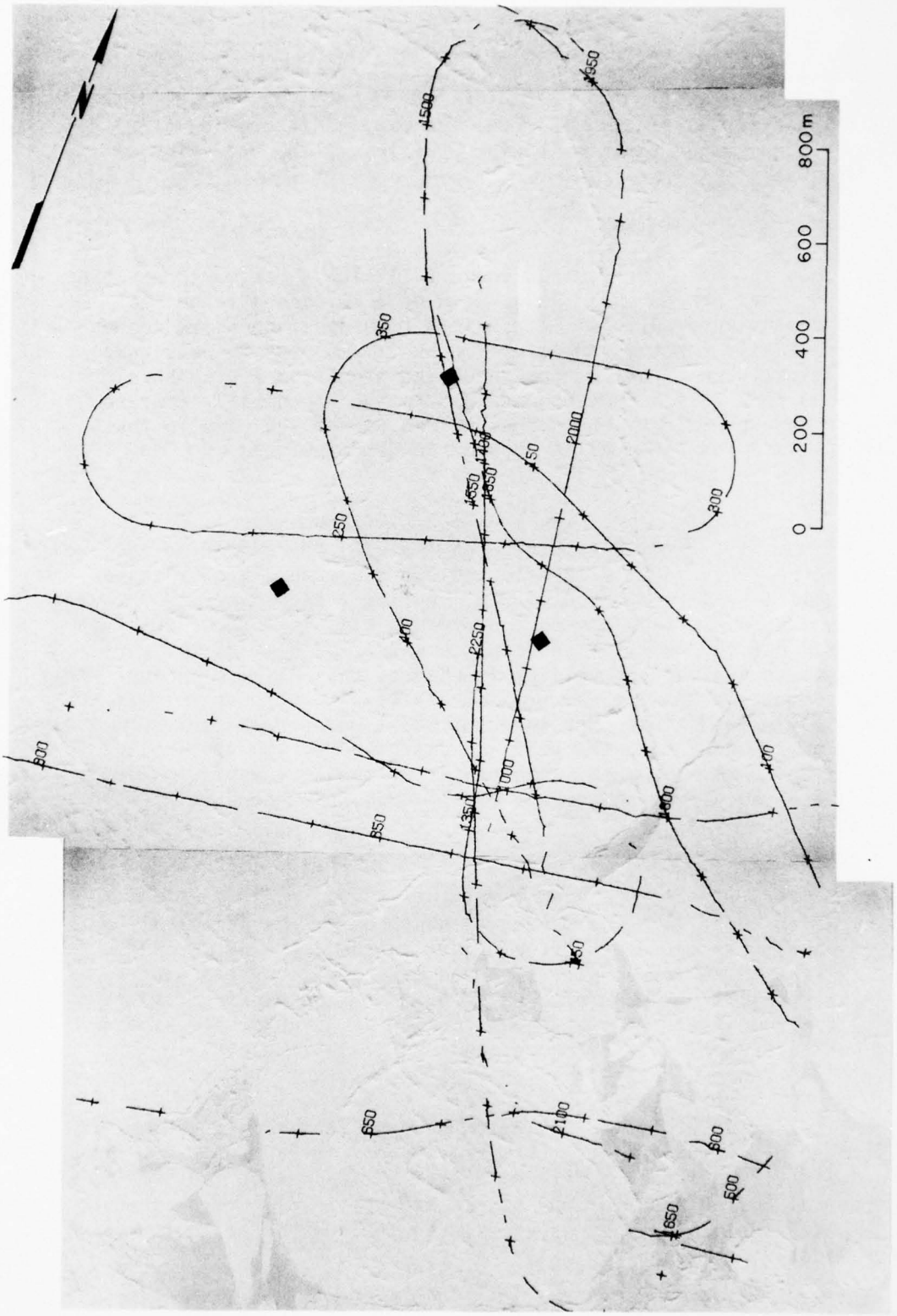

Figure 11. Track of the submarine during first profile run. The locations of the three tracking transducers are indicated.

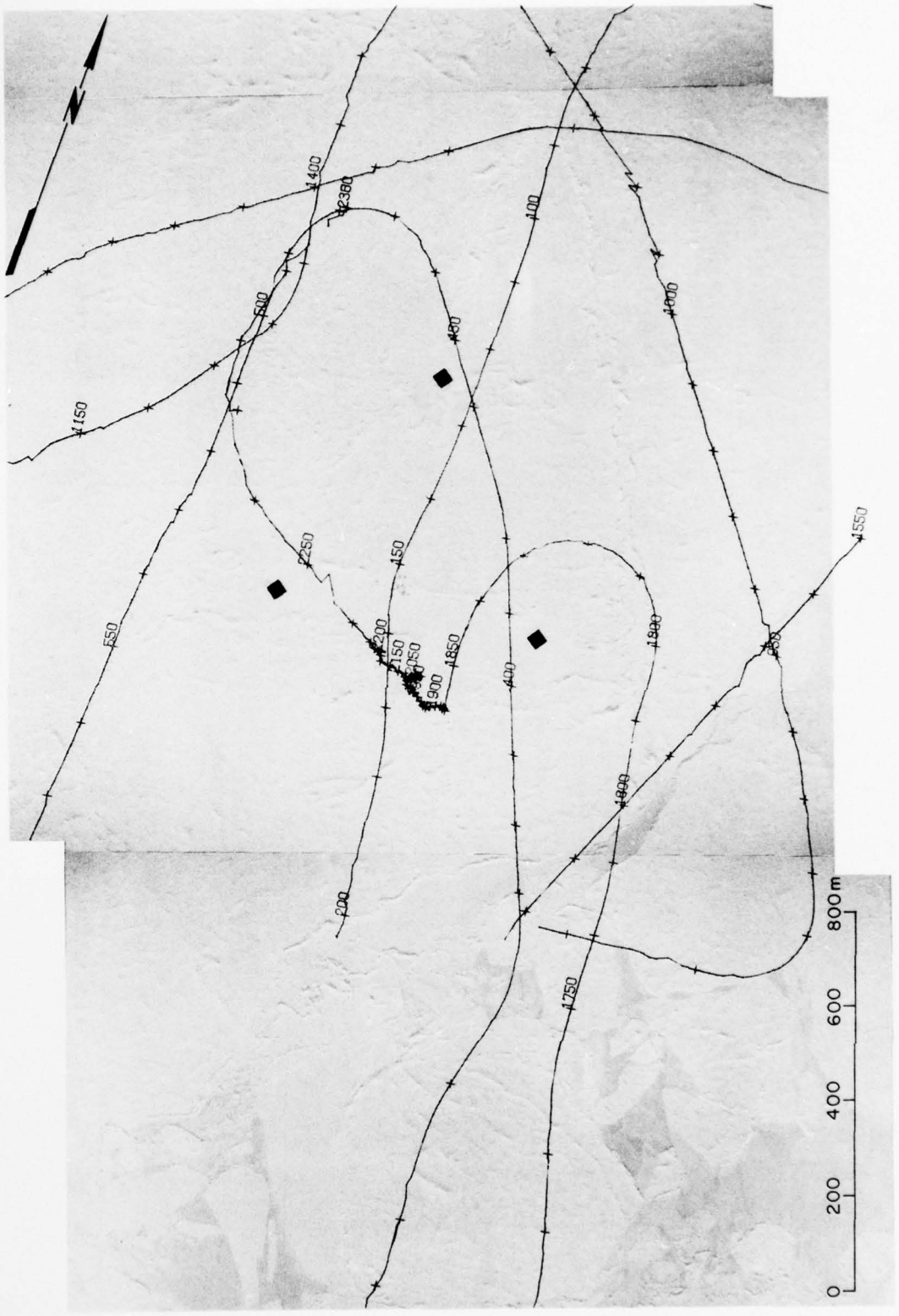

Figure 12. Track of the submarine during second profile run.

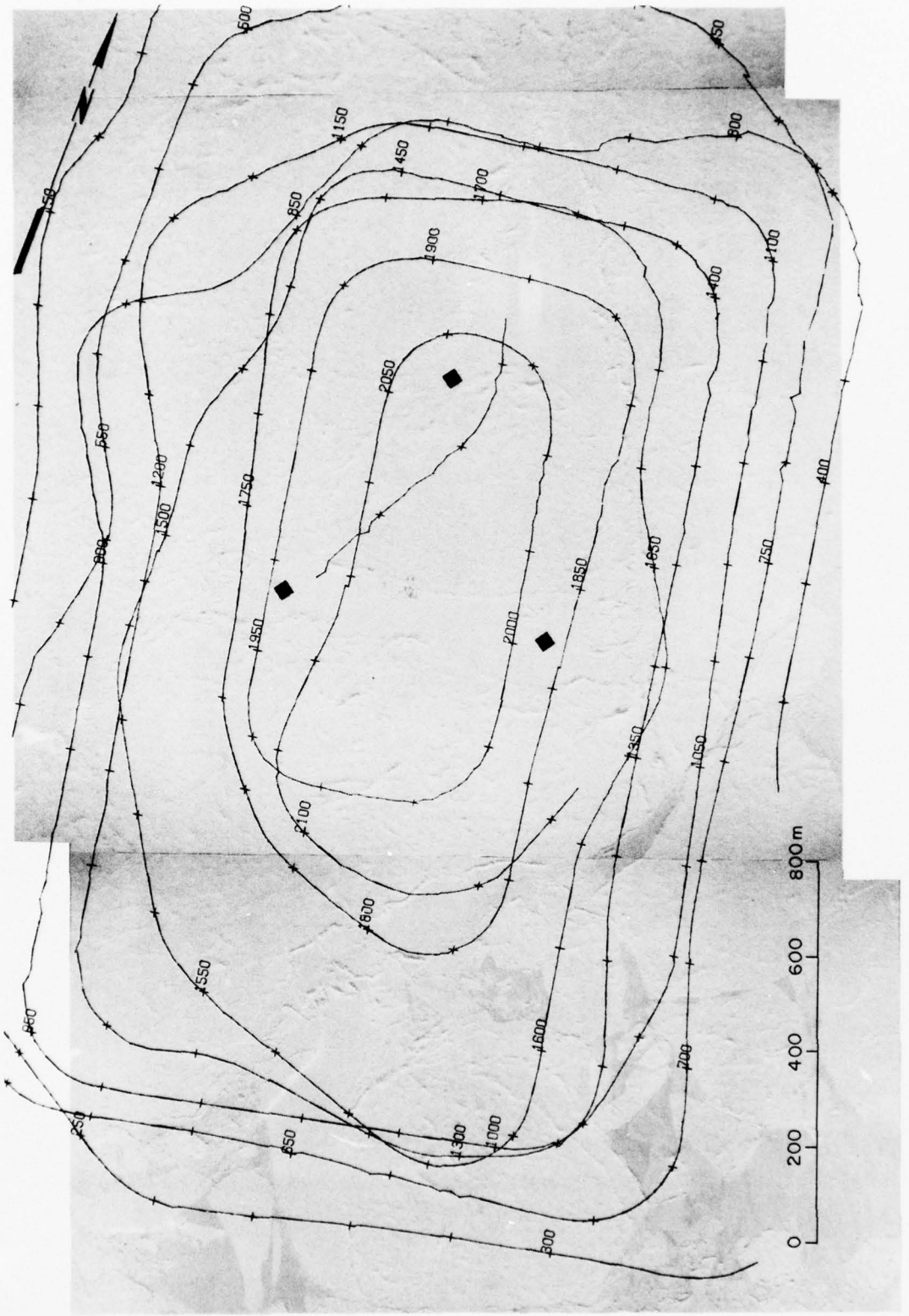

Figure 13. Track of the submarine during third profile run.

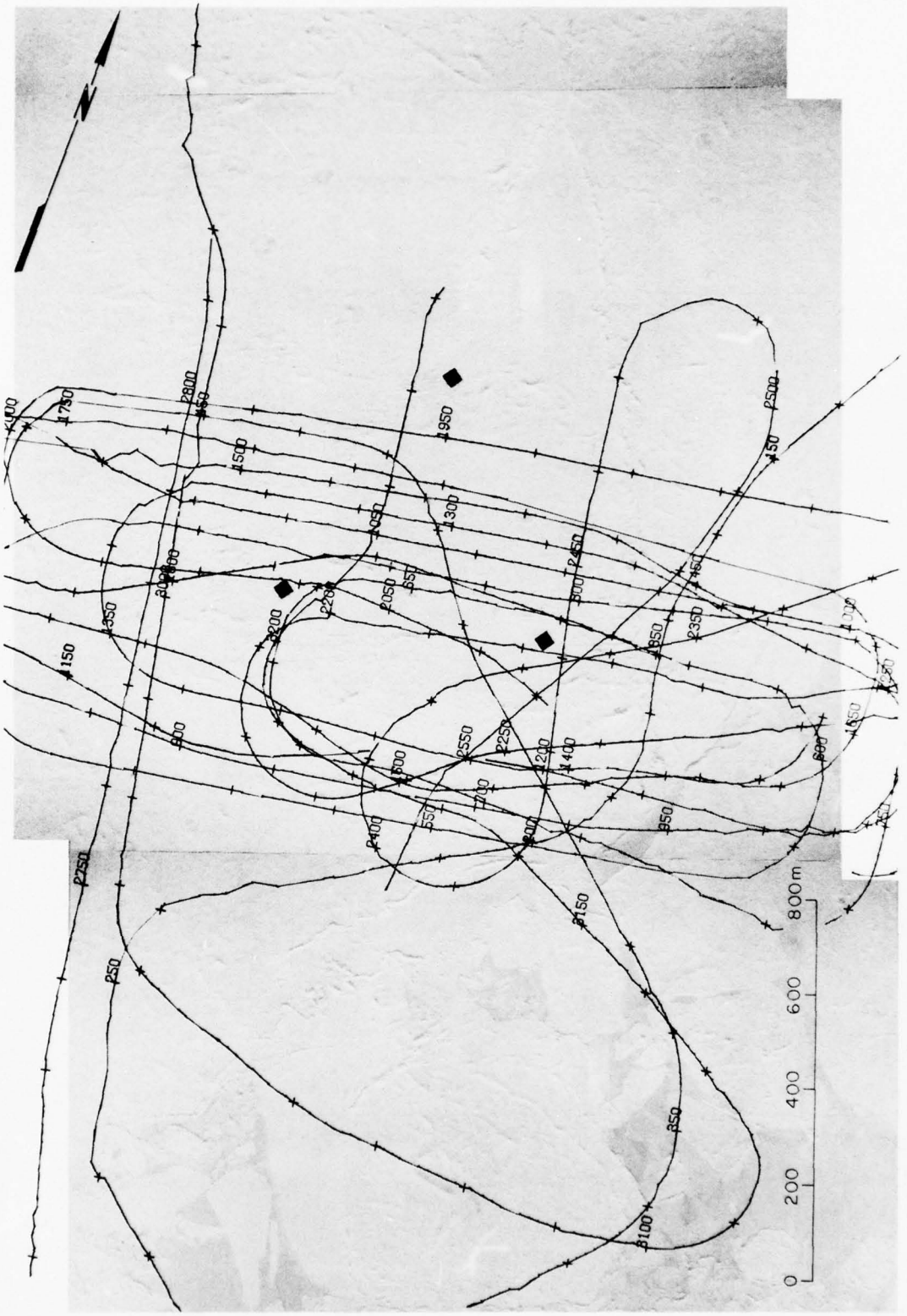

Figure 14. Track of the submarine during last profile run.

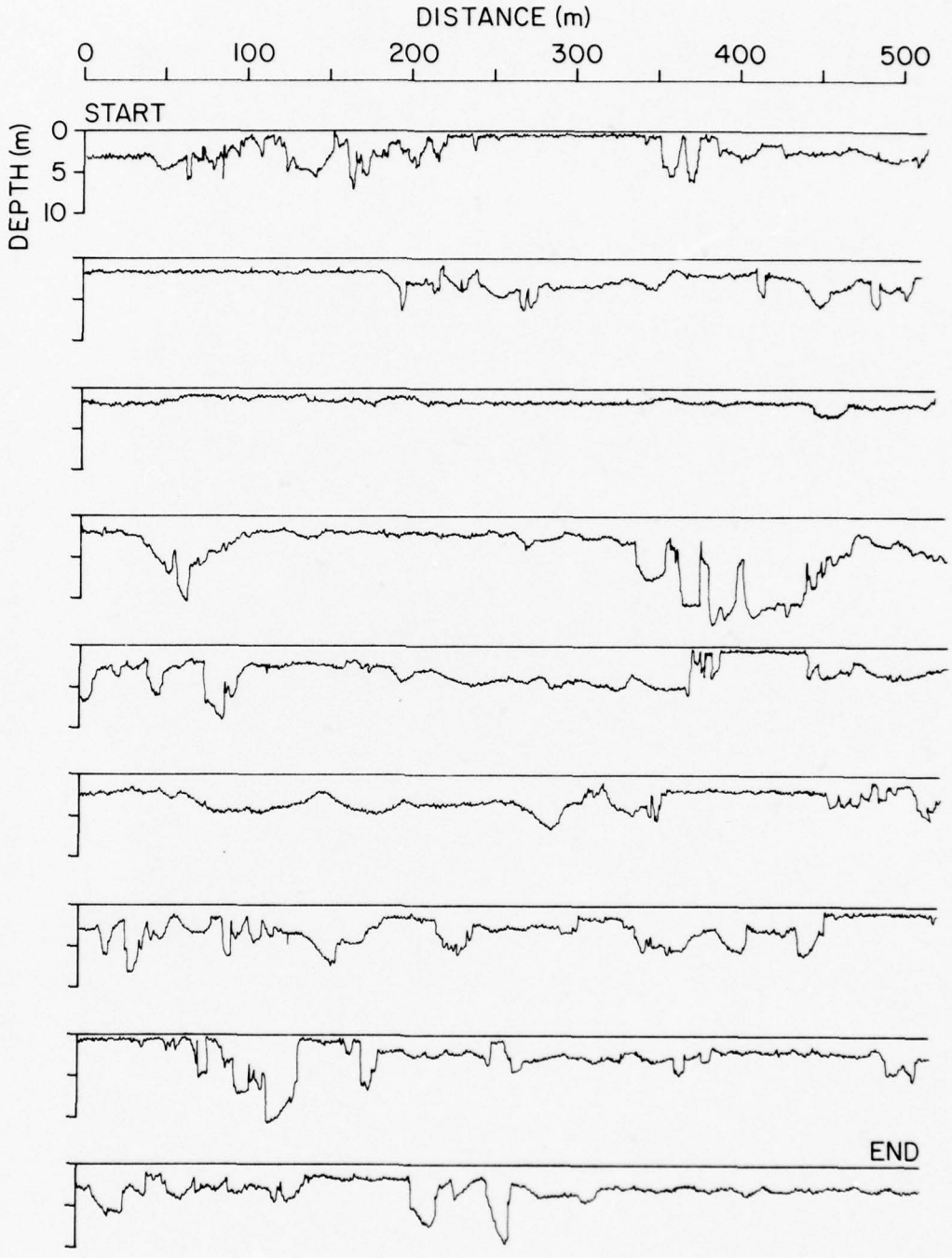

Figure 15. Sample of a continuous portion of the under-ice profile.

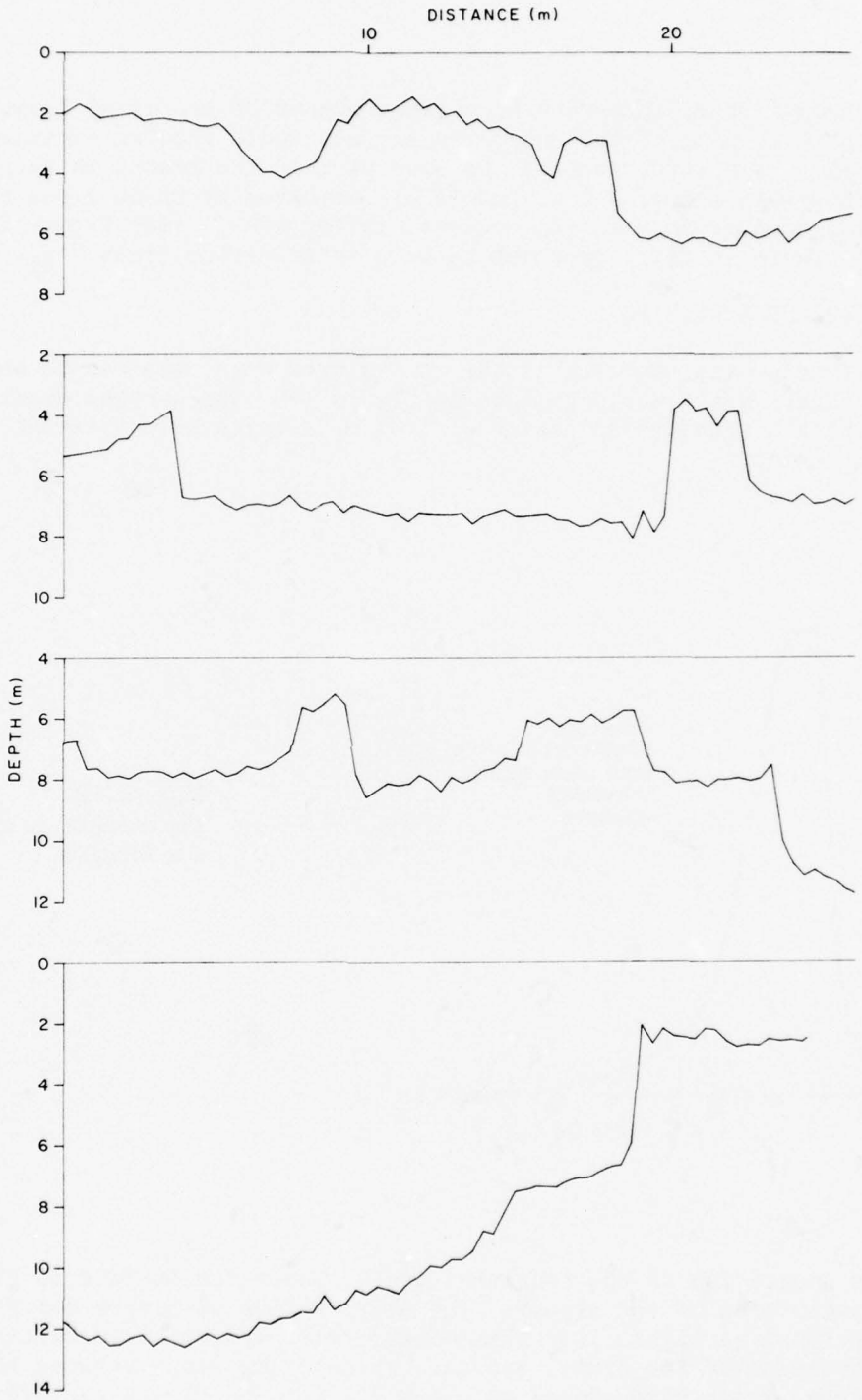

Figure 16. Typical under-ice profile with horizontal and vertical scales equal. The steep slopes are truly represented.

Although there appear to be a great number of profiling lines, topographic mapping of the under-ice surface would require considerably more data. In a later section, we have plotted the tracks in three depth intervals (>8 m, 4-8 m, and <4 m) indicated by three types of lines for comparison with the acoustic reflections. (See Figure 52, p. 88.) There is fair agreement between intersecting lines.

D. ICE DRAFT STATISTICS

All under-ice profiles in the 2x3 km area were examined to obtain the ice draft distributions shown in Figure 17. The average draft was 3.31 m with a standard deviation of 1.87 m. Drafts were referenced to the sea surface.

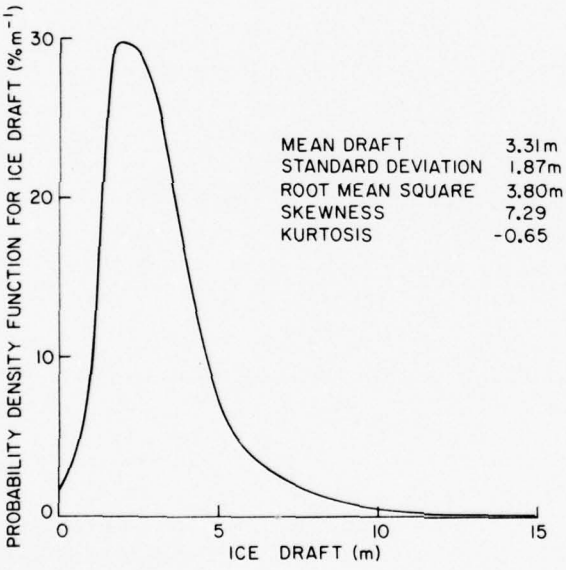

Figure 17. Distribution of ice drafts.

An indication of the roughness of the under-ice surface is given by the distribution of the slopes. The distribution of slopes for the 2x3 km area is shown in Figure 18. This distribution was obtained by taking six-point averages of the draft, and then calculating slope between these average points, which were spaced at about 1.8 m. The slopes averaged 9.7 ± 11.3°.

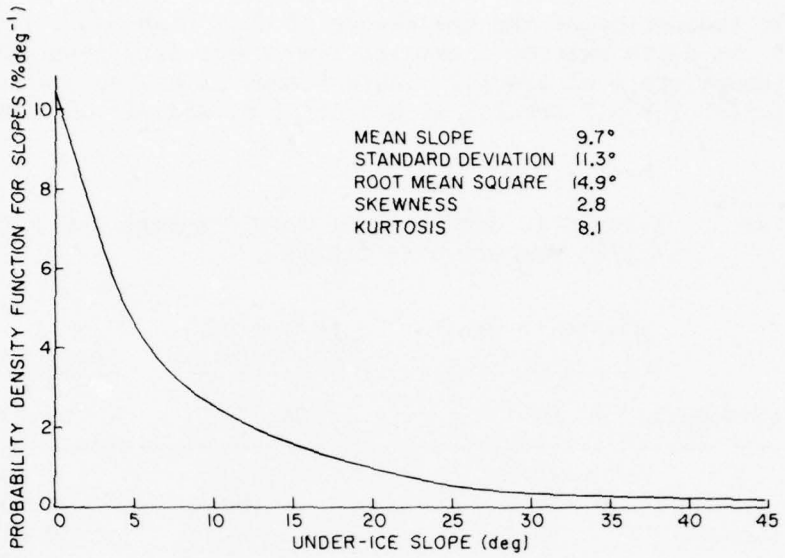

Figure 18. Distribution of under-ice slopes between averages of six data points (six points equal 1.8 m of distance). For greater detail on the slopes above 45°, see Figure 19.

A close examination of some of the profiles (see Figure 15) shows that there were many very large changes in a one-data-point increment. In many instances, the draft changed by several meters between adjacent data points, which were spaced at about 0.3 m. Such an abrupt change indicates a steep slope or the end of a projecting block. The presence of an appreciable number of these jumps indicates that the under-surface had retained the ruggedness created when the pressure ridges were formed, and that very little erosion had taken place.

Detailed observations of ice-ridge structure, especially that of the underside, are scarce. Kovaks et al.[9] reported the underwater portion of a ridge as massive and rounded, yet some of their test holes were only half the assumed thickness of the ice, giving the impression that the ridge may still have had blocks and cavities similar to those detailed here. Side-scanning sonars or wide-beam under-ice profilers are apt to attribute an erroneously smooth shape to the keels.

The fact that the under-ice surface retains considerable roughness is important to the prediction and explanation of acoustic reflection and backscattering. Some of the proposed models based on a rounded geometry[10] would not be suitable for predicting reflections at frequencies in the region above 1 kHz. The jagged blocks present many reflecting surfaces, some of which happen to be perpendicular to the probing beam and thus would produce large echoes.

As an indication of the prevalence of such high-angle faces, we tabulated the depth changes exceeding 1 m in one data interval of the profile (about 0.3 m of track). Table I summarizes the number of these "steep slopes" for all tracks, with a total of 438,815 data points.

Table I. Changes in depth in one data interval (~0.3 m of track) for all five tracks.

	Change in Draft (m)	Number of Data Points	Percentage
(Gradual)	0- 1	434,775	99.009
	1- 3	3,539	0.806
	3- 5	430	0.098
(Steep)	5- 7	54	0.012
	7- 9	11	0.003
	9-11	1	0.000
	11-13	2	0.001
	13-15	3	0.001

The distribution of slopes for the steep slopes in Table I is given in Figure 19. A second ordinate scale gives the number of these steep slopes per kilometer of track. There were 4040 steep slopes for the 143 km of track, which is an average of 28 per kilometer. (This value compares well with the 12 keels per kilometer noted in the next section if one considers each keel to have two steep slopes, one on each side.) This is one steep slope per 36 m of travel.

The slopes represented by these one-interval depth changes are important to acoustic studies. The average slope calculated between adjacent data points will usually be less than the maximum slope, thus the slopes shown in Figure 19 may be a little lower than the true slopes.

E. ICE KEEL STATISTICS

Ice keels have been defined in several ways. Those that use a specific dimension would appear to be useful for only a selected range of keel sizes. The Rayleigh criterion used by several researchers, in which a draft is defined as a keel if its depth is more than twice that of the adjacent valleys, is more general.

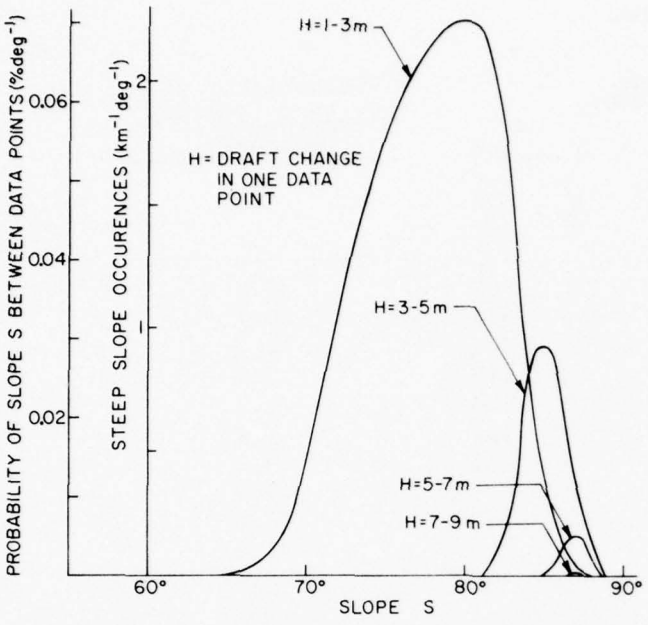

Figure 19. Slope distributions for various values of H (H = draft change in one data point).

The under-ice profiles taken from a submarine in the area of ice station APLIS have been examined and keels selected using the Rayleigh criterion. The results for four of the submarine runs are given in Table II.

Hibler Distribution

Hibler, Weeks and Mock[7] have developed a theoretical distribution function for pressure ridges from fundamental assumptions about the randomness of ridges. They assume that, for a given net deformation over a region, all possible collections of ridges that yield this deformation are equally probable. The theory applies also to pressure keels. For a given minimum keel draft h_o, they predict the distribution of keel drafts to be given by

$$P(h)\ dh = 2\lambda\bar{h}\ e^{\lambda h_o^2}\ e^{-\lambda h^2}\ dh\ ,$$

where $\bar{h}$ is the average keel draft. The values we used for $\bar{h}$ and h_o were 6.38 m and 3.5 m, respectively. A value of 3.5 m for h_o was selected because the number of keels with drafts of 2 and 3 m appeared to be very low compared to the values for greater h, probably a result of the keel definition employed.

Table II. Number of ice keels, based on Rayleigh criterion.

h	Number of Keels Track 1	2	3	5	Sum	Probability of Height h, for $h>h_o$ (percent)
2	15	5	16	16	52	
3	22	25	52	42	141	
h_o						
4	66	65	105	132	368	22.0
5	63	54	83	146	346	20.7
6	54	55	83	111	303	18.1
7	35	35	64	84	218	13.0
8	27	33	50	53	163	9.7
9	17	19	42	43	121	7.2
10	9	14	22	26	71	4.2
11	5	9	9	8	31	1.9
12	5	5	8	8	26	1.6
13	5	4	5	6	20	1.2
14			3	3	6	0.4
15			1	0	1	0.0
16				1	1	0.0
17				1	1	0.0
TOTAL (for h = 4-17 m)					1675	100.0

Track Length (km):
Track 1 = 20.5, Track 2 - 27.1, Track 3 - 42.3,
Track 5 - 53.3, Sum - 143.2

Average Keel Draft - 6.38 m

Average Keel Density - 11.7 keels per kilometer for h>3.5

With these values the Hibler equation becomes

$$P(h)\,dh = 0.338\, e^{-0.0206h^2}\, dh\ .$$

The logarithm of this relation is plotted in Figure 20 for comparison with the observations. The Hibler equation appears to fit the data very well. The dropoff with ridge draft is much faster than the examples given in References 7 and 8; however, (1) the ice formed in the Chukchi Sea is not nearly as thick as that in the Arctic Ocean and (2) the submarine avoided the larger keels and thus they were not counted.

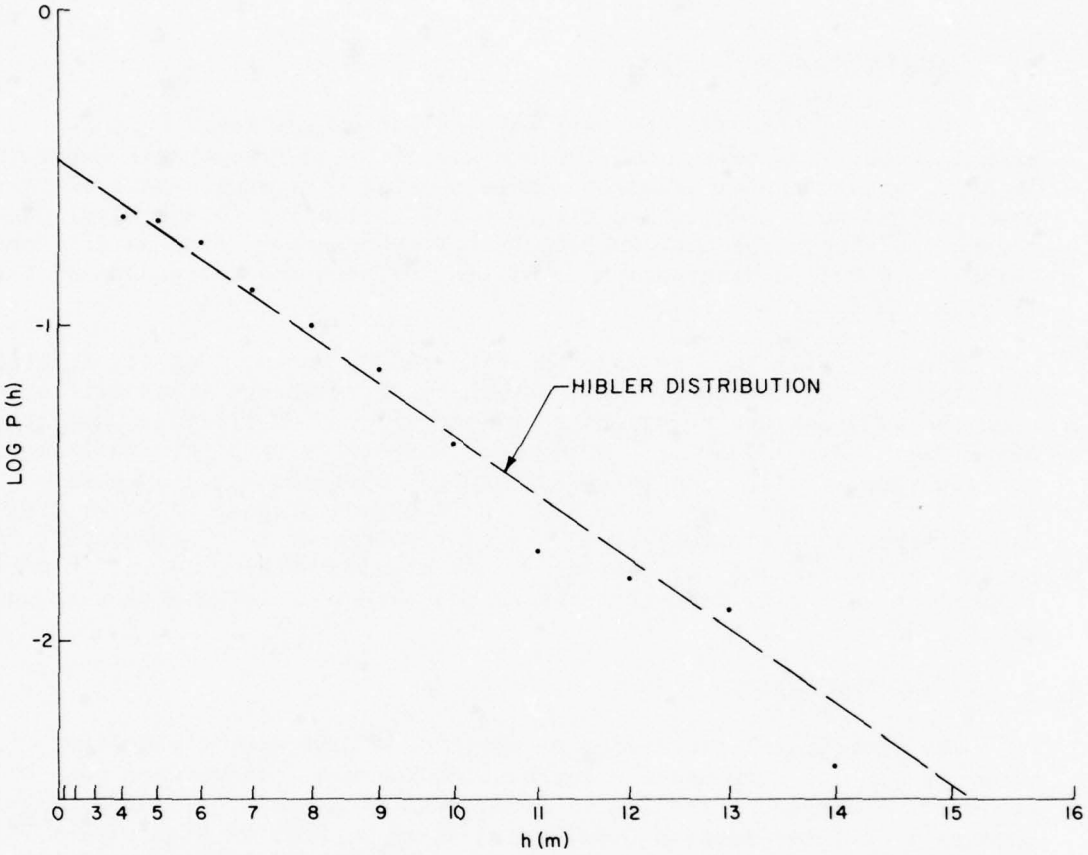

Figure 20. Distribution of keel drafts for all profiling runs near APLIS.

The good fit at low keel drafts verifies that the keel shadowing effect mentioned by Wadhams[8] is smaller for a narrowbeam sonar. Although Wadhams states that simple irregularities on the bottom will contaminate the measurement of reflections from keels with a draft less than 5 m, our value at 4 m appears in line with the Hibler distribution. Again, this may result from a smaller scale of the ice features in the Chukchi Sea compared to those in the Arctic Ocean at 84°N latitude.

VI. AERIAL OBSERVATIONS

The aerial observations were carried out by the Naval Oceanographic Laboratory of the Naval Ocean Research and Development Activity (NORDA), using several types of remote sensing equipment. Most of these observations were made from a Birdseye P-3A belonging to the Naval Oceanographic Office. The microwave equipment was operated from an Air Force C-130. A detailed description of all the flights and the equipment used is given in Reference 11.

Birdseye flights were made on 28 March, 30 March, 1 April, 3 April and 5 April. Passes were usually north-south, with one sweep directly over the camp and others spaced on either side. The altitude was either 305, 1220, 1830 or 3050 m. Photographs were taken at a rate sufficient to give some overlap. An infrared scanner, operated simultaneously, scanned an area about the same width as the photographs. A laser profile was obtained approximately along the center line of the photographs. A passive microwave imaging system was operated from the C-130 on 30 March, 1 April and 3 April; the microwave images covered a large area surrounding APLIS.

A. AERIAL PHOTOGRAPHS

The photographs taken from an altitude of 305 m give excellent views of the ice camp and the surrounding terrain. These were used to construct a mosaic of the 2x3 km study area at a scale of 1:4200. This appears in a later section (see Figure 51 on p. 86). A high elevation view of the area is shown in Figure 21. The several huts are visible and the locations of the tracking hydrophones are indicated. The hydrophones on the refrozen lead used for a landing strip are about 300 m from APLIS.

B. INFRARED IMAGERY

The infrared image of the area surrounding the ice camp is presented in Figure 22. For our convenience we have printed the warm areas dark and the cold areas light. The refrozen lead used as a landing strip shows as gray. The somewhat darker streak passing through the camp is a more recently refrozen break 1 or 2 m wide. A close comparison with the visible-light photograph taken at the same time shows dark areas corresponding to bright reflections on the photograph, indicating that sunlight is an interference if the purpose of the infrared image is to record the temperature of the ice and thereby estimate the proximity of the warmer water beneath.

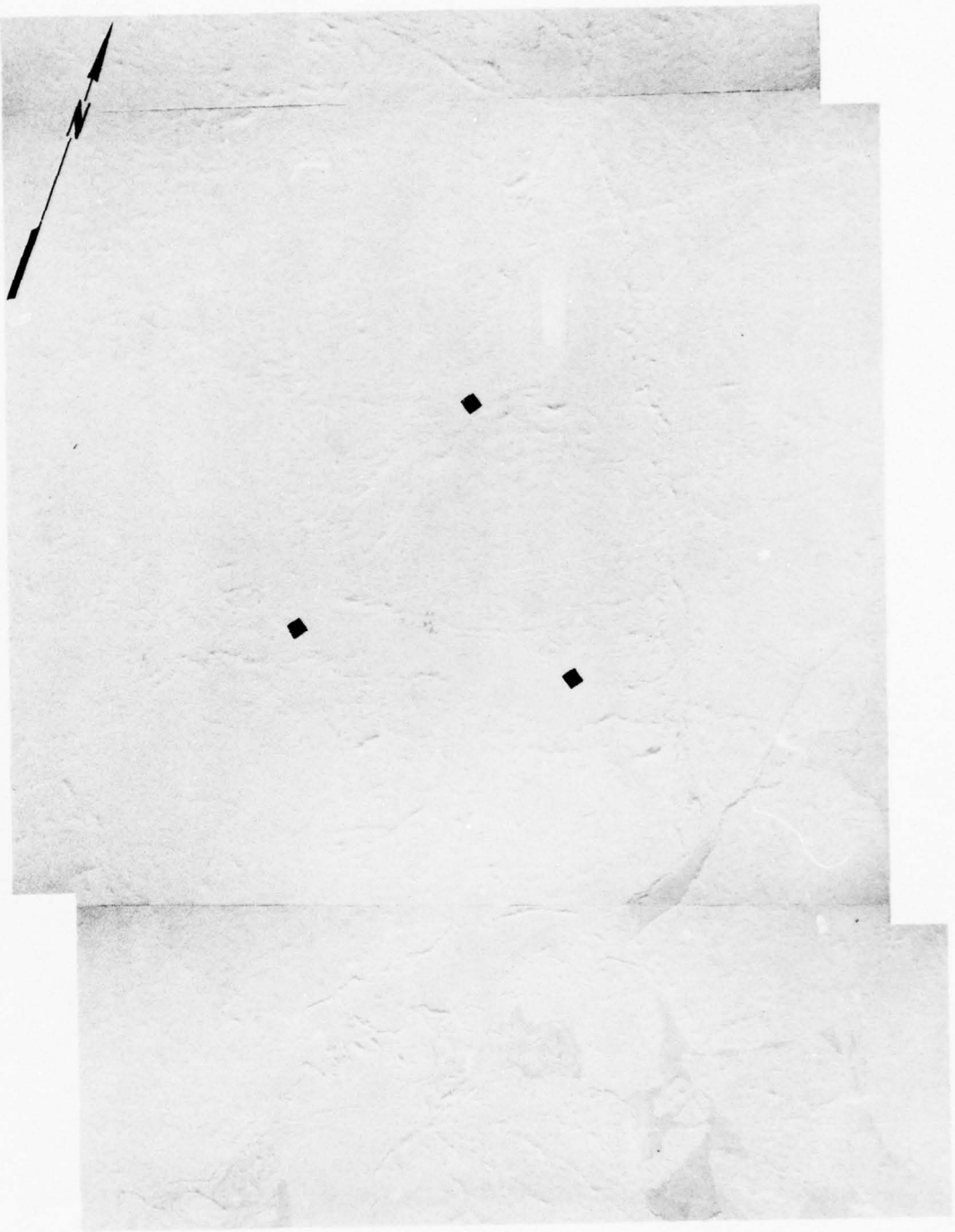

Figure 21. Aerial photograph of the area surrounding APLIS at a scale of 1 cm = 130 m.

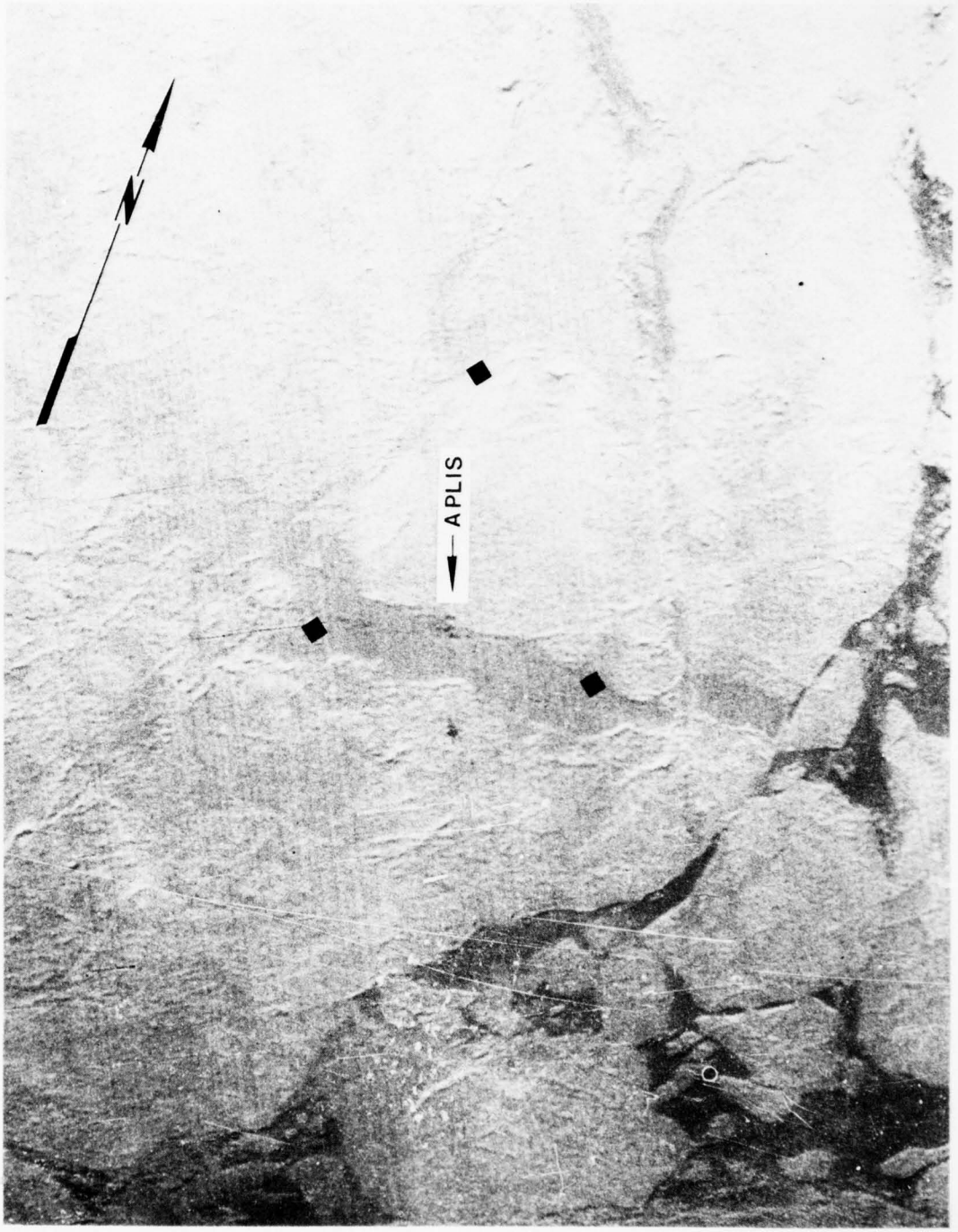

Figure 22. Infrared image of the area shown in Figure 21 (there is some distortion in the north-south direction).

Figure 23. Microwave image of the area surrounding APLIS showing areas and profiles selected for discussion (there is some distortion in the north-south direction).

C. MICROWAVE IMAGERY

Background

One of the goals of the Birdseye remote sensing mission was to test the use of the MICRAD passive microwave imaging system for sea ice investigations. This system has a 1° beam width, which gives it a high resolution. The MICRAD system was operated from an Air Force C-130 at a frequency of 33.6 GHz.[11]

According to NORDA researchers,[12] first-year ice has a high emissivity whether flat or ridged, and multi-year ice has a low emissivity, especially when it has changed in some manner, most likely because of stress. Radiometric temperatures vary from 130°K for open water or thin ice to 240°K for the early stages of ice development, with multi-year ice falling between these extremes.

A mosaic of the microwave imagery for a large area surrounding APLIS was provided by NORDA. We have enlarged the portion within 5 km of the camp and reproduced it in Figure 23 at the same scale as the preceding figures. The warmer radiometric temperatures appear darker, thus the first-year ice appears dark while the older ice appears light. Open water should appear very light, but there may not have been any open water at this time.

As discussed in Reference 12, sudden changes in the radiometric temperature cause the MICRAD system to "overshoot," i.e., the change appears too large for a short portion of the scan. This can be observed in the MICRAD image as dark shadows extending in the direction of the scan. A larger false effect is the brightness along the edge of the film strip. In examining the image, allowances must be made for these characteristics.

In the following paragraphs, we will examine the MICRAD image of the area surrounding APLIS and relate it to the properties of the floe determined from under-ice profiles, photography, infrared imagery, and hole drilling.

Results

The MICRAD image presented in Figure 23 does not reproduce all the gray shades that we were able to observe on the original. Therefore, in the discussion that follows, we may describe characteristics of the image that cannot be observed in the figure. The numbers in parentheses refer to the numbered features in Figure 23. Figure 24 shows typical under-ice profiles through each area and a summary of the observed surface appearance and MICRAD image.

The large refrozen lead (1) used as a landing strip for APLIS is a very high emitter (dark). It is uniformly 2 m thick and appears to have frozen without disturbance.

The long newly ridged area (2) along the northeast side of the floe is also a high emitter (dark). Although there is some unbroken new ice along this break, the dark area is much wider and must include the ridging along the edge; this ridging was severe, with keels as deep as 12 m (see profiles 2a and 2b in Figure 24, and Figure 39 on p. 64). The lead must have opened, frozen over to 2 m thick, and then rafted to produce the deep keels. Despite all this stress and deformation, the emissivity remains high--the same as new 2-m thick ice. In this case the microwave emission depends more on the age of the ice, rather than on the stress, deformation, or ridge thickness.

A large area of high emissivity occurs in the northeast part of the area (3). The emission is highly variable and shows some large-scale patterns that do not appear on the aerial photograph in Figure 21. The under-ice profiles (Figure 24, profiles 3a and 3b) indicate the area consists of ice 2 to 3 m thick with considerable ridging to depths of 7 or 8 m.

The floe across the lead from APLIS has medium emissivity (dark gray) in the central and nothern portions (4). The aerial photograph shows some high ridges in this area, and the keels must have been very deep because the submarine detoured around part of this area. The runs that were made (see Figure 24, profile 4) showed a very irregular bottom with keels ranging from 2 to 10 m. Such variation in thickness seems to appear as a variation in the MICRAD image. We have attempted to match MICRAD variations with thickness variations, but there is too much distortion in the image for a close cross correlation. The rough surface and irregular bottom indicate that this ice is not as old as some of the other floes in the area.

An area of high emission also occurs along the central western edge of the occupied floe (5). This area has ridges young enough to be plainly visible in the photograph and many deep irregular keels (see Figure 24, profile 5). Although this ice appears to have ridged the previous year and is therefore at least a year old, it has a high emissivity. (This feature is discussed further in Section VII-C.)

The eastern area (6) shows very low emission (very light). The surface appears in the photograph to be eroded and fairly smooth. The under-ice profiles (Figure 24, profile 6) show the ice to be 4-5 m thick with very little ridging.

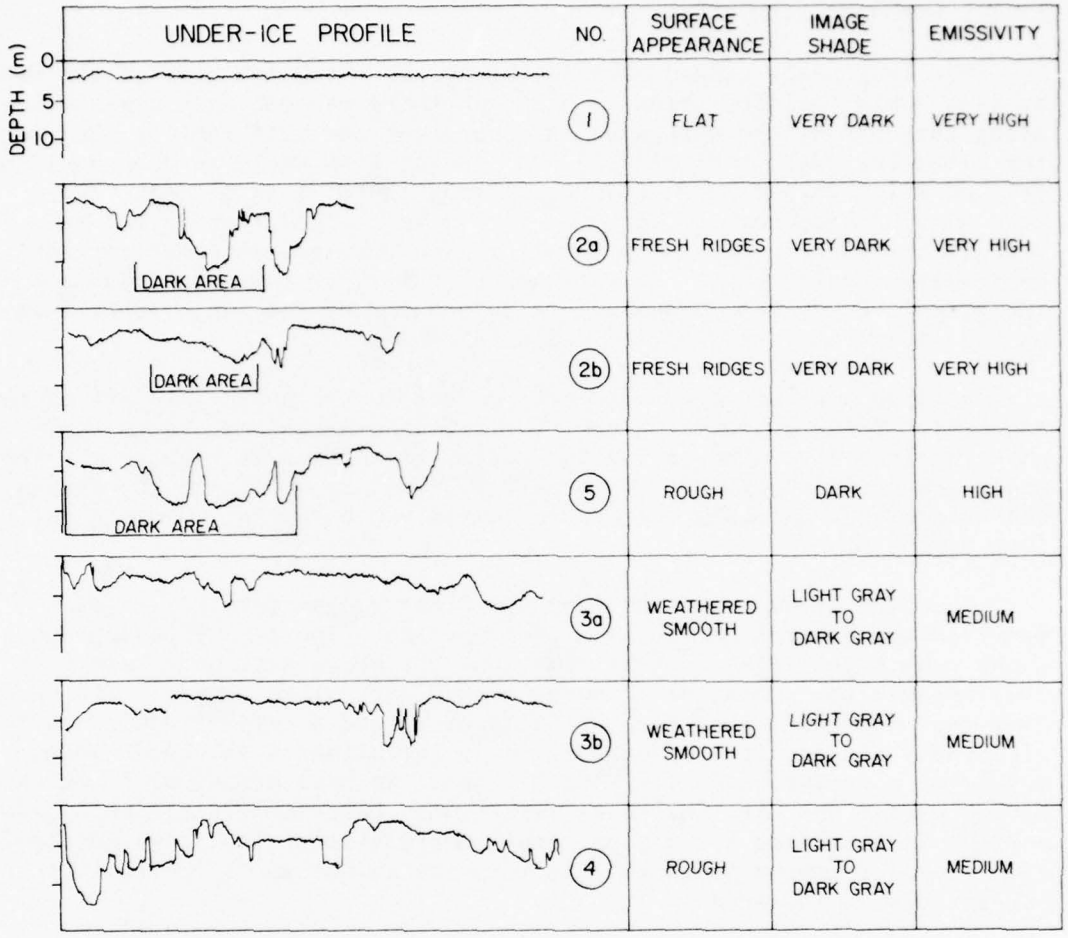

Figure 24. Under-ice profiles across the areas outlined in Figure 23. The left ends of the profiles start at the circular ends of the lines in Figure 23. The emissivity as given merely corresponds to the image shade.

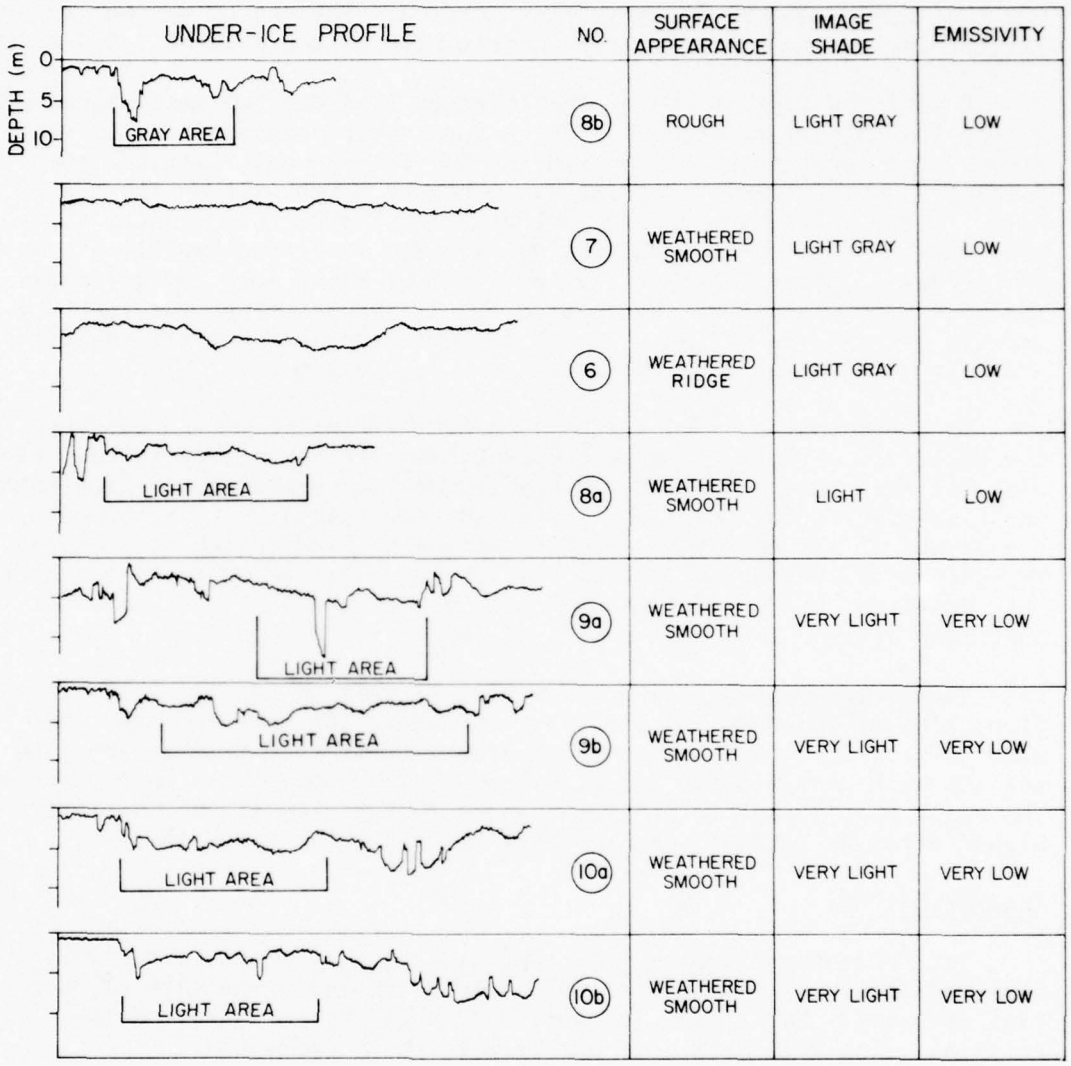

NO.	SURFACE APPEARANCE	IMAGE SHADE	EMISSIVITY
8b	ROUGH	LIGHT GRAY	LOW
7	WEATHERED SMOOTH	LIGHT GRAY	LOW
6	WEATHERED RIDGE	LIGHT GRAY	LOW
8a	WEATHERED SMOOTH	LIGHT	LOW
9a	WEATHERED SMOOTH	VERY LIGHT	VERY LOW
9b	WEATHERED SMOOTH	VERY LIGHT	VERY LOW
10a	WEATHERED SMOOTH	VERY LIGHT	VERY LOW
10b	WEATHERED SMOOTH	VERY LIGHT	VERY LOW

Figure 24 continued.

An area of very light gray (7) extends to the north of APLIS. This large area appears old in the photograph. There are marks of much ridging that has eroded to a nearly flat surface. The bottom of the ice (Figure 24, profile 7) is fairly uniform with a thickness of 2.5-4 m.

Beyond the eastern end of the refrozen lead are two small areas with a very low emissivity (8,9) that have apparently broken off multi-year floes. They bear marks of old ridging but erosion has flattened the surface. One of these floes (8) has a higher emissivity on the north half. Close inspection of the photograph in Figure 25 indicates that this end has more pronounced ridging, and the under-ice profile of this end (Figure 24, profile 8b versus profile 8a) shows more irregularity. The under-ice profile of the other floe (9) shows thicker ice (see Figure 24, profiles 9a and 9b). The bottom is irregular but the variations are more rounded, as if older than those in profile 8b.

The southeastern edge of the floe south of APLIS (10) shows very low emissivity. This could be caused by the overshoot (see Section VI-C) when the scan passed from the thinly frozen lead south of the floe onto the floe itself, but the light area seems too extensive. An estimate of the extent of the overshoot can be obtained by examination of area (8). The overshoot does not extend to the northern half of area (8) and therefore would not extend over about one-third of area (10). We conclude that much of area (10) must represent low emissivity.

The surface appearance of area (10) is that of an old, well-eroded floe, similar to areas (6) and (7). The under-ice profiles show the area to be 3-5 m thick with some scattered keels to 7 m. Profiles 10a and 10b both show rounded keels, except for one sharp keel on profile 10b. The right end of profile 10b shows sharp features as it extends into the higher emission (darker) area of the floe, which is 6-8 m thick.

Interpretation

The foregoing examples show that new ice, 1-2 m thick, has very high emissivity. In older ice, the heavily ridged areas also produce high emission. Multi-year ice with a rounded bottom shape has low emission. Ice thickness does not seem to be an influence.

These observations lead to the postulation that the age of the ice alone governs the microwave emission. Ridges are formed when the pack is under pressure. Floes pressing together often raft the ice that has formed between the floes. These ridges are of younger ice than the existing floes. When the resulting conglomerate passes through a season or two, the ridged areas will always be younger and will have a higher emissivity. This would explain why the deep keels along the pressure ridge (2) have a higher emissivity than the adjacent floes, and why the

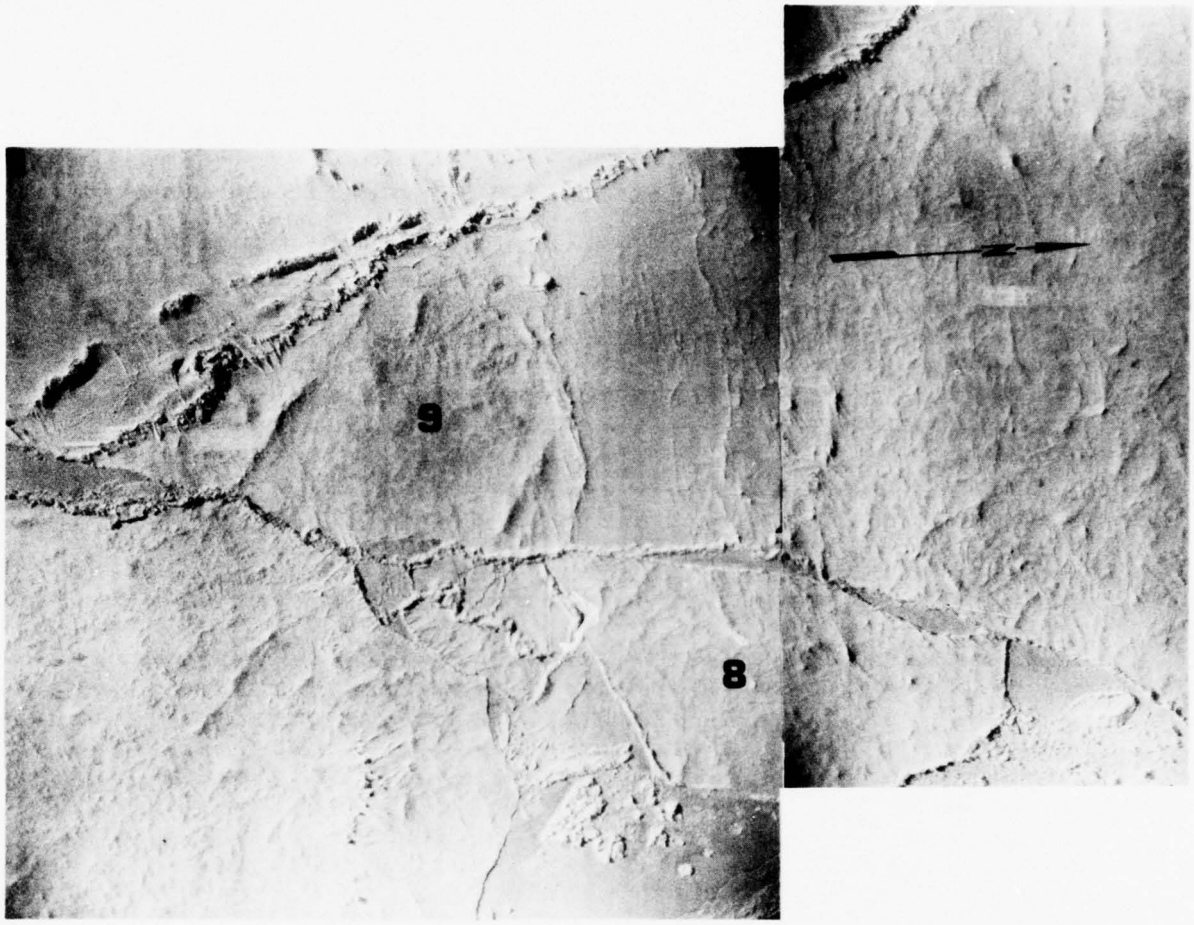

Figure 25. Aerial photograph of two floes of multi-year ice.

ridged areas in multi-year ice (4,5) have a higher emissivity than the nearby undisturbed floes. The floes that have eroded during several seasons have very low emissions.

According to this postulate, if a floe cracks under pressure and a ridge is formed, no increase in emissivity would be expected at the break, since all the ice would be the same age. However, if water seeps into the broken ice and freezes, there could be an appreciable amount of new ice, and the emissivity at the break would be high. We have no examples to indicate whether the high emissivity observed between floes corresponds with the broken ice or the newly formed ice between the blocks.

Our study of ice floes in the vicinity of APLIS indicates that the age of the ice alone determines the radiometric temperature. Several possible reasons have been given for the age effect,[12] such as weathering, brine drainage, and increased porosity. The variability in the emission from multi-year floes can be attributed to the variability in the age of the components of an old floe. Ketchum and Lohanick[12] postulate, and show supporting examples, that stress and deformation decrease emissivity. This additional effect is not evident in our study. In several cases, an area of ridging that must have been heavily stressed seems to emit more.

D. LASER PROFILING

Digital laser data on seven-channel magnetic tape were provided by NORDA. In addition, some statistical analyses of ice heights were provided.

Figure 26 is an example of a laser profile that passed very close to the ice camp. Aircraft motion has not been removed, thus the gradual rise from left to right may not be real. The two peaks at approximately 50 m may be two of the huts or some of the boxes piled around the camp.

Other laser profiles in the area have been included in Section VII where they are compared with the aerial photographs and the corresponding under-ice profiles. However, there were not many areas where the laser profile coincided with an under-ice profile (i.e., where the two tracks were parallel and within 50 m). It should be kept in mind that the location of the laser track is not accurately known because the laser instrument was gyro-stabilized to the vertical, while the camera was mounted rigidly in the plane. As a result, the laser track was not always along the center line of the photographs.

E. ICE ELEVATION STATISTICS

Statistics of the ice elevation were obtained by NORDA from the laser profile data. The number of points analyzed and the statistical results for each pass are shown in Table III. Weighted averages are shown at the bottom of the table.

The overall mean elevation of 0.30 m computed from the laser data was probably referenced to the surface of the 1-m thick refrozen leads. Adding the freeboard of the refrozen leads results in an average elevation of 0.44 m above sea level. When this value is compared with the average ice draft of 3.31 m obtained from the under-ice profiles (see Section V-D), we obtain a ratio of ice draft to ice elevation of 7.5, which is a reasonable value for free floating ice of density 0.91. In calculating this ratio, the effects of the snow on top of the ice and the voids within the ice have been ignored (the under-ice profiles with many very steep slopes indicate that voids are prevalent). Also the

laser profile runs extended farther north than the under-ice profiles, covering a region of thin ice north of the floe and thus reducing the average ice elevation.

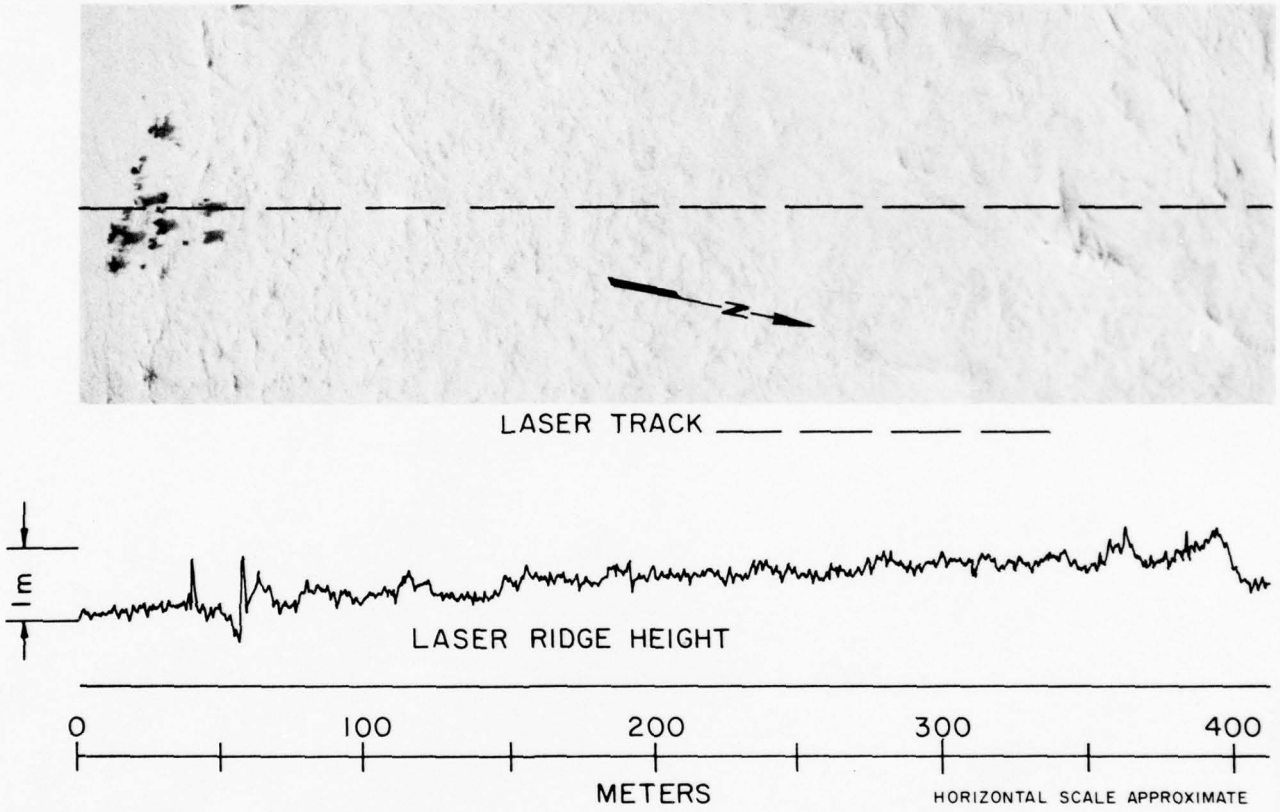

Figure 26. A laser profile through Ice Camp APLIS.

F. RIDGE STATISTICS

NORDA processed most of the runs, correcting for aircraft motion and systematic errors. NORDA tabulated the number of sails and analyzed them statistically, using every third data point. The results for each pass are given in Table IV. A peak is defined as a sail if the adjacent valleys are less than one-half the height (called the Rayleigh criterion). The nine passes across the area show 4.6 sails per kilometer, with an average sail height of 1.55 m. When this average height is compared with the average keel depth determined in Section V-E, we obtain a keel draft to sail height ratio of 4.1. This is lower than the ratio of 7.5 for ice draft to ice elevation, and corresponds to the linear density of keels being over twice the density of sails.

Table III. Ice elevation statistics computed by NORDA from the laser profiles.

Line	Direction	No. of Points	Mean Height (m)	rms (m)	Standard Deviation (m)	Skewness	Kurtosis
Easternmost Line	N	3,652	0.25	0.36	0.26	2.49	13.21
Center Line	S	2,988	0.26	0.36	0.25	2.25	11.35
East of Center Line	N	3,984	0.34	0.45	0.29	2.45	13.57
Easternmost Line	S			NOT USABLE			
West of Center Line	N	3,652	0.32	0.44	0.30	2.84	17.67
Westernmost Line	N	3,984	0.30	0.42	0.29	3.12	17.26
East of Center Line	S	3,652	0.34	0.47	0.33	3.28	20.49
West of Center Line	S	2,656	0.26	0.35	0.22	2.63	15.00
Westernmost Line	S	3,984	0.31	0.41	0.27	2.48	13.31
Total or Average		28,552	0.30	0.41	0.28	2.69	15.23

Table IV. Laser Profile Ridge Statistics

Date 28 March 1977

Altitude 305 m
Data Point Spacing 1.5 m
Aircraft Speed 200 km/hr

Location	Flight Direction	Run Length (km)	Sail Frequency (/km)	Number of Sails Height Interval (m) 1-1.5	1.5-2	2-2.5	2.5-3	3-3.5	Total
Easternmost Line	N	5.66	3.71	13	3	4	1		21
Center Line	S	4.63	3.02	7	5	2			14
East of Center Line	N	6.18	5.83	23	9	3	1		36
Easternmost Line	S	7.72	4.79	18	10	3	1	2	34
West of Center Line	N	5.66	4.59	18	4	3	0	1	26
Westernmost Line	N	6.18	3.72	14	5	2	2		23
East of Center Line	S	5.66	4.42	17	4	3	0	1	25
West of Center Line	S	4.12	1.70	3	3	1			7
Westernmost Line	S	6.18	3.88	17	5	2			24
Total		45.81		130	48	23	5	4	210
		Sails per kilometer		2.84	1.05	0.50	0.11	0.09	4.58
		Percent per interval		61.9	22.9	11.0	2.4	1.9	

Average sail height, $\bar{h}$ = 1.55 m

Root mean square = 1.61 m

Standard deviation σ = 0.46 m

Variance, $V = \frac{\sigma}{\bar{h}} = 0.29$

Hibler Distribution

Also of interest is the distribution of the sail heights. The distribution of sail heights greater than 1 m is shown in Figure 27 for the nine passes listed in Table III. As mentioned in Section V, Hibler, Weeks and Mock[7] have derived a theoretical distribution function for pressure ridges from fundamental assumptions about the randomness of the ridges. They assume that for a given net deformation over a region, all possible collections of ridges that yield this deformation are equally probable. For a given minimum sail height h_o, the predicted distribution of sail heights is given by

$$P(h)\ dh = \frac{2\sqrt{\frac{\lambda}{\pi}}\ e^{-\lambda h^2}}{\text{erfc}\ \sqrt{\lambda}\ h_o}\ dh\ ,$$

where

$P(h)\ dh$ = probability that the sail height will be between h and h+dh

erfc = 1 - error function

λ = a parameter determined from the average sail height.

For an average sail height of 1.554, they give a value for λ of 0.45, and the probability function becomes

$$P(h) = 2.19\ e^{-0.45h^2}\ .$$

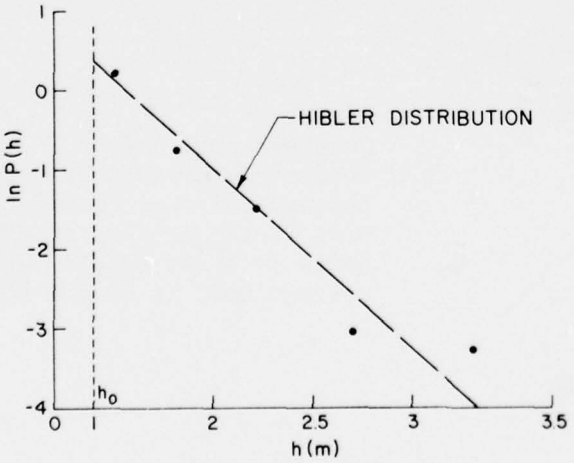

Figure 27. Observed sail height distribution compared to Hibler's theoretical distribution. P(h) is the portion of the sails in a 1-m height interval centered at height h.

This relationship has been plotted for comparison with the measured data in Figure 27; it shows good agreement with the data.

Wadhams' Distribution

A simpler relationship has been found by Wadhams[8] to fit data taken along a 1000-km track in the Arctic Ocean north of Greenland. This relationship is

$$n(h)\, dh = B\, e^{-bh}\, dh\ ,$$

where n(h) = number of sails with height h per kilometer of track. The constants b and B are obtained from the average sail height $\bar{h}$' the minimum height considered h_o, and the number of sails per kilometer of track μ:

$$b = (\bar{h}-h_o)^{-1}$$

$$B = \mu\, b\, e^{bh_o}\ .$$

For the 1976 APLIS data listed in Table IV, b = 1.82 and B = 51.49, to yield

$$n(h) = 51.49\, e^{-1.82h}\ .$$

This line is plotted for comparison with the data in Figure 28. The data are about as well represented by this distribution as by the Hibler distribution.

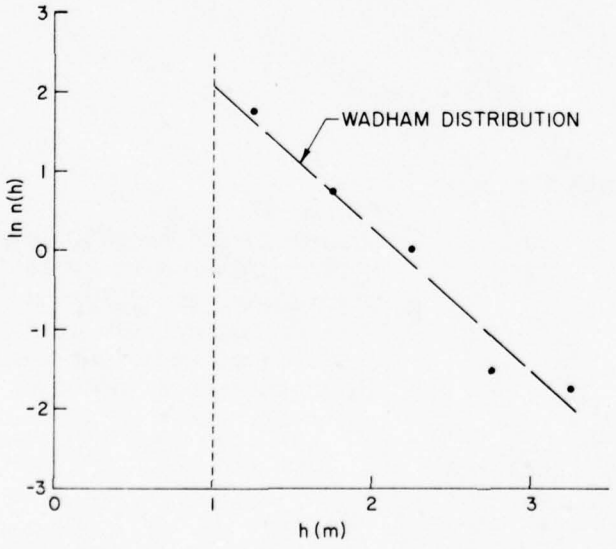

Figure 28.
Observed sail height distribution compared to Wadhams' theoretical distribution. n(h) is the portion of the sails in a 1-m height interval centered at height h.

G. COMPARISON WITH OTHER INVESTIGATIONS

A comparison between our measurements in the Chukchi Sea, Hibler's work in the Central Arctic, and Wadhams' study north of Greenland is given in Table V.

Note that the value of Wadhams' b for the APL data agrees well with the values of b obtained for the 1000-km track north of Greenland[8] but that our keel draft distribution drops off much faster (the value for λ is much larger). It is odd that the two areas show a good agreement in the sail height distribution and a large difference in the keel draft distribution. Two explanations are offered for this discrepancy:

(1) Our narrower sonar beam would detect more of the smaller keels.

(2) The measurements analyzed by Wadhams were made from 18 to 21 October when some of the smaller keels may have been eroded during the summer, while ours were made in April.

Table V. Comparison of our measurements, Hibler's work, and Wadhams' study.

	Investigator		
	APL Chukchi Sea	Hibler Central Arctic	Wadhams North of Greenland
Length of Track (km)			
Sails	46	--	1000
Keels	143	1400[a]	1000
No. of Sails	210	--	
No. of Keels	1675	5702	
Sail Density (km^{-1})	4.6		19.8
Keel Density (km^{-1})	11.7	4.0[a]	3.7
Sail Height Distribution			
Wadhams b	1.82		1.73
Hibler λ	0.45		
Keel Draft Distribution			
Hibler λ	0.021	0.012	0.005

[a]Estimated from map in Reference 7, Figure 4.

Measurements with an unmanned vehicle by Francois[13] have shown that the underside of the ice is an assortment of jumbled blocks with a size corresponding to the ice thickness at the time of the ridging, and that these blocks exhibit very little erosion. These characteristics are easily overlooked when broad-beam sonars are used to profile the ice. Many models assume that ice keels reconsolidate and are rounded off. We contend that this does not occur, except in areas where warm water enters, and that sharp, irregular blocks persist. (See Section V.)

VII. ICE PACK FEATURES

Occupancy of the ice camp for three weeks provided an opportunity for the personnel to become familiar with the floe. The holes drilled through the ice established its thickness at several locations. Laying out cables to remote transducers required considerable walking and snow-mobiling over the surface and allowed observation of surface features.

Combining this information with the under-ice profiles obtained by the submarine, laser profiles of the upper surface, aerial photographs, infrared imagery, and microwave imagery, we are able to describe some of the features of the ice pack in great detail. In this section, we have selected several features and present all the available information regarding them. They are labelled in Figure 29, a high-altitude aerial view, and are discussed individually.

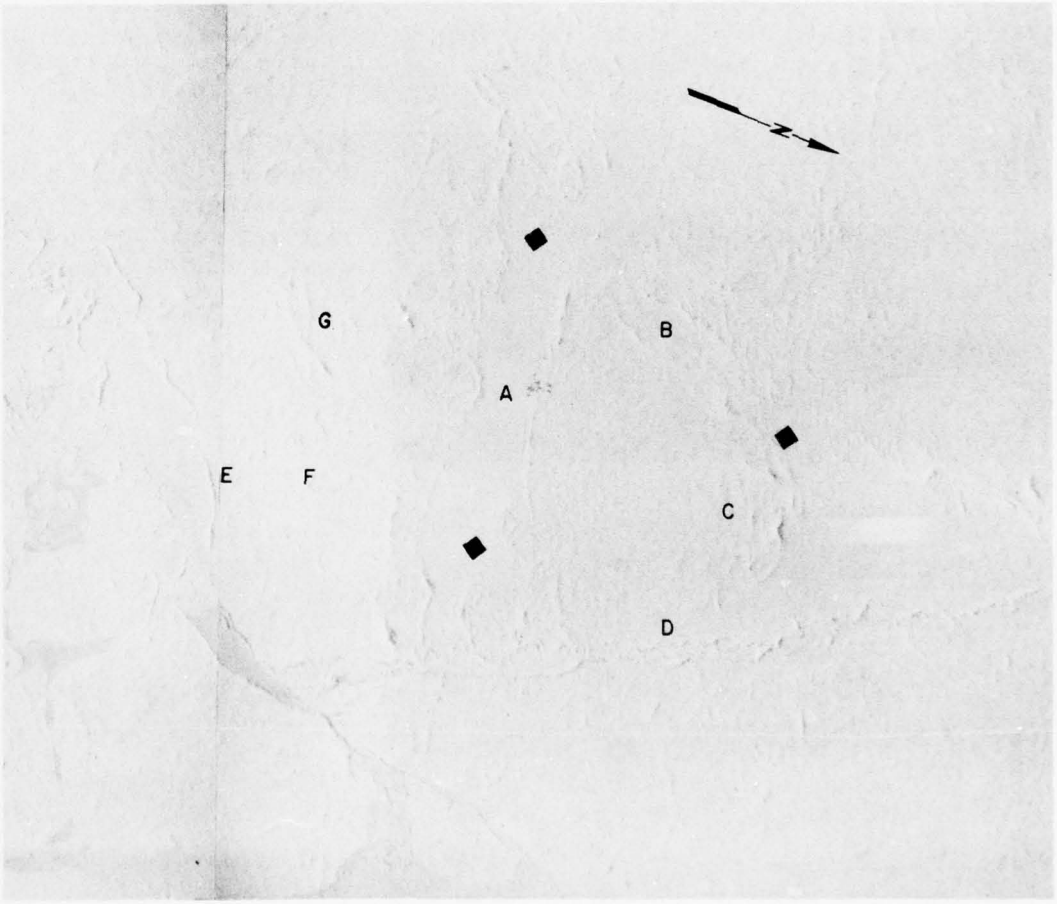

Figure 29. Index to the ice features discussed.

A. LARGE REFROZEN LEAD

Feature A is the large refrozen lead that was used as a landing strip. Ice Camp APLIS was established along the northern edge at about the middle.

As indicated in the photographs, the lead was flat and smooth. The southern edge ended very abruptly in some high ridges, which are shown in Figures 30 and 31. The northern edge was more subtle, especially in the eastern portion where an older break delineated a large separation which occurred much earlier than the break that created the lead. A more recent crack, 2-4 m wide, which occurred after the lead opened and thinly refroze, extended through the camp to both ends of the lead. A hole drilled through this refrozen crack showed the ice to be 1.2 m thick.

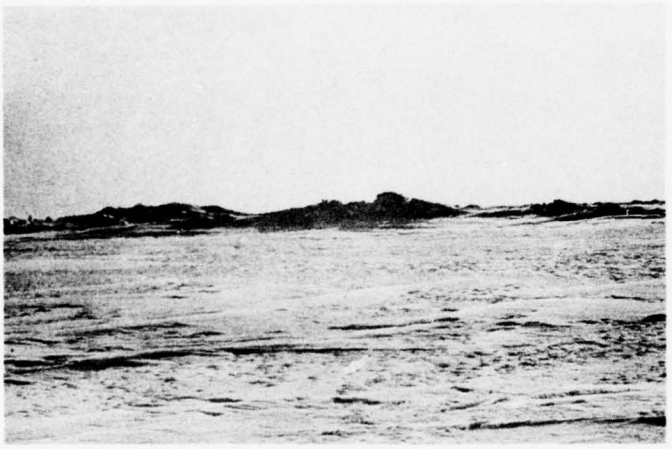

Figure 30.
A view of the ridge along the southern edge of the refrozen lead used for a landing strip.

Figure 31.
Another view of the ridge shown in Figure 30.

The lead was crossed many times during the under-ice profiling, and several laser profiles of the top surface were taken during the Birdseye flights. Nearly coincident topside and bottomside profiles near the western end of the lead are shown in Figure 32. The laser profile shows a low-level, flat portion corresponding to the lead. (The noise level of about 0.2 m shown in the figure seems to exist throughout the laser recordings.) The sails and keels agree quite well in location and magnitude (note that the ratio of the top and bottom scales plotted in the figure is 1:5). The most recent crack appears in the under-ice profile as a small portion that is less thick than the rest of the lead (1.0 m compared to 1.7 m).

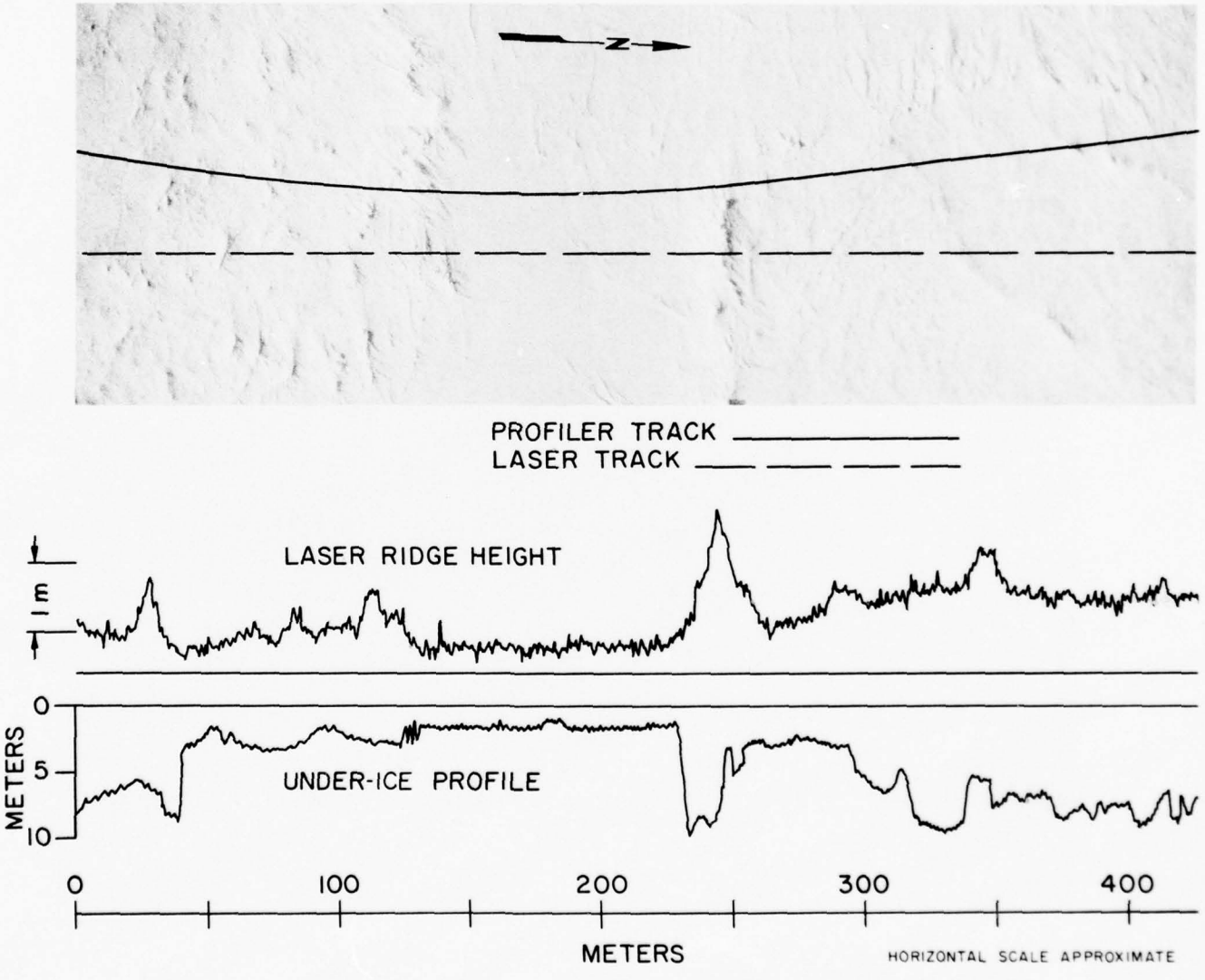

Figure 32. Comparison of laser and under-ice profiles across western portion of refrozen lead (feature A).

The southern edge of the western portion of the lead is shown in Figure 33a. Although the ridge at the edge is quite prominent in the photograph, the under-ice profiles (Figure 33b) show keels only 4-5 m deep.

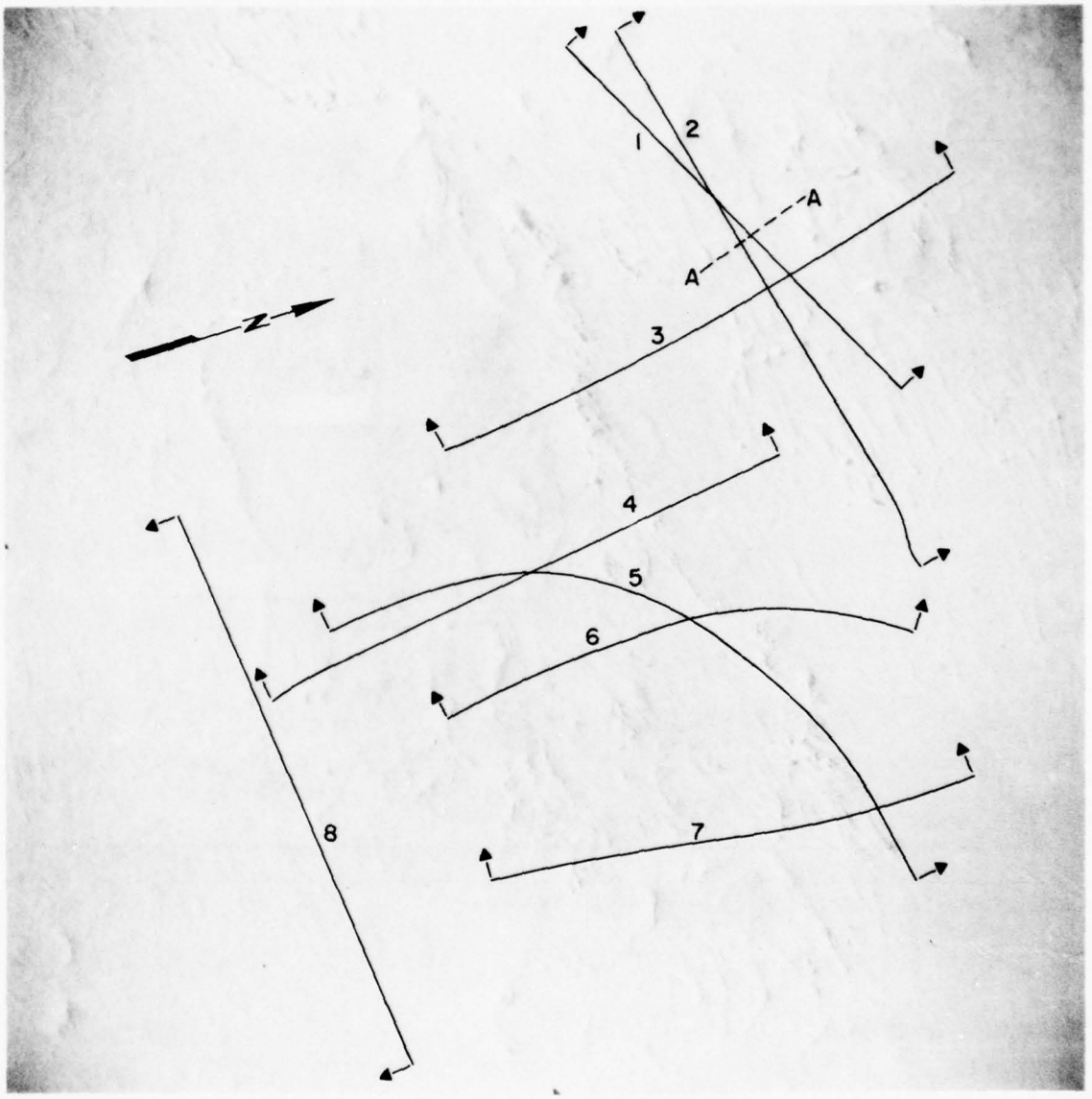

Figure 33a. Under-ice profile lines across the western end of the refrozen lead (feature A).

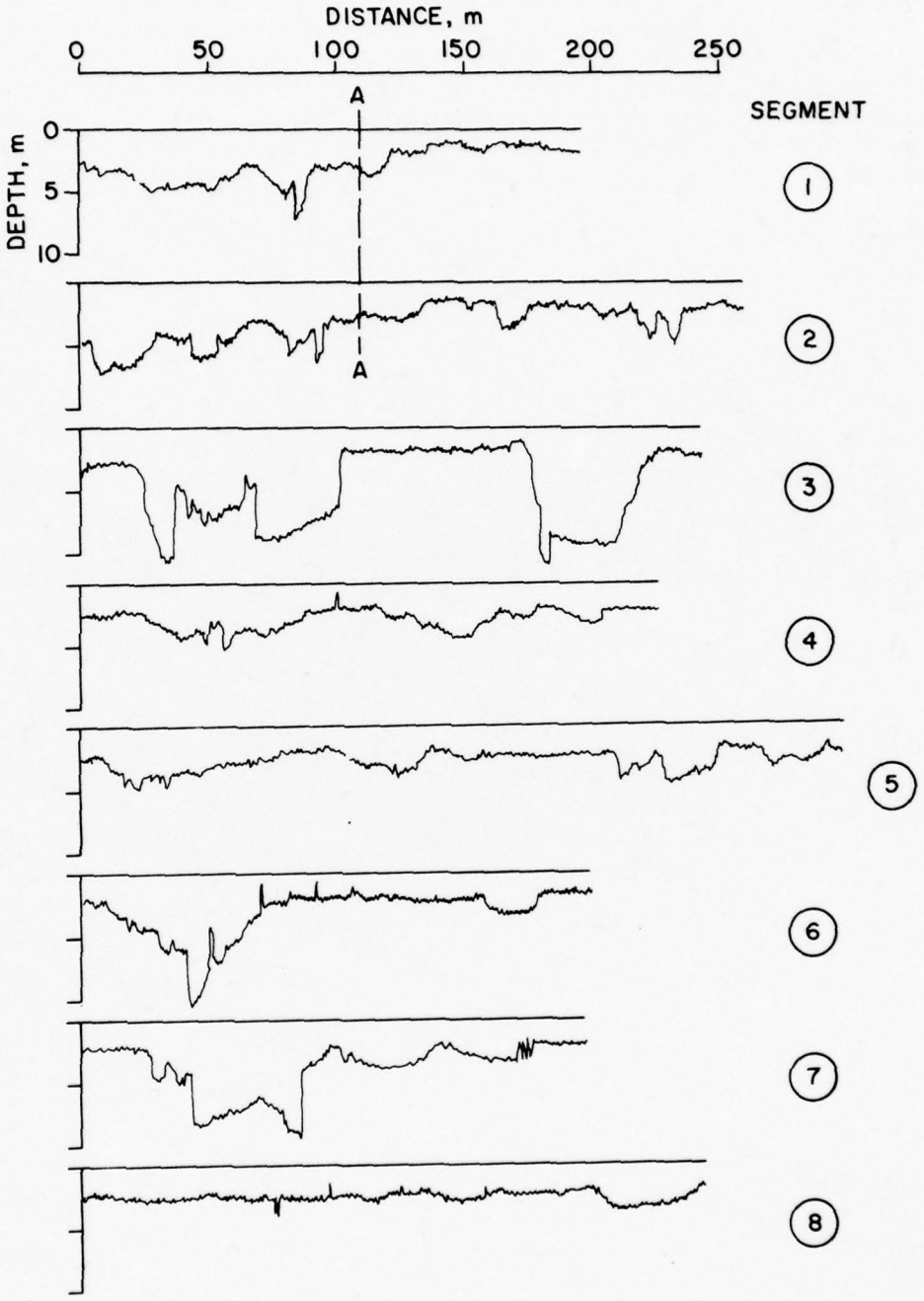

Figure 33b. Under-ice profiles across the western end of the refrozen lead (feature A).

Some of the character of the eastern end of the lead can be seen in the photograph in Figure 34a. A series of under-ice profiles covering the eastern half of the lead is presented in Figure 34b. In profiles 1 to 7, the lead is observed as a flat, thin portion bounded by severe ridging at the edges. The severity of the ridging along the edge appears to agree with the roughness seen in the photograph. The recently refrozen crack appears as the thinnest portion of segments 2, 3, 4 and 5.

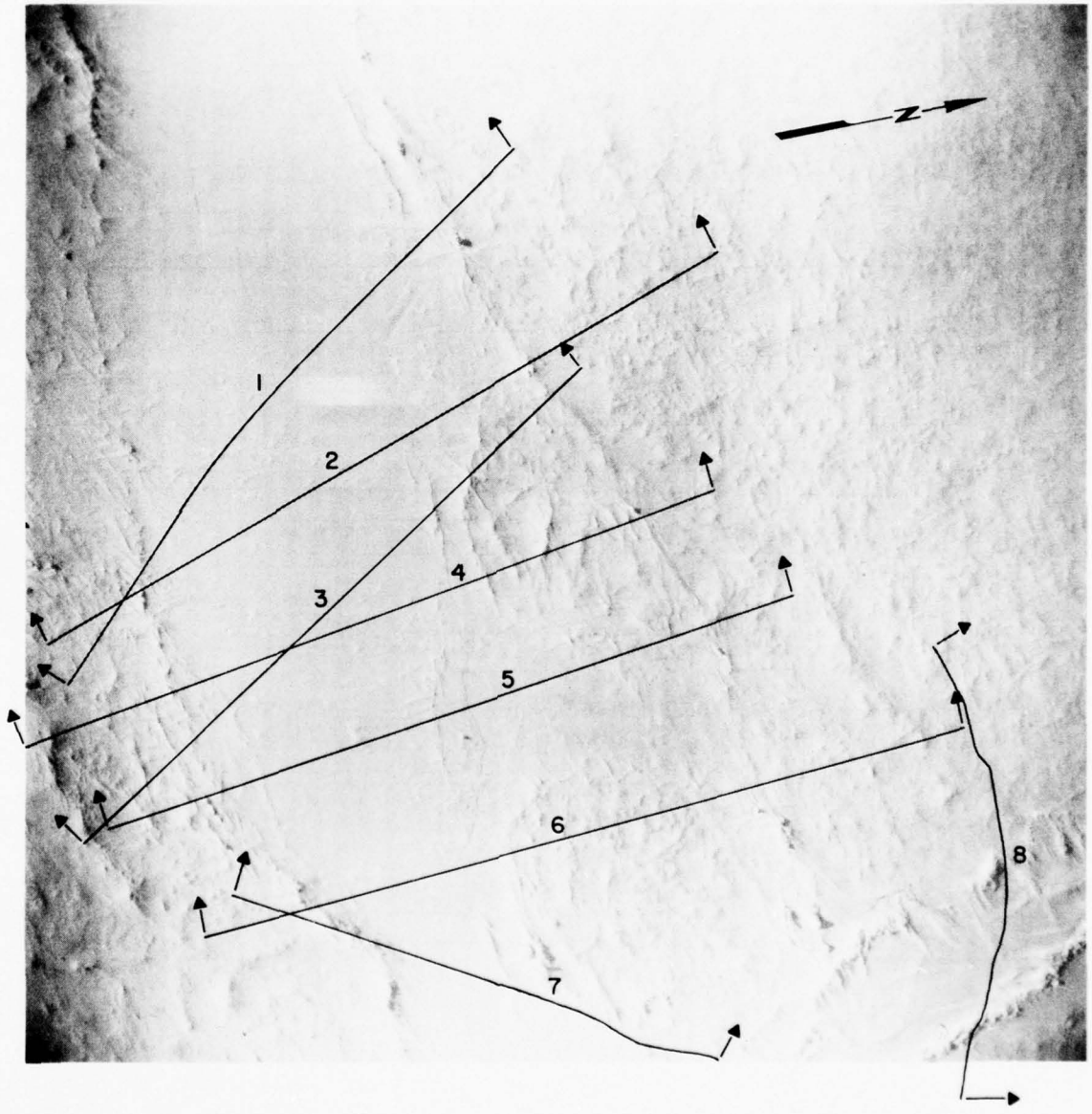

Figure 34a. Under-ice profile lines across the eastern end of the refrozen lead (feature A).

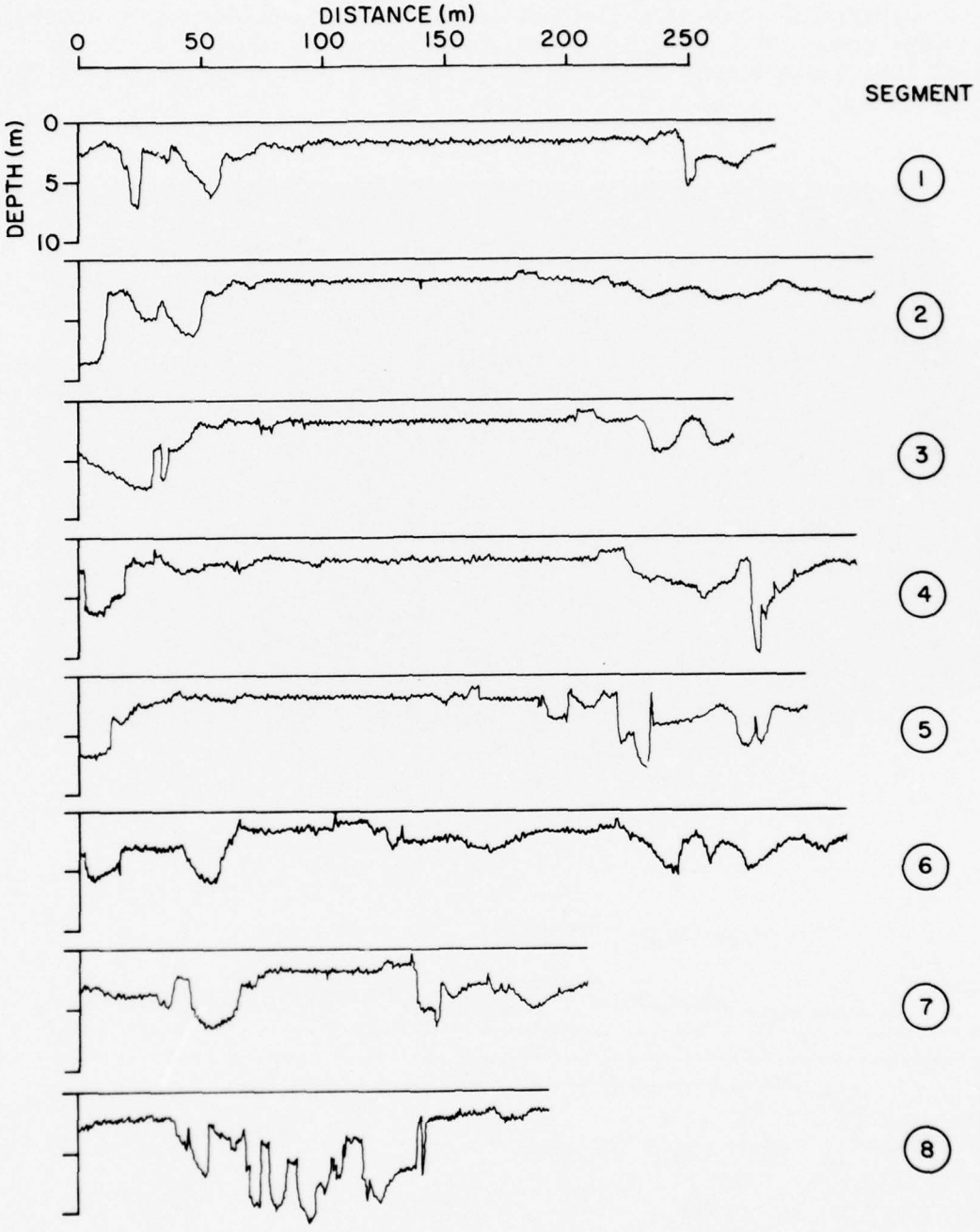

Figure 34b. Under-ice profiles across the eastern end of the refrozen lead (feature A).

Segment 5 is shown again in Figure 35 with a nearby laser profile for comparison. The agreement between topside and bottomside features is very good. Note, however, that the area on the south side of the lead that appears very rough in the photograph does not have much ridging beneath it.

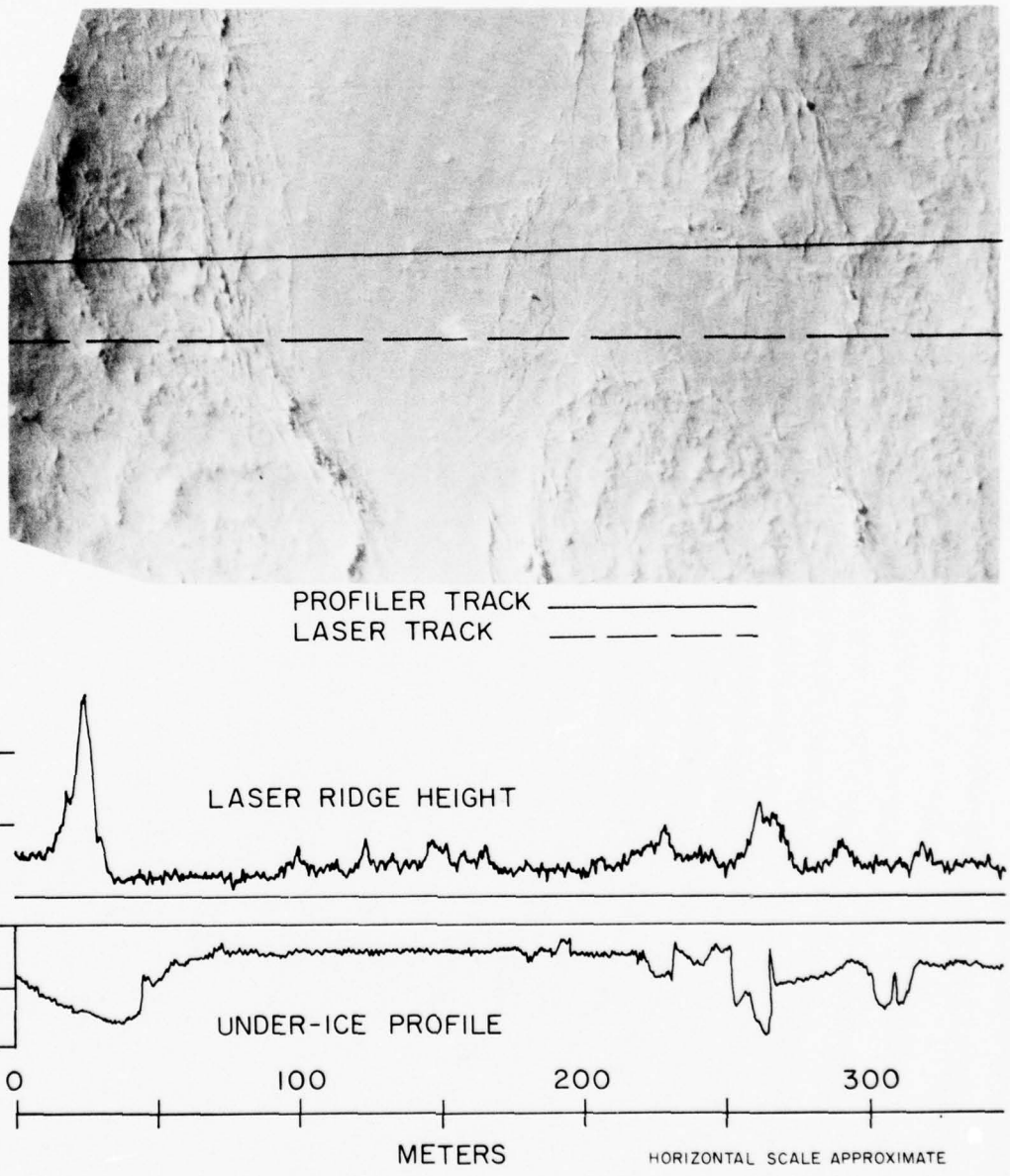

Figure 35. Comparison of laser and under-ice profile for segment 5 in Figure 34a.

On the infrared image (Figure 22, previous section), feature A appears a uniform dark gray. The slightly thinner, refrozen crack appears noticeably darker, toward the shade of open water. On the MICRAD image (Figure 23), this area appears very dark, which is characteristic of first-year ice.

B. MULTI-YEAR FLOE

Feature B appears to be a thick, old floe that was frozen into a mass of younger, but multi-year, floes. In the aerial photographs, it appears to have a uniform, flat surface; its cold appearance on the infrared image indicates a thick floe. About 100x300 m in size, it was located 300 m northwest of APLIS (see Figure 29).

Several under-ice profiling tracks passed under this floe. Their locations are shown in Figure 36a, and the corresponding under-ice profiles in Figure 36b. Segment 1 is actually south of this feature, but has been included because it shows a very sharp, deep ridge along the edge of the lead. Segment 2 crosses the floe itself, and shows a large mass extending 10 m deep. Sections taken successively farther north show this mass continuing along the west side of the floe. Even though the floe appears to be several years old, the bottom is still very rugged with many irregular blocks. In the photograph the thick middle of the floe appears only slightly different from the adjacent floe which is only 3 m thick. It has some smooth, icy surfaces that may indicate refrozen melt ponds.

Segment 7 includes a section of thick ice that appears to be similar to feature B but separate from it. This area again shows large patches of glare ice.

Segment 8 passes through the old floe longitudinally, beginning, on the left, at the large ridge along the edge of the lead.

This 10-m thick floe shows on the infrared image (Figure 22) as a lighter gray than the surroundings; in fact, this gray is the lightest shade observed. On the MICRAD image (Figure 23), this area is light at the south end because of the overshoot at the sudden change from lead to thick ice. Near the north end, past the overshoot region, it remains light gray as would be expected for multi-year ice.

A laser profile through part of the floe can be seen in Figure 32. The ridge at the edge of the lead appears at 250 m. The record beyond the edge shows the ice elevation as about 1 m above the lead; however, variations in the plane's altitude make the absolute elevation uncertain.

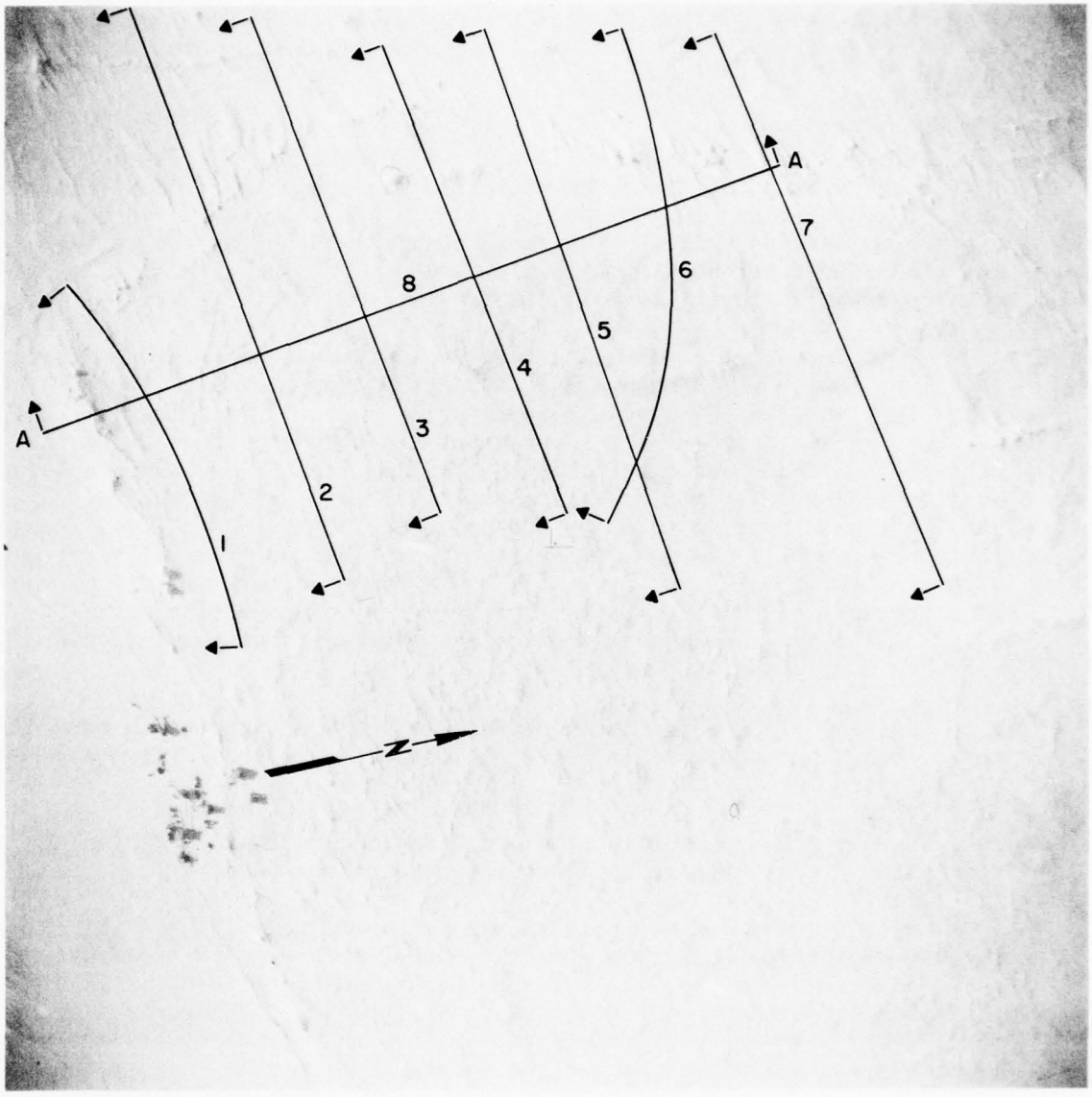

Figure 36a. Under-ice profile lines across a multi-year floe (feature B).

C. LARGE CENTRAL RIDGE

Feature C is the large, rough-looking area north of APLIS. The tracking transducer placed in this area had to be lowered because of the deep keels.

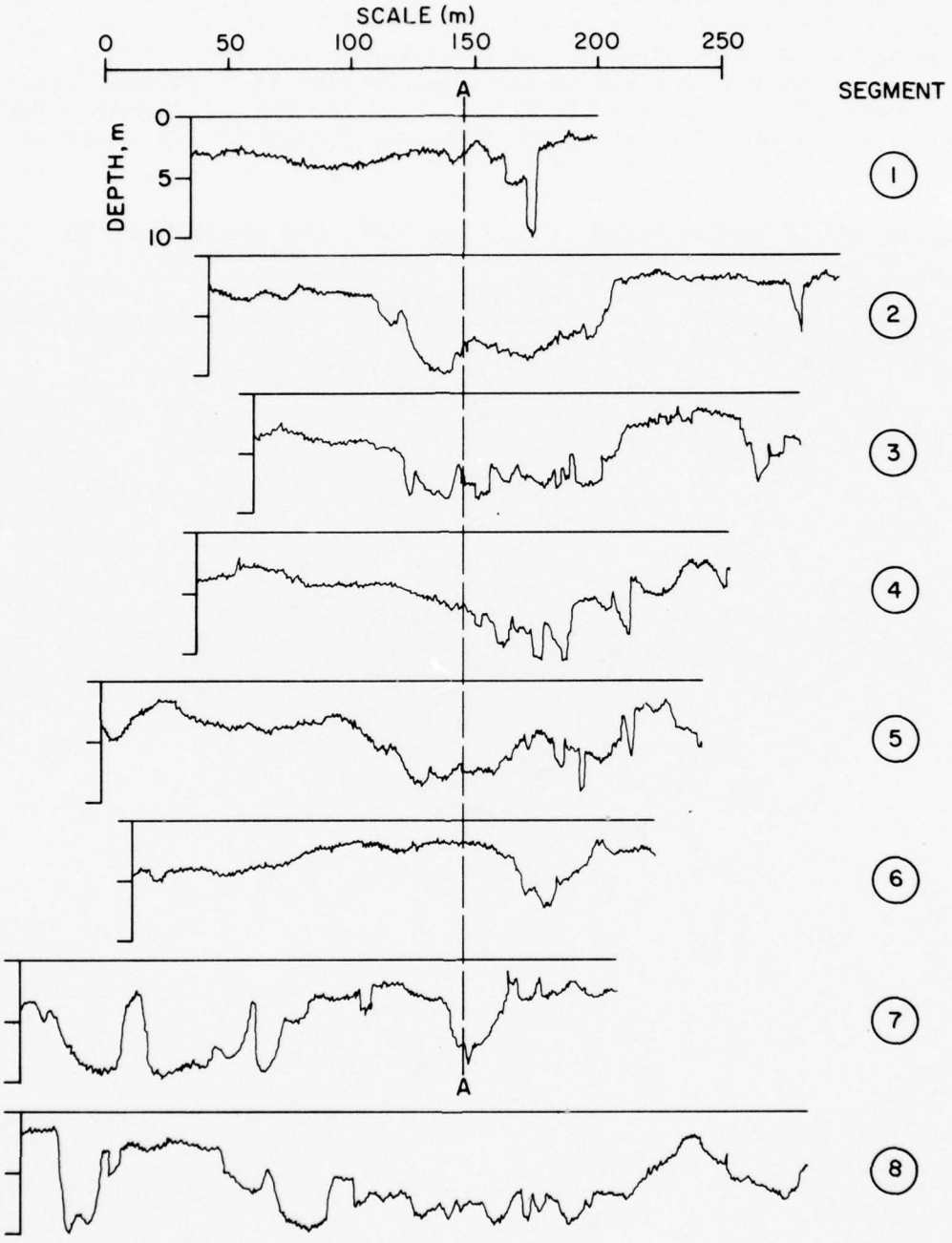

Figure 36b. Under-ice profiles across a multi-year floe (feature B).

The tracks of the under-ice profiling runs through this area are shown in Figure 37 along with the corresponding profiles. The rough-looking area at the bottom of the photograph corresponds to the very irregular area 5-10 m thick to the right of line A-A. Sudden changes in ice depth of 5 to 7 m indicate a very rugged bottom. The large ridges seen near the bottom of the photograph were avoided by the submarine, but probably were 15-20 m deep.

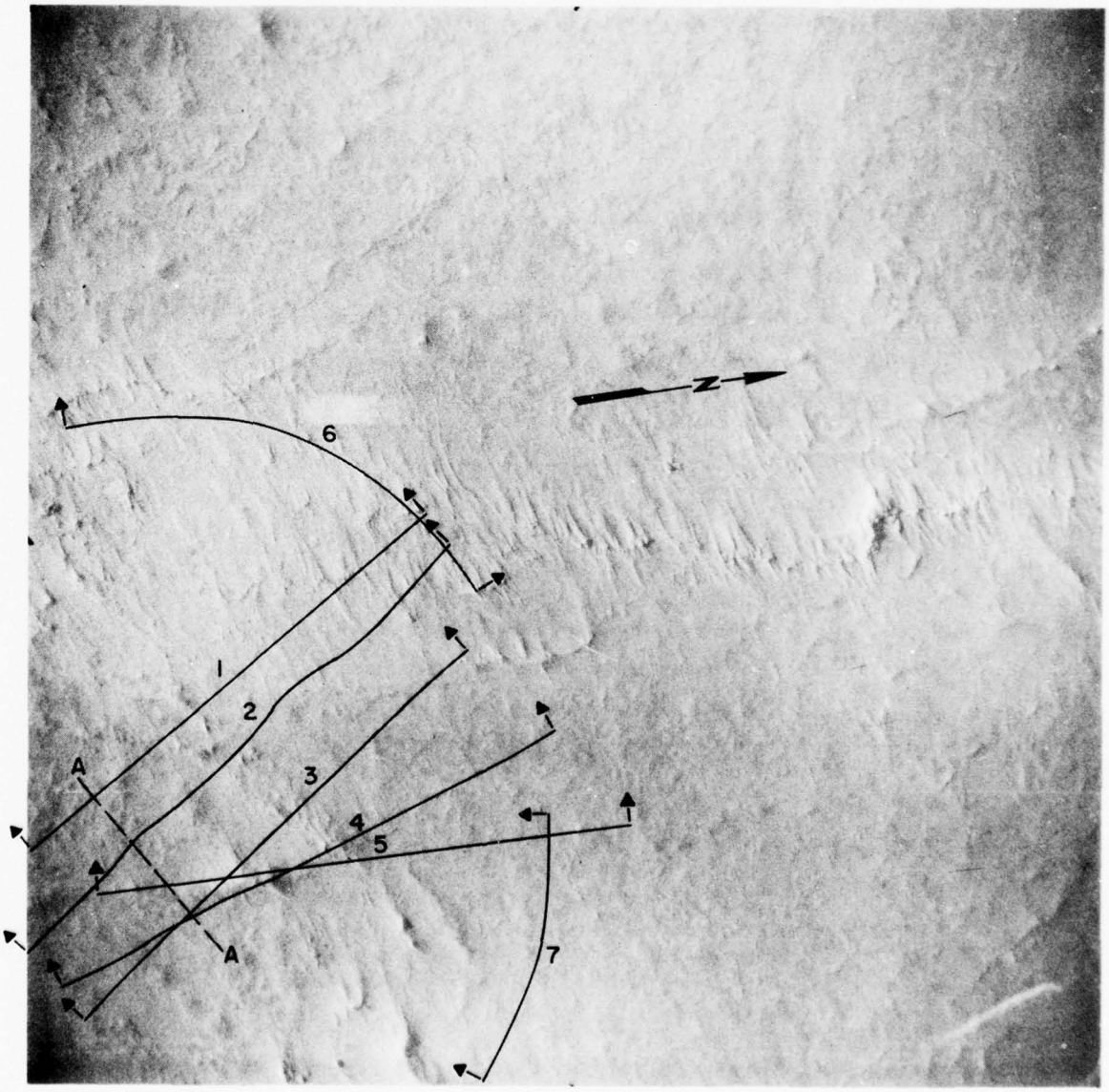

Figure 37a. Under-ice profile lines across a large ridge (feature C).

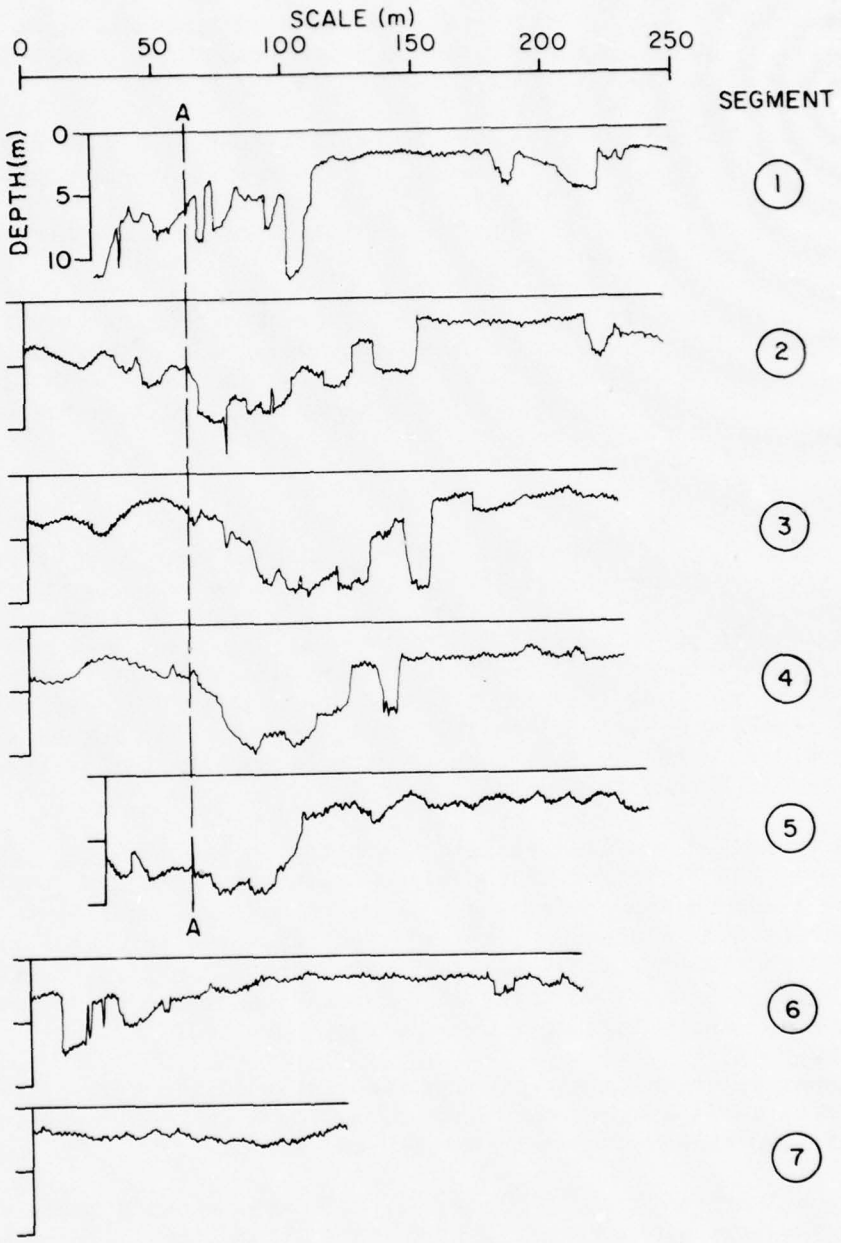

Figure 37b. Under-ice profiles across a large ridge (feature C).

The change in the character of the ice seen near the right ends of segments 2, 3, and 4 in the photograph corresponds to a change from rugged ice 5-10 m thick to fairly smooth ice 2-3 m thick.

A laser profile and an under-ice profile that passed through feature C about 50 m apart are shown in Figure 38. A peak about 2 m high and 30 m long occurs near the end of the ridge. The under-ice profile shows deep keels in this region which end 50 m farther north, where a younger floe begins.

In the infrared image (Figure 22), this area appears very light. Most of the lightness, however, is on the north side of the ridges and may be related to the shadows found there. In the MICRAD image (Figure 23), this area appears light gray as would be expected for multi-year ice.

D. A YOUNG RIDGE

The ice camp was established on the southern edge of a large triangular floe whose northern vertex was about 800 m across from the camp (see Figure 29). Both the eastern and western sides of this triangle were rimmed with pressure ridges. On the eastern side, however, the ridge was much younger and the sails were high and abrupt. We have designated the portion of this ridge within the area profiled by the submarine as feature D. At the northern end, this feature formed a single pressure ridge. The remainder appeared to be double as if a lead had formed, refrozen, and then undergone pressure.

The under-ice profiles crossing this region are shown in Figure 39. Segment 3 is the first one that crosses feature D. The 3-m thick floe above the ridge in the photograph appears to have met the 7-m thick floe below without much ridging. Segment 4 indicates the thicker floe is very rough on the bottom. Segments 6 and 7 cross the ridge farther south. Segment 6 shows no keels at the location of the ridge seen on the photograph while segment 7 shows a very deep keel.

Segment 8, which passes through the center of the ridges seen on the surface, shows a very rough bottom, ending with thin ice which indicates a lead that had opened recently and refrozen.

In the infrared image (Figure 22), this area shows a large variation in shading, with light and dark areas alternating. There is very little warmth (darkness) along the ridge itself. Apparently, it was under great pressure when it formed. The MICRAD image shows a darkness similar to that for new ice.

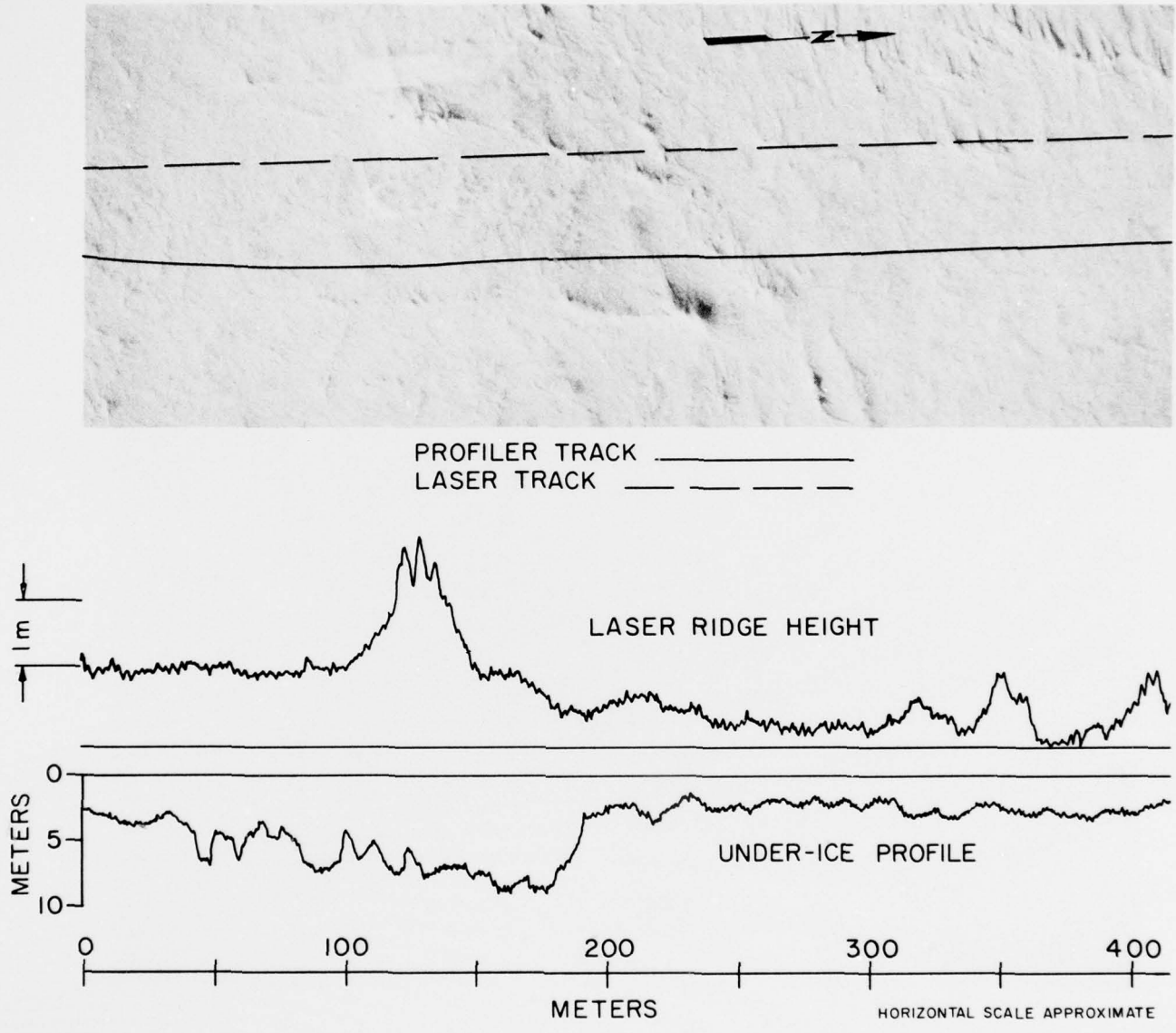

Figure 38. Nearly coincident laser and under-ice profiles through feature C.

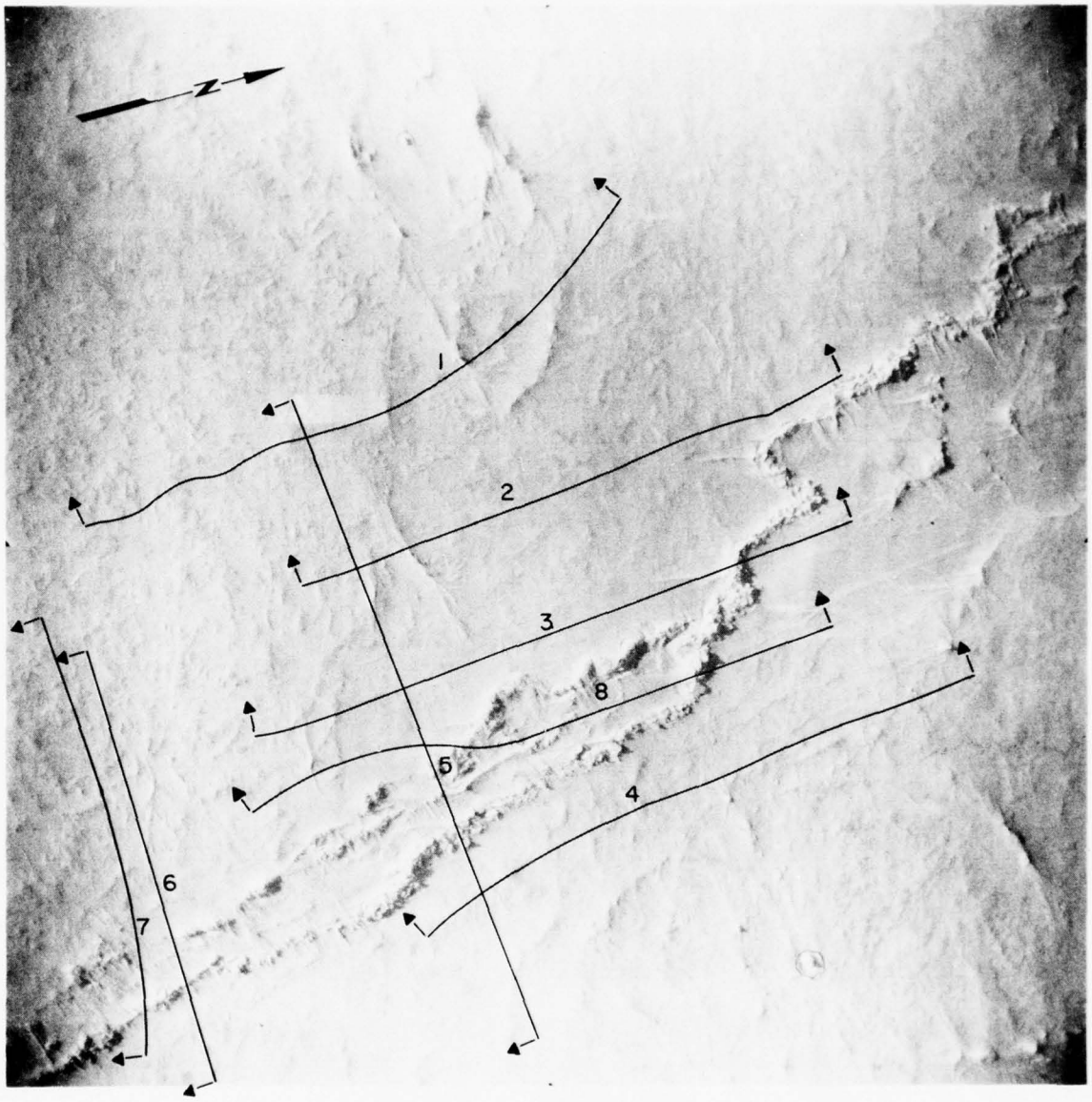

Figure 39a. Under-ice profile lines across a young ridge (feature D).

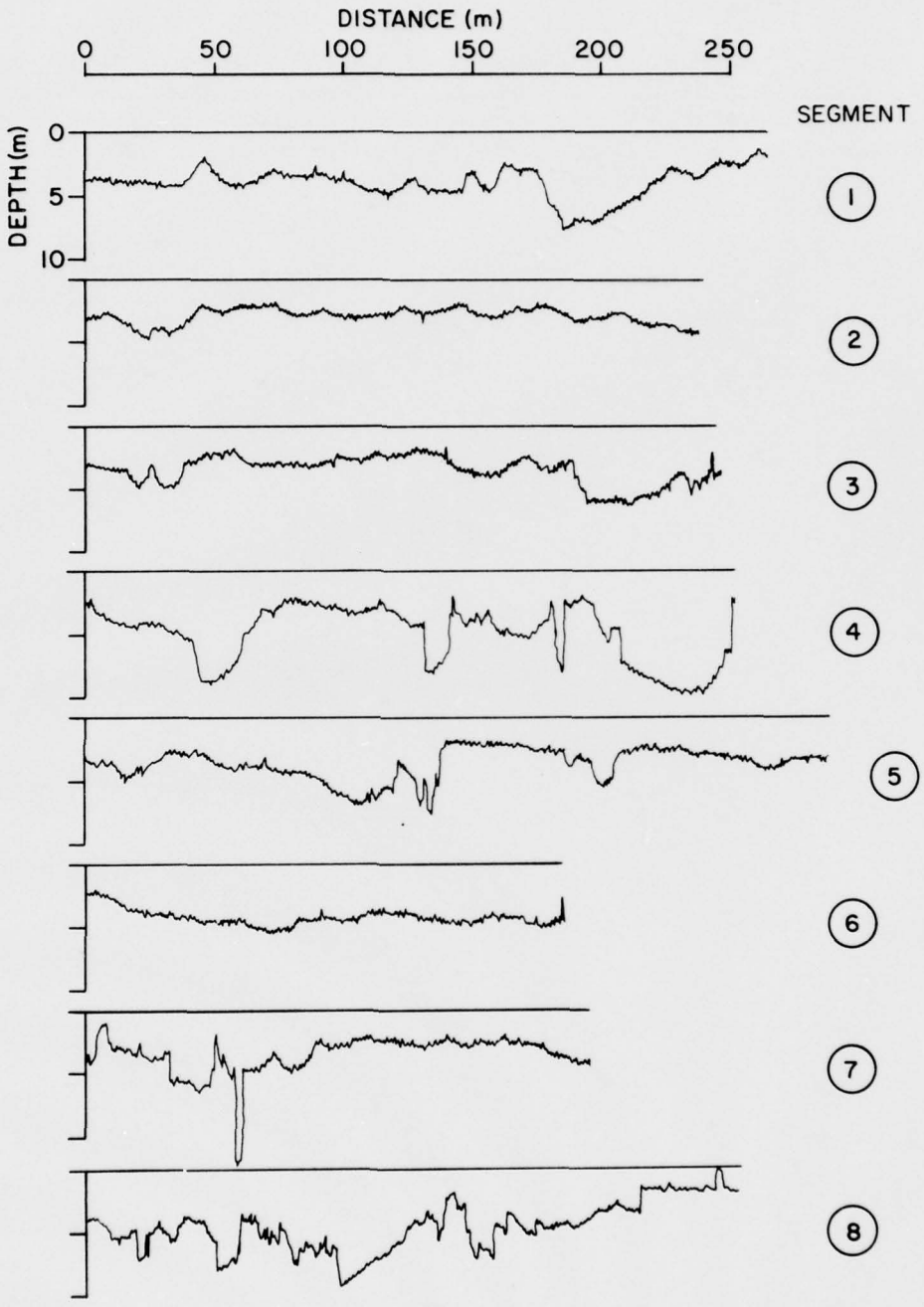

Figure 39b. Under-ice profiles across a young ridge (feature D).

E. RECENT RIDGING

Feature E, on the southeast side of the floe south of APLIS, appeared to be a fracture line that had opened, refrozen, and then closed and ridged perhaps twice in recent weeks. Individual, 3-m high blocks on the latest ridge can be seen in the photograph in Figure 40a. The under-ice profiles corresponding to the tracks shown on the photograph are given in Figure 40b.

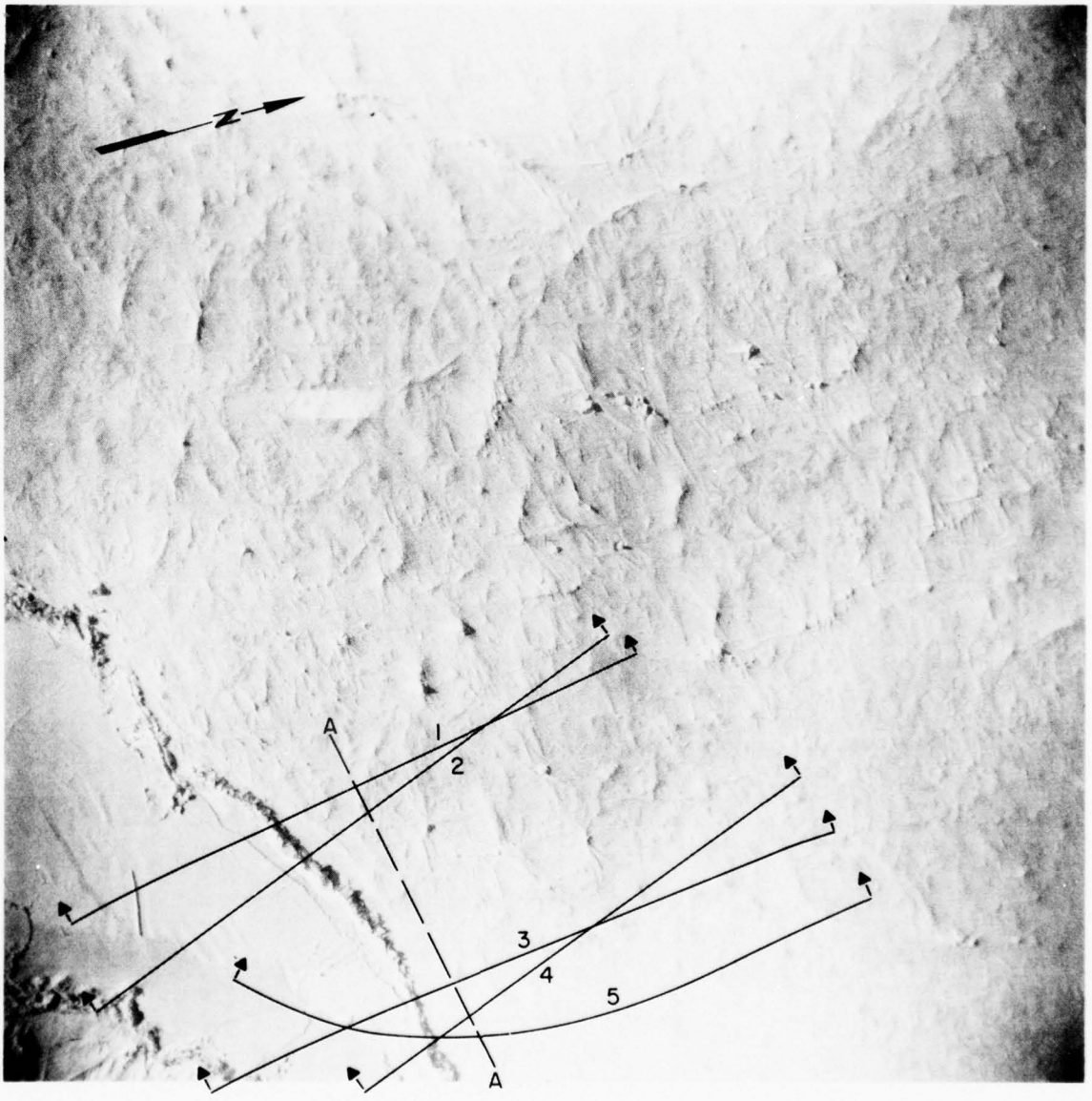

Figure 40a. Under-ice profile lines across a recently formed ridge (feature E).

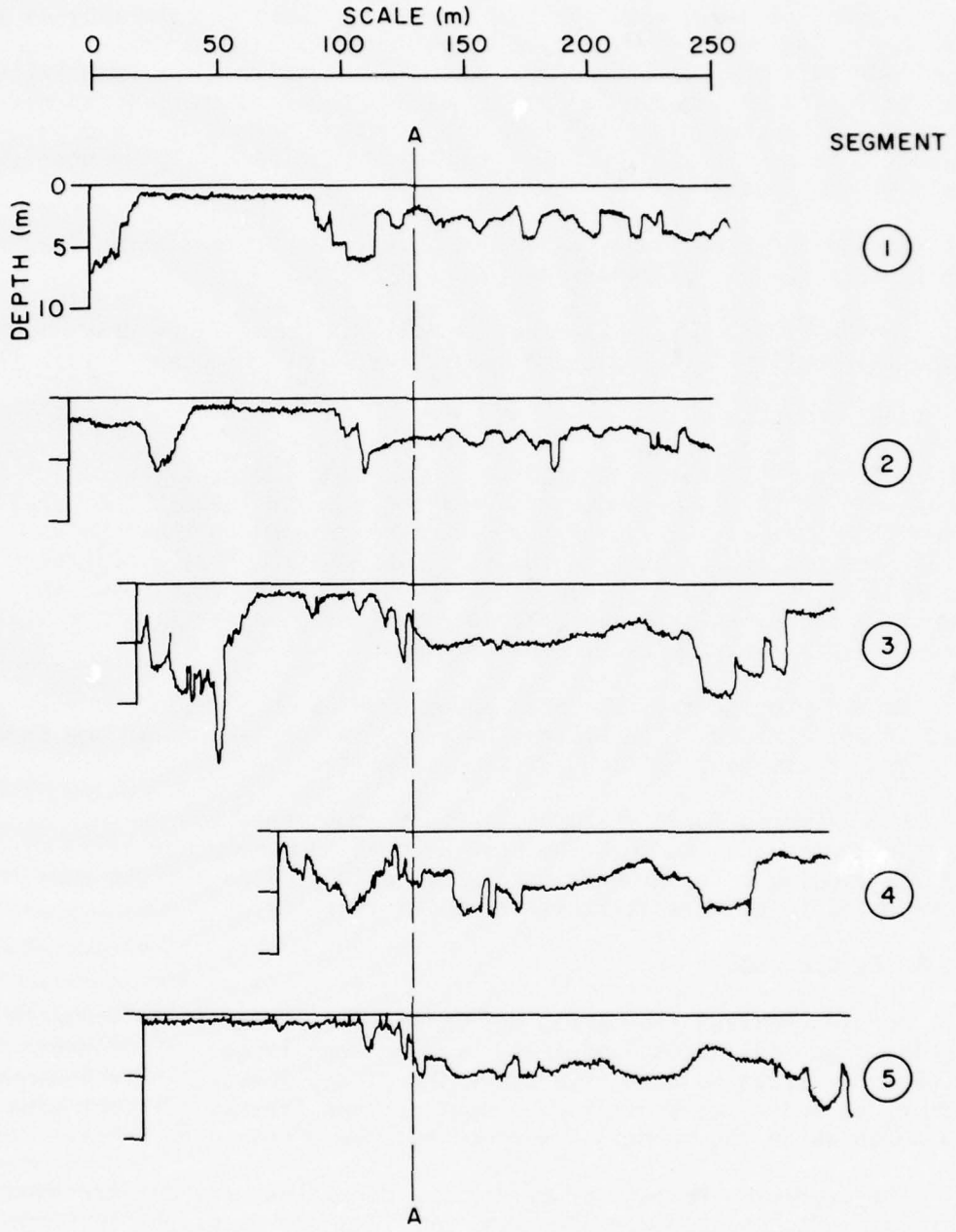

Figure 40b. Under-ice profiles across a recently formed ridge (feature E).

Segments 1 and 2 show the thin ice on the lead and the ridging at the edge. Segment 3 shows a very deep, sharp keel on the other side of the lead; this keel is 15 m deep, which is certainly incongruous with the small size of the rubble seen on the surface. Segment 4 appears to be so close to the end of the lead that no thin ice is observed. Segment 5 crosses from thin ice to the old floe, revealing several sharp keels at the transition.

In the infrared image, this lead appears dark, indicating that the ice is very new and perhaps less than a meter thick.

In the MICRAD image, the area is dark with some light gray spots along the southern side that are apparently chunks of a multi-year floe.

F. LARGE HUMMOCK

Southeast of APLIS was a large, smooth-looking area that was found to be quite thick. The under-ice profiles passing through this area are shown in Figure 41. The profiles have been grouped to show the similarity between tracks that are nearly coincident. These groups are labelled A, B, and C; a dashed line serves as a reference point for comparing the profiles. Near the intersections the profiles are similar. Not far away they vary considerably.

In the photograph, this area appears to be an old floe, surely a year or more in age. The bottom, however, is very irregular and shows no signs of erosion, melting, or consolidation.

The infrared image (Figure 22) shows some variation in this area, but the appearance is about the same as that of many other areas with no surface ridging. The MICRAD image shows this area as a light gray, as is reported to be characteristic of multi-year ice.

G. THICK OLD FLOE

Across the lead from APLIS was an old floe. The large ridge in its center, about 400 m south of APLIS, can be seen in the aerial photographs. Profiles beneath this ridge showed the deepest keels encountered during the under-ice profiling, except perhaps for the adjacent area to the north which the submarine avoided because of the deep keels.

The several submarine tracks that crossed this feature are shown in Figure 42a, and the corresponding profiles are displayed in Figure 42b. Although this appears to be an old floe, the underside is extremely rough. The profiles show blocks extending 10 m below the bottom of the floe, which is only about 5 m thick. In contrast, the upper surface is so smooth that it is almost unrecognizable as a ridged area.

A laser profile through this floe is shown in Figure 43. The 2.5-m high peak seems to correspond with the major ridge seen in the photograph. At the right end of the profile is the refrozen lead near APLIS.

The infrared image (Figure 22) shows light areas corresponding to the north side of the visible ridges. Every shadow on the photograph shows as a light patch on the infrared image. The thickness of the ice appears to affect the shade of gray, but the ridges may be apparent only because of the sun's radiation which warms the southern side of the ridges and fails to warm the northern side.

The MICRAD image for this area is variable, but mostly a light gray. This seems to be true for multi-year ice, no matter how thick.

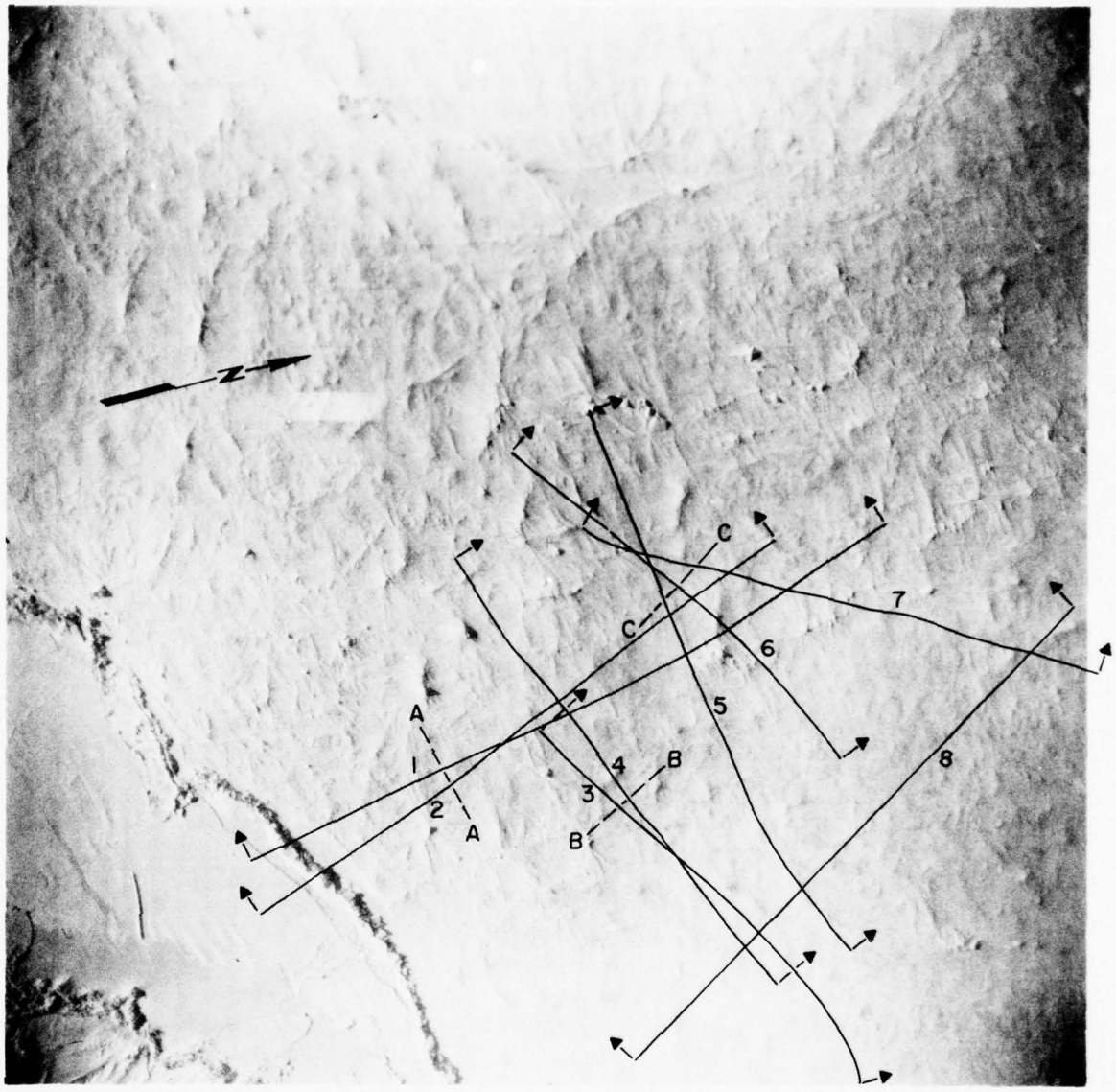

Figure 41a. Under-ice profile lines across a large hummock (feature F).

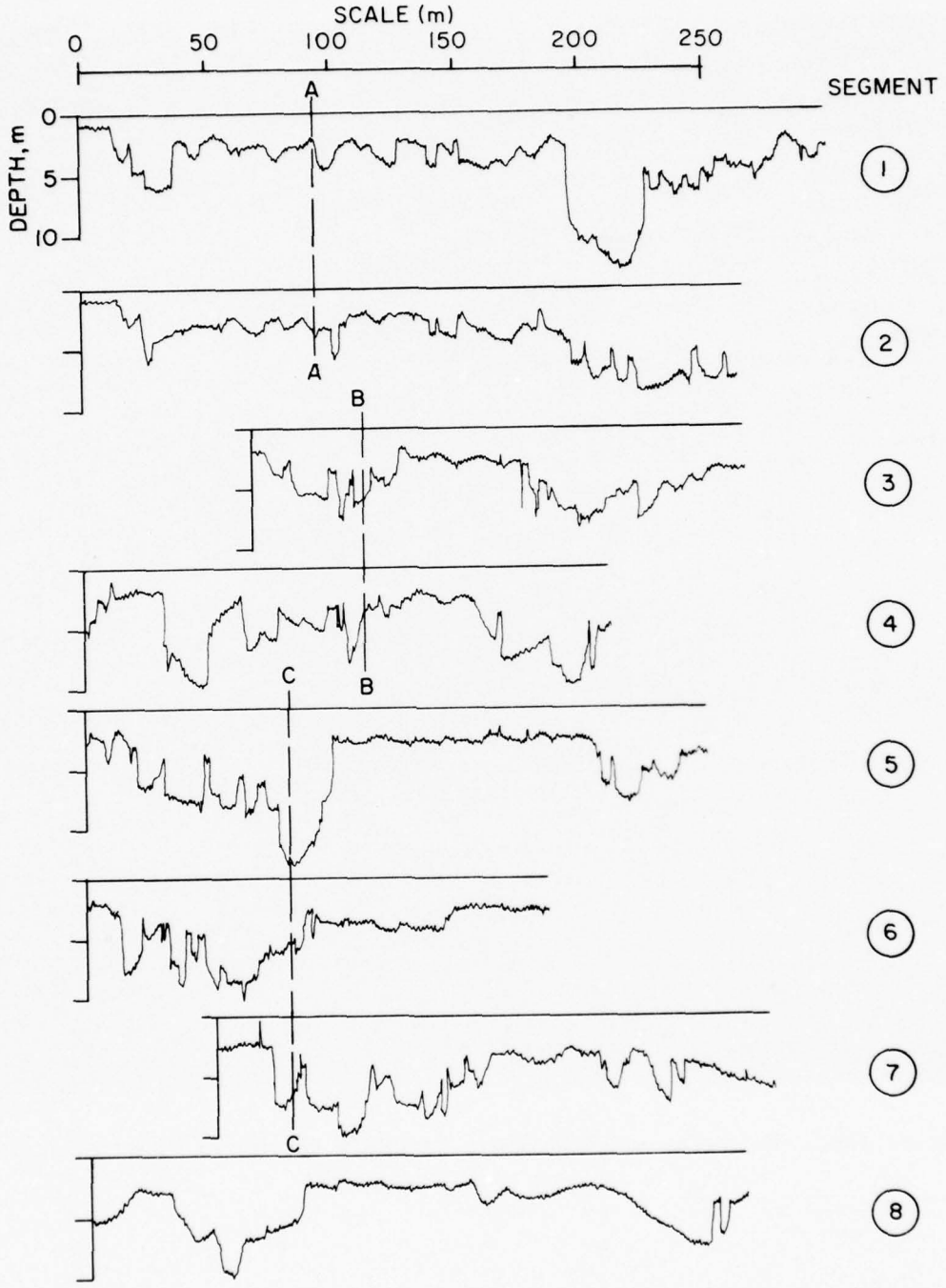

Figure 41b. Under-ice profiles across a large hummock (feature F).

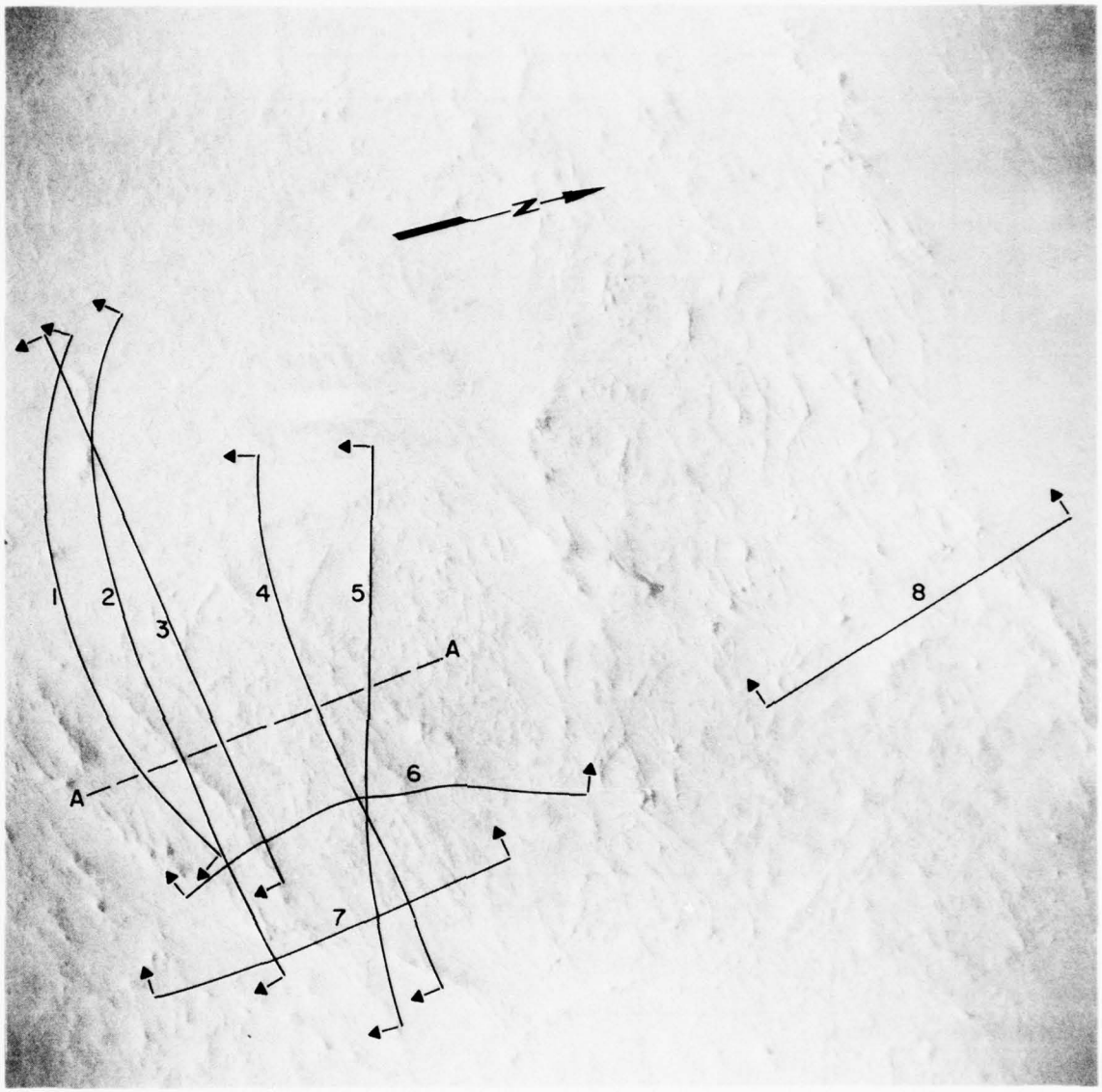

Figure 42a. Under-ice profile lines across a thick old floe (feature G).

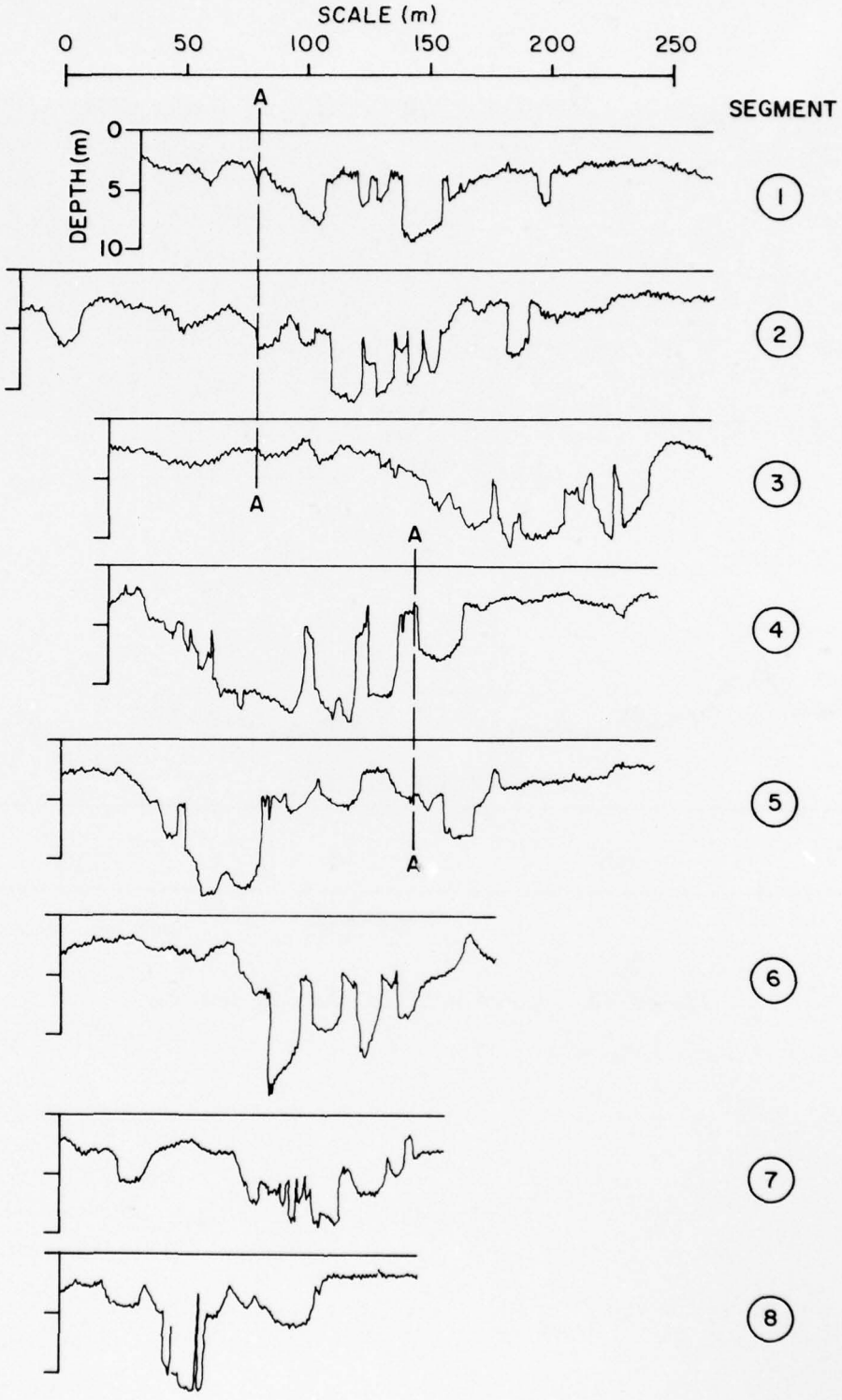

Figure 42b. Under-ice profiles across a thick old floe (feature G).

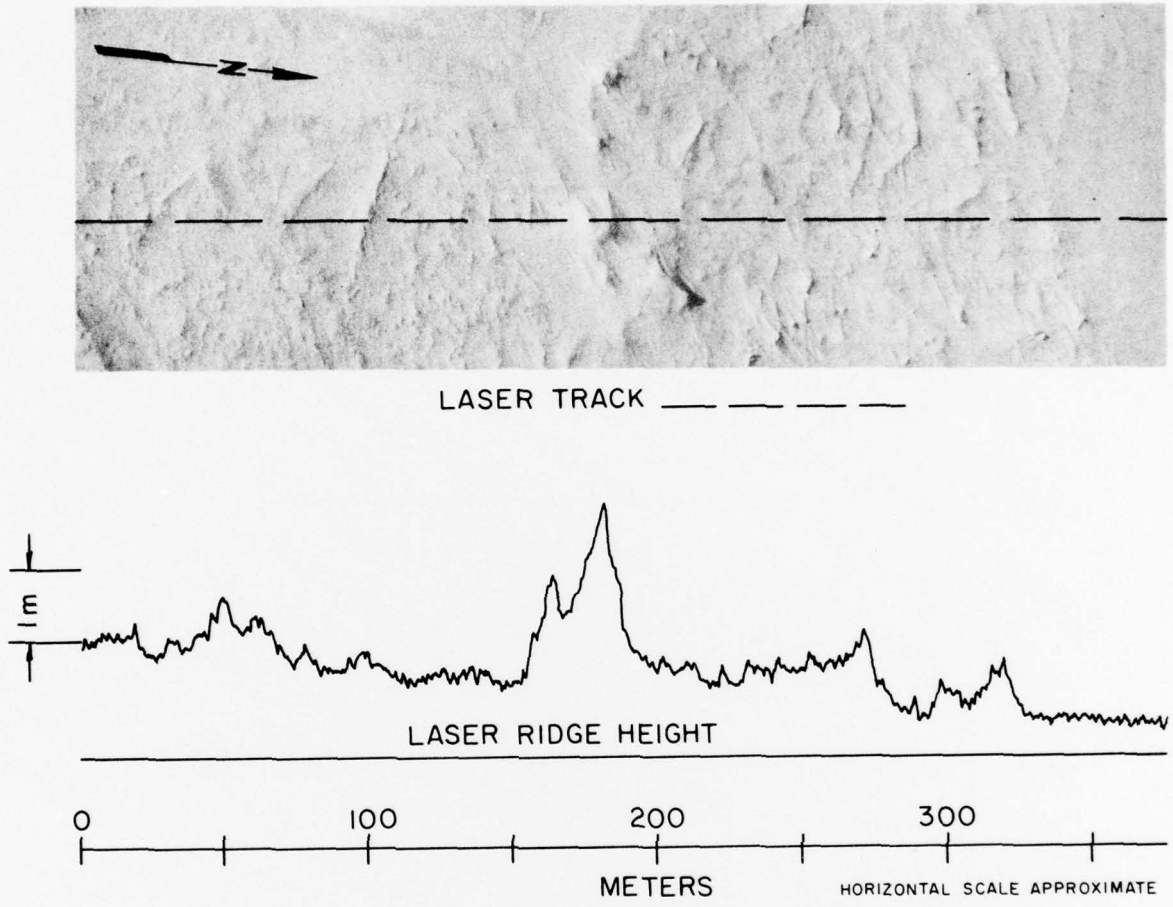

Figure 43. Laser profile through feature G.

VIII. ACOUSTIC REVERBERATION FROM THE UNDER-ICE SURFACE

Reverberation measurements were conducted in the same manner and with the same equipment as the under-ice reflection measurements discussed in an earlier report.[5] Only the backscatter from a flat field of ice is considered to be truly surface reverberation, which we would expect to be dependent on the small-scale character of the surface. The separation of this return from the reflection from ice keels was difficult, especially since there wasn't much flat ice in the area of measurement. However, the return from the flat area near the ice camp was examined for reverberation, or at least the upper bound to it.

A. REVERBERATION EQUATIONS

Development of the reverberation equations is discussed in detail in a previous report.[5] In brief, for the arrangement shown in Figure 44, the equation for the scattering strength is

$$S = I - I_1 + 30 \log R + 2\alpha R + 2B(\theta) + 10 \log c\tau/2 - 10 \log 2\pi - SRI, \quad (3)$$

where

I = received intensity, in decibels

I_1 = source intensity, in decibels

R = range, in meters

α = absorption coefficient, in decibels/meter

$B(\theta)$ = transducer pattern reduction, in decibels

τ = pulse length, in seconds

SRI = surface reverberation index.

The angle to the underside of the ice is given by

$$\sin \theta' = \frac{D-t}{R} .$$

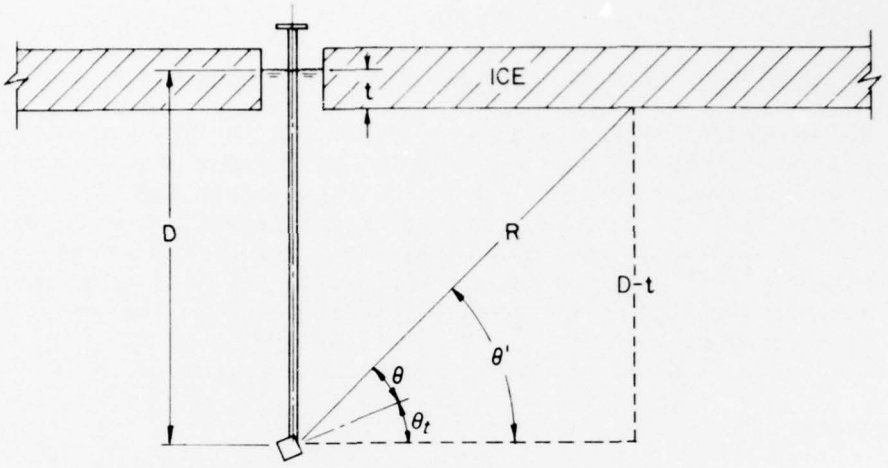

Figure 44. Geometrical relationships for reverberation calculations.

B. REVERBERATION AT 20 kHz

Two of the 20-kHz runs, Nos. 17 and 19, had sufficiently low attenuator settings that low returns were accurately recorded. In Run 17, the pulse length was 1 msec; in Run 19, it was 4 msec. These returns were digitized at 5-msec intervals, and the scattering strength was calculated according to Eq. 3. The results are plotted in Figure 45. At grazing angles lower than sin $\theta \simeq 0.2$ (long range), the reflections from ice keels predominated. At sin $\theta = 0.2$, the reverberation was masked by an electronic target used for calibration. At higher angles, the scattering coefficient increased as in previous years. The two runs were in good agreement. The results are close to those obtained in the Chukchi Sea at 20 kHz in 1974.[4]

C. REVERBERATION AT 60 kHz

Two of the 60-kHz runs, Nos. 2 and 4, were also analyzed for reverberation. After digitizing the tape record at 5-msec intervals, the scattering strengths were calculated using Eq. 3. The results are plotted in Figure 46. The data connected by a dashed line in the figure are considered invalid because of their closeness to the tape noise level; the solid line represents portions that are above noise.

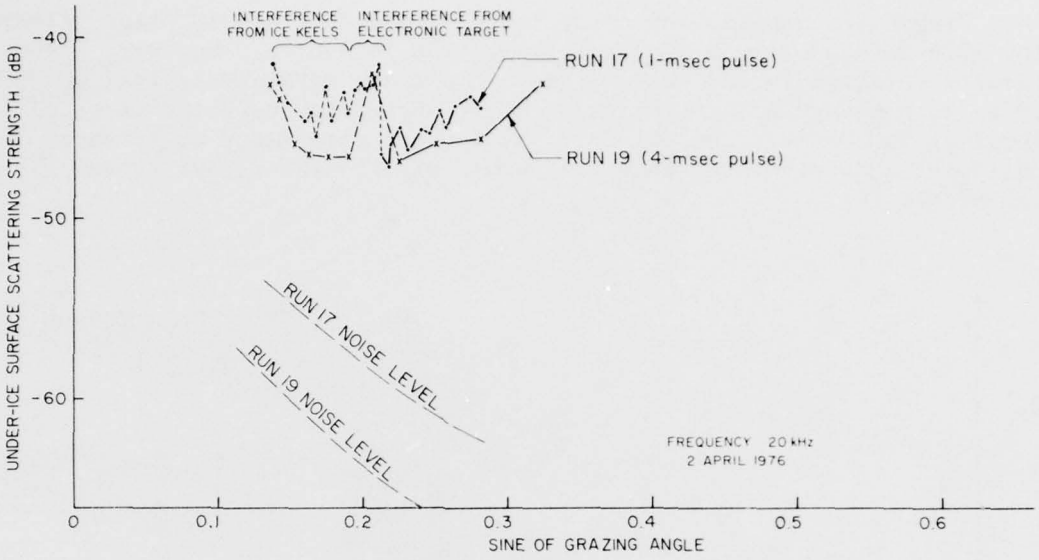

Figure 45. Under-ice surface reverberation at 20 kHz.

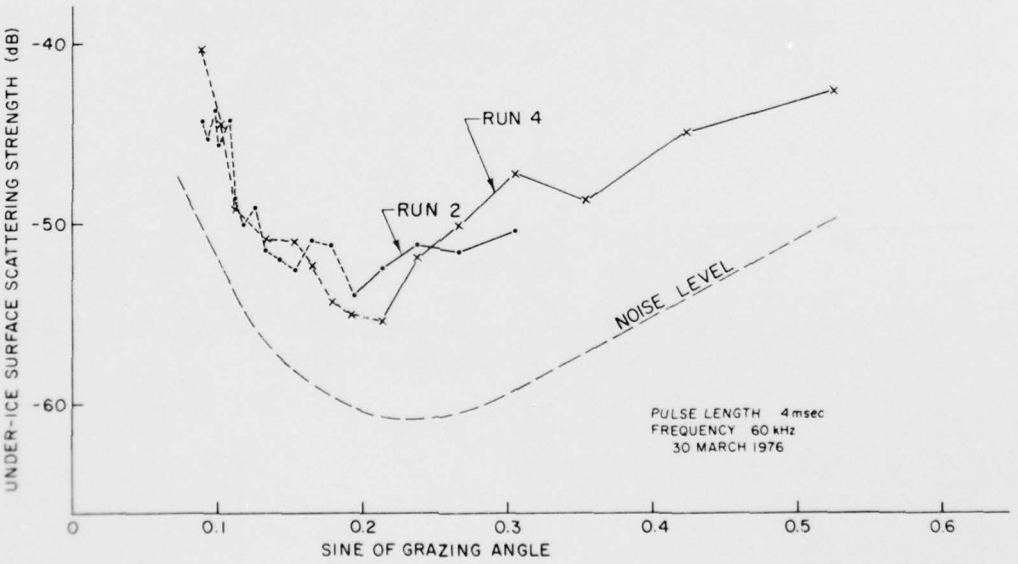

Figure 46. Under-ice surface reverberation at 60 kHz.

Figure 47 compares the results with those obtained in prior years. The 1976 data appear to agree well with the 1974 data. However, the results obtained in 1975 were higher than those obtained in 1974 and 1976, even though all three measurements were taken near the first of April in the eastern Chukchi Sea. There were some minor differences in equipment and method but none that would explain the higher values for the middle year.

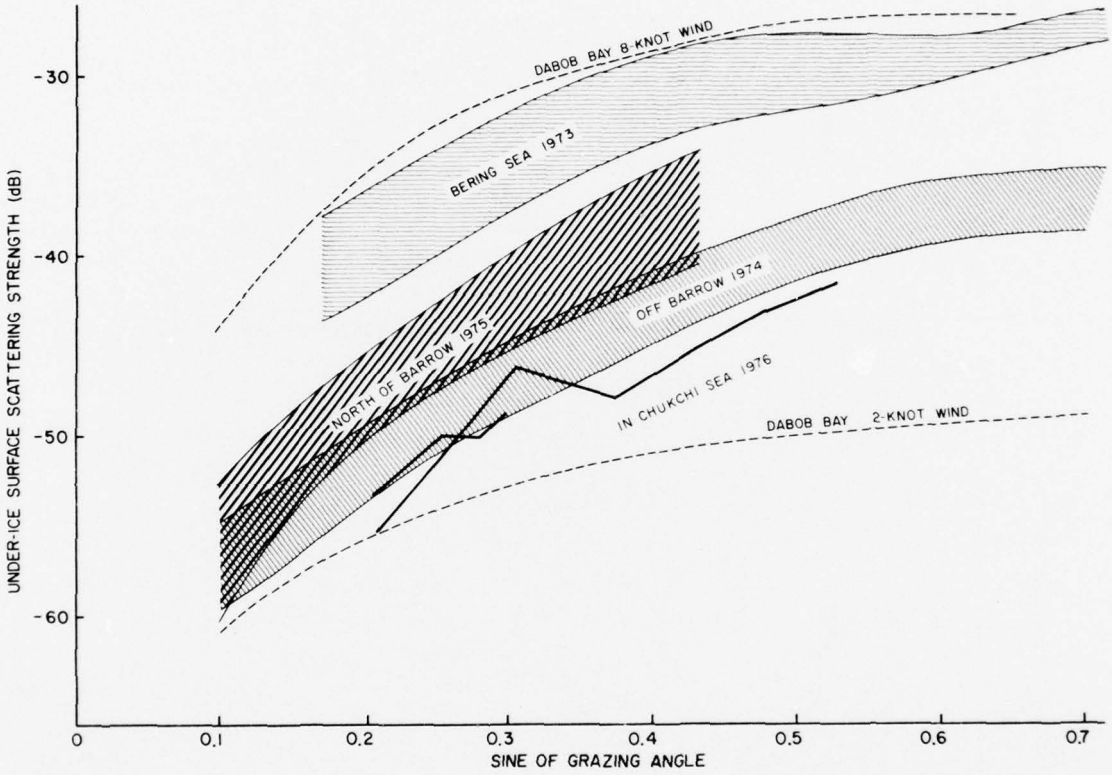

Figure 47. Comparison of 1976 surface reverberation results at 60 kHz with our measurements in previous years.

IX. REFERENCES

1. APL-UW 7223, "Studies in the Marginal Ice Zone of the Chukchi and Beaufort Seas: A Report on Project MIZPAC-71B," Applied Physics Laboratory, University of Washington, by G.R. Garrison and E.A. Pence, 31 January 1973.

2. APL-UW 7311, "Studies in the Marginal Ice Zone of the Chukchi Sea: Analysis of 1972 Data," by G.R. Garrison, E.A. Pence, H.R. Feldman, and S.R. Shah, Applied Physics Laboratory, University of Washington, 14 March 1974.

3. APL-UW 7410, "Studies in the Marginal Ice Zone of the Bering Sea: Analysis of 1973 Bering Sea Data (U)," by G.R. Garrison, E.A. Pence, E.W. Early, and H.R. Feldman, Applied Physics Laboratory, University of Washington, 19 November 1974 (Confidential).

4. APL-UW 7514, "Acoustic Studies from an Ice Floe near Barrow, Alaska, in April 1974," by G.R. Garrison, E.A. Pence, and E.W. Early, Applied Physics Laboratory, University of Washington, 29 February 1976.

5. APL-UW 7608, "Acoustic Studies from an Ice Floe in the Chukchi Sea in April 1975," by G.R. Garrison, R.E. Francois, and E.W. Early, Applied Physics Laboratory, University of Washington, 20 August 1976.

6. APL-UW 7710, "Oceanographic Measurements in the Chukchi Sea and Baffin Bay - 1976," by G.R. Garrison, Applied Physics Laboratory, University of Washington, 15 October 1977.

7. W.D. Hibler III, W.F. Weeks, and S.J. Mock, "Statistical aspects of sea-ice ridge distributions," J. Geophys. Res., 77(30): 5954-5970 (1972).

8. P. Wadhams, "A comparison of sonar and laser profiles along corresponding tracks in the Arctic Ocean," A Symposium on Sea Ice Processes and Models, September 6-9, 1977, Vol. II, International Commission on Snow and Ice, Arctic Ice Dynamics Joint Experiment.

9. A. Kovaks, W.F. Weeks, S. Ackley, and W.D. Hibler III, "A study of a multiyear pressure ridge in the Beaufort Sea," AIDJEX Bulletin 12, February 1972.

10. TN 6130-5-75, "A Simple Geometrical/Statistical Model of Sea Ice Ridges," by O.I. Diachok, Naval Oceanographic Office, Washington, D.C., 1 November 1975.

11. NORDA Technical Note 1, "Mission Report, Spring 1976, Arctic Airborne Remote Sensing Program and Preliminary Analysis of High Resolution Passive Microwave Sea Ice Imagery," by R.D. Ketchum, Jr., S.G. Tooma, Jr., and H. Li, Naval Ocean Research and Development Activity, Bay St. Louis, Mississippi, June 1976.

12. R.D. Ketchum, Jr. and A.W. Lohanick, "Microwave scanning the arctic ice pack," A Symposium on Sea Ice Processes and Models, September 6-9, 1977, Vol. II, International Commission on Snow and Ice, Arctic Ice Dynamics Joint Experiment.

13. APL-UW 7712, "High Resolution Observations of Under-Ice Morphology," by R.E. Francois, Applied Physics Laboratory, University of Washington, 31 March 1977.

X. ACKNOWLEDGMENTS

Field support was provided by the Naval Arctic Research Laboratory through funding by the Office of Naval Research. Working with the officers and crew of the USS GURNARD (SSN-662) was a pleasure. The preparation of profile data tapes by Terry Luallin of NOSC is greatly appreciated. The cooperation of NORDA in arranging and conducting the overflights added greatly to our knowledge of the surrounding ice.

APPENDIX

PROCESSING OF UNDER-ICE PROFILE DATA

The material in this appendix was furnished by Mr. Terry Luallin of the Arctic Submarine Laboratory, Naval Ocean Systems Center, San Diego, California.

1. During SUBICEX 1-76 a high frequency, narrow beam sonar was installed on the USS GURNARD (SSN-662) to profile the underside of the Arctic ice sheet. The sonar system was modified to provide outputs to a signal processing system that digitized the sonar signals and produced a digital magnetic tape of ice drafts with a resolution of 0.1 foot. Due to mechanical limitations within the sonar system, the digital ice draft data has an absolute accuracy in the range of $\pm$ 1 foot, with a demonstrated standard deviation for smooth ice of 0.3 foot.

2. The digitized magnetic tapes were unpacked and processed by the Arctic Submarine Labortory on a UNIVAC 1108 - 1110 computer system at the Naval Ocean Systems Center. The edited and corrected data was converted to BCD format for transmittal to the Applied Physics Laboratory.

3. After the initial unpacking, spurious profile points resulting from multiple echos, fish, air bubbles, etc., were eliminated by two correction programs. Any points that were deleted were set to -10.0. Multiple adjacent deleted points were left at this value, but single points were filled by linear interpolation. These were flagged by adding 200 to the interpolated value.

4. The first correction program deleted any points that were greater than or equal to 150 feet. At the beginning of a tape, or following one or more zeros recorded by the system, the program searched for the first valid data point by computing the absolute difference between adjacent points ($|X_i - X_{i+1}|$), and requiring that the difference be less than 5.0 feet. For example, if the difference between the first two points satisfied this criterion, the program assumed that X_1 was correct and used it as its current X_i value. If, however, the difference was greater than 5.0, it deleted X_1, made X_2 the current X_i value, and computed a new difference ($|X_2 - X_3|$). It continued in this manner until it found a difference that was less than 5.0, at which time it accepted the current X_i value as the first valid data point.

5. After the program chose a valid X_i value, it computed the absolute difference between adjacent points and compared the difference with a threshold number that was set to 20.0 feet. If the D_1 difference ($|X_i - X_{i+1}|$) was less than the threshold, the program accepted X_{i+1} as a valid point and used it as its next X_i value. However, if the difference was greater than 20, it computed a D_2 equal to $|X_i - X_{i+2}|$, and, if necessary, a D_3 equal to $|X_i - X_{i+3}|$. The program accepted X_{i+1} as a valid point only if both D_2 and D_3 were also greater than the threshold value. If D_2 was less than 20, X_{i+1} was deleted, and X_{i+2} was selected as the next X_i value. If D_2 was greater than 20 but D_3 was less, both X_{i+1} and X_{i+2} were deleted, and X_{i+3} was chosen as the next X_i value.

6. Since the system recorded zeros during periods when it didn't receive any data, zero words were not used to compute the differences. The program required that if D_1 ($|X_i - X_{i+1}|$) was greater than the threshold, both X_{i+2} and X_{i+3} must be non-zero, and both D_2 and D_3 must be greater than 20 or the data was rejected. In the case that D_1 was greater than 20 and X_{i+2} was zero, the program deleted X_{i+1}. If D_1 and D_2 were greater than 20, but X_{1+3} was zero, both X_{i+1} and X_{i+2} were deleted. In either case, or if X_{i+1} was zero, the program searched for the next valid X_i value by using the technique described in paragraph 4 above.

7. In order to maintain continuity between data records, the program included the first three data points from the succeeding record with the current record when it computed the differences.

8. The second program subtracted a surface offset correction from each of the profile points. This correction was determined from an analysis of both analog and digital data, and is used to shift the mean data points in areas of open water to read zero. A few points that were already very near zero became negative. The offset was usually one to two feet.

9. This program also eliminated spurious points that might have been missed by the first program by deleting any points during a variable time period that exceeded the maximum possible ice depth which was determined by examining the analog records. Points deleted by this program were not interpolated and appear as -10.0.

Distribution List

Addressee	No. of Copies
Commander Naval Weapons Center China Lake, California 93555 Attn: Library	1
Commander Naval Ocean Systems Center 271 Catalina Boulevard San Diego, California 92152 Attn: Library	1
Director Naval Research Laboratory Washington, D. C. 20375 Attn: Technical Information Division	3
Director Ordnance Research Laboratory Pennsylvania State University State College, Pennsylvania 16801	1
Commander Submarine Force U. S. Atlantic Fleet Norfolk, Virginia 23511	2
Commander Submarine Force U. S. Pacific Fleet N-21 FPO San Francisco, California 96610	1 1
Commander Naval Air Development Center Warminster, Pennsylvania 18974	1
Commander David W. Taylor Naval Ship Research and Development Center Bethesda, Maryland 20084	1
Chief of Naval Material Department of the Navy Washington, D.C. 20360 NMAT 08T NMAT 08T24 NMAT 08T245	2 1 1
Director Applied Physics Laboratory University of Washington 1013 Northeast 40th Street Seattle, Washington 98105 Mr. Robert E. Francois Mr. E. A. Pence Dr. G. R. Garrison Library	1 1 1 1
Director Arctic Submarine Laboratory Code 54, Building 371 Naval Ocean Systems Center San Diego, California 92152	25
Superintendent Naval Postgraduate School Monterey, California 93940 Library Dr. R. G. Paquette Dr. R. H. Bourke	2 1 1
Polar Research Laboratory, Inc. 123 Santa Barbara Street Santa Barbara, California 93101	2
Chief of Naval Operations Department of the Navy Washington, D. C. 20350 NOP-02 NOP-22 NOP-095 NOP-098	1 1 1 1
Commander Submarine Squadron THREE Fleet Station Post Office San Diego, California 92132	1
Commander Submarine Group FIVE Fleet Station Post Office San Diego, California 92132	1
Director Marine Physical Laboratory Scripps Institute of Oceanography San Diego, California 92132	1
Commanding Officer Naval Intelligence Support Center 4301 Suitland Road Washington, D. C. 20390	1
Commander Naval Electronic Systems Command Hq. Department of the Navy Washington, D. C. 20360 NESC 03 PME 124	1 1 1
Director Woods Hole Oceanographic Institution Woods Hole, Massachusetts 02543	1
Commanding Officer Naval Coastal Systems Laboratory Panama City, Florida 32401	1
Commanding Officer Naval Submarine School Box 700, Naval Submarine Base, New London Groton, Connecticut 06340	1
Assistant Secretary of the Navy (Research and Development) Department of the Navy Washington, D. C. 20350	2
Director of Defense Research and Engineering Office of Assistant Director (Ocean Control) The Pentagon Washington, D. C. 20301	1
Commander Naval Sea Systems Command Department of the Navy Washington, D. C. 20362	4

Addressee	No. of Copies
Chief of Naval Research Department of the Navy 800 North Quincy Street Arlington, Virginia 22217	1
Code 102-OS	1
Code 220	1
Code 461	1
Project Manager Anti-Submarine Warfare Systems Project Office (PM4) Department of the Navy Washington, D. C. 20360	1
Commanding Officer Naval Underwater Systems Center Newport, Rhode Island 02840	1
Commander Naval Air Systems Command Headquarters Department of the Navy Washington, D. C. 20361	2
Commander Naval Oceanographic Office Washington, D. C. 20373	
Attn: Library	2
Director Defense Supply Agency Defense Documentation Center Cameron Station Alexandria, Virginia 22314	12
Director Defense Advanced Research Project Agency 1400 Wilson Boulevard Arlington, Virginia 22209	1
Commander, SECOND Fleet Fleet Post Office New York, N. Y. 09501	1
Commander, THIRD Fleet Fleet Post Office San Francisco, California 96601	1
Commander Naval Surface Weapons Center White Oak Silver Spring, Maryland 20910	
Mr. M. M. Kleinerman	1
Library	1
Officer-in-Charge New London Laboratory Naval Underwater Systems Center New London, Connecticut 06320	1
Commander Submarine Development Group TWO Box 70 Naval Submarine Base - New London Groton, Connecticut 06340	1
Oceanographer of the Navy Hoffman II 200 Stovall Street Alexandria, Virginia 22332	1

Addressee	No. of Copies
Commandant U. S. Coast Guard Headquarters 400 Seventh Street, S. W. Washington, D. C. 20590	2
Commander Pacific Area, U. S. Coast Guard 630 Sansome Street San Francisco, California 94126	1
Commander Atlantic Area, U. S. Coast Guard Building 125, Room 204 Governors Island New York, N. Y. 10004	1
Department of Oceanography University of Washington Seattle, Washington 98195	2
Commanding Officer Naval Arctic Research Laboratory Barrow, Alaska 99723	
Library	2

REPORT DOCUMENTATION PAGE

READ INSTRUCTIONS BEFORE COMPLETING FORM

1. REPORT NUMBER

2. GOVT ACCESSION NO.

3. RECIPIENT'S CATALOG NUMBER

4. TITLE (and Subtitle)

COMPREHENSIVE STUDIES OF ARCTIC PACK ICE IN APRIL 1976

5. TYPE OF REPORT & PERIOD COVERED
Data presentation and analysis, 1976

6. PERFORMING ORG. REPORT NUMBER
7724

7. AUTHOR(s)
G.R. Garrison, R.E. Francois, E. W. Early, T. Wen

8. CONTRACT OR GRANT NUMBER(s)
N00123-74-C-2064 and N00123-77-C-1013

9. PERFORMING ORGANIZATION NAME AND ADDRESS
Applied Physics Laboratory
University of Washington
1013 NE 40th, Seattle, Washington 98105

10. PROGRAM ELEMENT, PROJECT, TASK AREA & WORK UNIT NUMBERS
62759N, F 52555, ZF 52555001, MR 01-C2

11. CONTROLLING OFFICE NAME AND ADDRESS
Director, Arctic Submarine Laboratory
Naval Ocean Systems Center
San Diego, California 92152

12. REPORT DATE
May 1978

13. NUMBER OF PAGES
83

14. MONITORING AGENCY NAME & ADDRESS(if different from Controlling Office)

15. SECURITY CLASS. (of this report)
Unclassified

15a. DECLASSIFICATION/DOWNGRADING SCHEDULE

16. DISTRIBUTION STATEMENT (of this Report)

Approved for public release, distribution unlimited.

17. DISTRIBUTION STATEMENT (of the abstract entered in Block 20, if different from the report).

18. SUPPLEMENTARY NOTES

19. KEY WORDS (Continue on reverse side if necessary and identify by block number)

Chukchi Sea
Ice Morphology
Remote Sensing of Sea Ice
Reverberation from Sea Ice

20. ABSTRACT (Continue on reverse side if necessary and identify by block number)

During the occupancy of a camp on an ice floe in the Chukchi Sea, studies were made of both the upper and lower surfaces of the pack ice surrounding the camp. Hole drilling and surface observations provided accurate information on ice thickness and composition. A submarine was tracked acoustically as it profiled the underside of the ice. Two aircraft examined the upper surface using photography, infrared imagery, laser profiling and microwave imagery. The highly detailed under-ice

20. ABSTRACT (Continued)

profiles show the underside of the ice to be very irregular with little erosion regardless of the age of the ice. The upper surface erodes much faster, and thus gives little evidence of the roughness below. Radiation patterns reveal thickness and age characteristics of the floe but their interpretation requires further investigation.

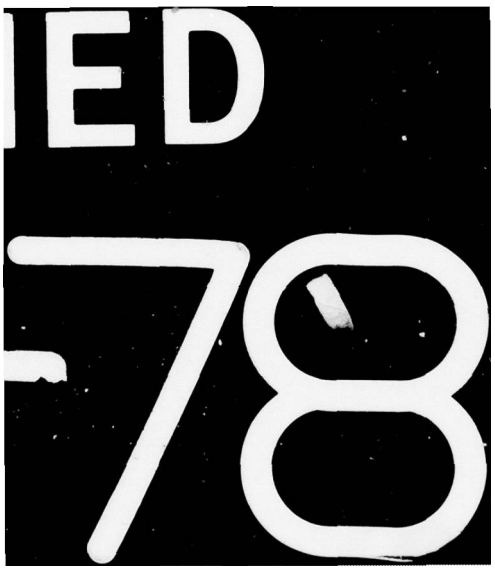
ED
78